THESIS

TITANIA NANOTUBES AS POTENTIAL INTERFACES FOR VASCULAR APPLICATIONS

Submitted by

Sean Edward Kelley

Department of Mechanical Engineering

In partial fulfillment of the requirements

For the Degree of Master of Science

Colorado State University

Fort Collins, Colorado

Spring 2015

Master's Committee:

Advisor: Ketul C. Popat

Melissa Reynolds
Walajabad S. Sampath

ABSTRACT

TITANIA NANOTUBES AS POTENTIAL INTERFACES FOR VASCULAR APPLICATIONS

The primary fatality of the public worldwide is cardiovascular disease. Surgery is usually the modern answer to these complications including transplanting organs and artificial implants with the latter typically being most successful. Generating long term synergy between the transplants and the surrounding tissue continues to be a problematic causing the necessity for comprehending the complex interactions that occur between the two sides at the cellular level. New implants comprising of either purely cellular platforms or a mixture of synthetic and cellular frameworks have demonstrated tremendous potential for tissue restoration. Preferably, the surface of an implant should be suitable for cells to adhere, proliferate, and in many cases differentiate while performing their required functions as if they were in their own natural environment. The surface of these implants must also have a minimum but ideally no immune response. Titanium and its alloys are extensively employed in biomedical devices, due to their beneficial mechanical and relatively high biocompatible properties. Smooth muscle cells are one of the two major cells varieties that are in contact with vascular stents; consequently the interaction between the cells and the nanotube titania (TiO_2) surface is of the utmost importance. The objective of this research is to examine the cellular response of smooth muscle cells to titania nanotubes as a prospective surface modification to complement titanium vascular stents.

ACKNOWLEDGEMENTS

In regards to my thesis and the pursuit of my Master's degree, the greatest thanks goes to Dr. Ketul Popat, who presented me with the opportunity to work in his laboratory and the pursuit of a higher degree. His leadership, consideration, and professionalism will never be forgotten and are attributes I will continue to try my best to emulate.

To Dr. Barbara Smith, for all of her kindness and patience as well as allowing me to serve as her undergraduate associate. My contribution to her PhD research paved the road to the pursuit of my Master's degree.

I would like to thank Dr. Melissa Reynolds for serving as my committee member and allowing me the opportunity to be a Chemisty 141 Teacher's Assistant my first semester.

I would like to thank Dr. Walajabad S. Sampath for serving as not only my committee member but for also being a very knowledgeable and helpful professor for the Material Science course.

I would like to thank all my fellow laboratory students, especially Jonathan Sorkin as well as Dr. Nathan Trujillo for all their help in performing the studies that are part of this thesis.

To Dr. Patrick McCurdy, I thank you for all your service with all the material analyses over the years.

To my undergraduate assistants, Mahli Ruff and Lizette Van Zyl, for producing the titania nanotubes samples that expedited my research and all other responsibilities that you offered your time to help with my research.

Last, to anyone that I did not mention, my thanks to you.

DEDICATIONS

I dedicate this work to God, my family, particularly my devoted parents and all my friends for all their love and support. None of this would be possible without all of you.

TABLE OF CONTENTS

LIST OF TABLES

LIST OF FIGURES

INTRODUCTION

With the tremendous escalation in the world's populace, there are enormous requirements each year for diverse biomedical transplants to reestablish missing or ailing tissues. Producing long time collaboration between the surrounding tissue and the transplants continues to be a challenge in biomedical engineering, calling for a deeper comprehension to the complex relations that occur between the two features at the cellular level. It is imperative to produce new generation alternatives to restore tissue at defect locations that will persist for the lifetime of the patient.

Titanium and titanium alloys are extensively exploited in biomedical apparatuses predominantly as solid tissue substitutes including cardiovascular treatments, such as implantable screws, femur head replacements, stents and much more, due to their advantageous mechanical and comparatively elevated biocompatible characteristics. The natural oxide film that generates on the surface of titanium and its alloys is a major contributor to decreased immune rejection.

Cellular surface proteins are nanometers in dimension, and so there is a need to create medical implants with nanoscale surfaces structures. Since these transplant surfaces relate directly with nanostructured extra-cellular matrices (ECM)s, the attributes of nanomaterials are vital in prompting tissue renewal. The surfaces of these implants should allow for cells to adhere, proliferate, differentiate with minimum to no immune response, while allowing the cells to continue performing their essential purposes.

Titania nanotubes were fabricated from commercially pure titantium by an electrochemical anodization process comprising a fluoride electrolyte solution. These nanotubes were found to be uniform, vertically oriented and reproducible.

The research presented in this master's thesis is one of the few studies fixated on the influence of titania nanotubes on vascular smooth muscle cells and the only study currently found that specifically utilizes human aortic smooth muscle cells. This investigation addresses the hypothesis that titania nanotubes will provide a suitable surface modification of titanium for human aortic smooth muscle cell adhesion, proliferation and differentiation. The study's purpose is to quantitatively and qualitatively determine if surface modification with titania nanotubes of titanium vascular stents is a worthwhile enterprise by their interaction with smooth muscle cells. The findings of the series of experiments in this document offer favorable results in regards to titania nanotubes as potential interfaces for vascular applications.

HYPOTHESIS AND SPECIFIC AIMS

Fundamental Hypothesis: Titania nanotubes provide a more beneficial substrate for vascular prostheses than flat titanium

Specific Aims

Hypothesis 1: Titania nanotubes can be produced from commercially pure titanium to be highly reproducible, uniform, vertically-oriented interfaces for vascular implantable devices using an electrochemical anodization process.

Specific Aim 1: Fabrication and material characterization of titania nanotubes as interfaces for vascular prostheses. This specific aim will be examined in depth in Chapter 2 and will discuss the following topics:

(a) Fabrication of reproducible, vertically oriented, uniform titania nanotube arrays by an electrochemical anodization reaction procedure.

(b) Assessment of material surface characterization of the titania nanotubes.

(c) Survey of mechanical surface characteristics of the titania nanotubes.

Hypothesis 2: Titania nanotube substrate will deliver beneficial topographies for devices in interacting with vascular tissue.

Specific Aim 2: Ascertain smooth cell adhesion, proliferation and differentiation on titania nanotubes. This specific aim will be examined in depth in Chapters 3 and 4 which will discuss the following topics:

(a) Valuation of the outcome of titania nanotubes on the adhesion, proliferation, viability, cellular structure, and morphology of human aortic smooth muscle cells.

(b) Differentiation of human aortic smooth muscle cells from a proliferative, synthetic phenotype to a more contractile phenotype.

CHAPTER 1

LITERATURE REVIEW

1.1 Introduction

With the enormous escalation in the world's populace, there are vast requirements each year for diverse biomedical transplants to restore ailing or missing tissues. It is plainly imperative to generate new generation alternatives to restore tissue at defect locations that will endure for the lifetime of the patient [1]. Since cellular surface proteins are nanometers in dimension, there is a strong need to produce medical implants with surfaces on the nanoscale. Since these transplant surfaces interact closely with nanostructured extra-cellular matrices (ECM)s, the characteristics of nanomaterials are crucial in promoting cell growth, migration and differentiation as well as influencing tissue restoration [1].

In their native environment, cells are incased by nanofeatures, when communicating with other cells; through membranes of nano-size structures or with the extra-cellular matrix (ECM), founded by biomolecules arranged in diverse geometrical arrays such as nanofibers, nanocrystals, nanopores [2]. Examples of various nanostructured materials can be viewed below in **Figure 1.1.1.**

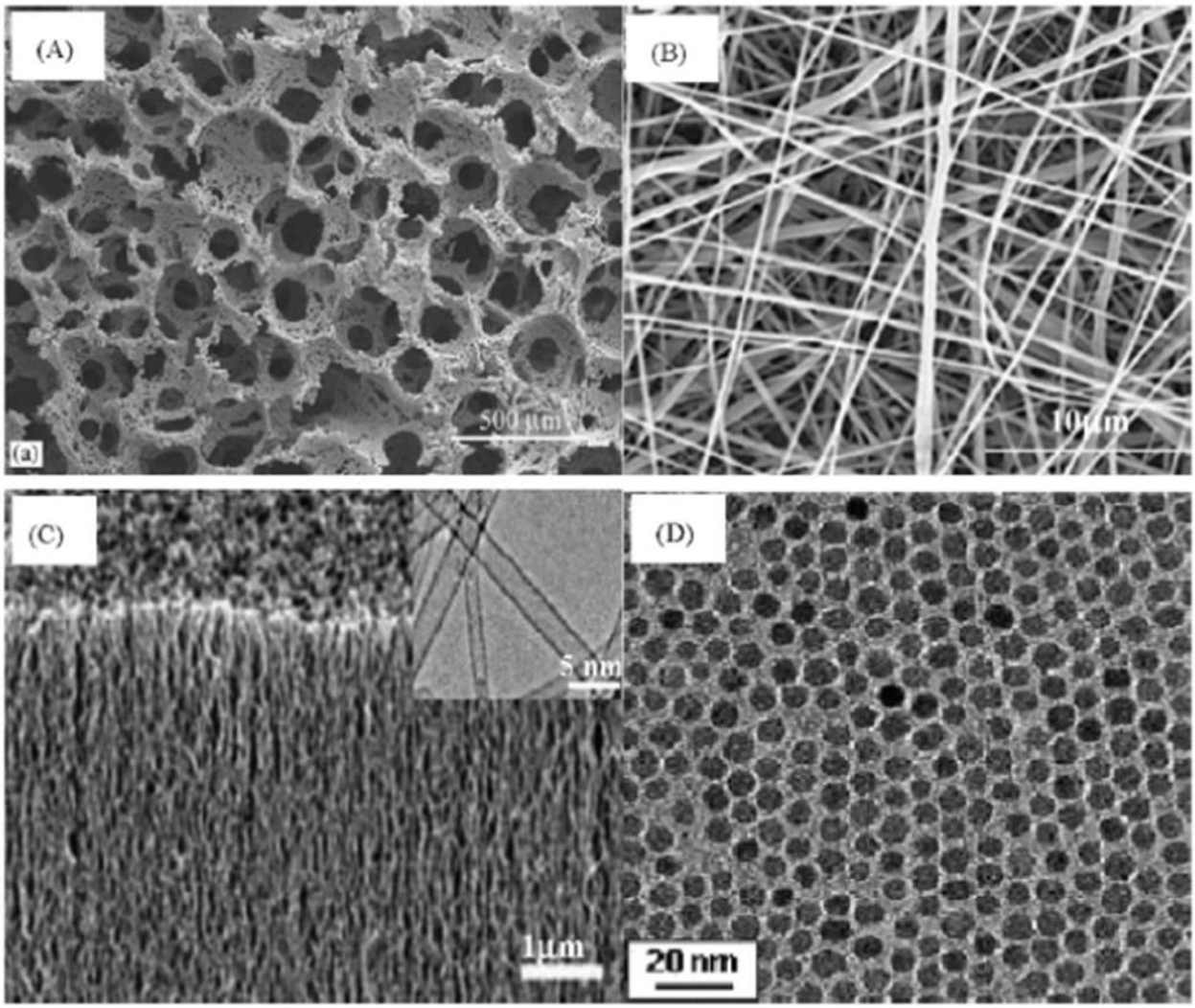

Figure 1.1.1: (A) Ploy(L-lactic acid) (PLLA) nanofibrous framework (B) Plycaprolactone/hydroxyapatite/gelatin nanofibers (C) Carbon nanotubes (D) Fe_3O_4 nanoparticles. Reprinted from Zhang, Lijie, and Thomas J. Webster. "Nanotechnology and nanomaterials: promises for improved tissue regeneration." Nano Today 4.1 (2009): 66-80 [1].

In vivo, cells are fixed within tissue, attached to an assorted arrangement of frameworks known as the extracellular matrix (ECM) [3]. The ECM consists primarily of interlinked protein fibers such as proteoglycans, collagen, fibronectin and elastin that are on the order of 10–450 nm diameters [4]. These interwoven fibers offer tensile strength to the ECM, while other proteins and proteoglycans produce hydrated gels which serve to withstand compressive forces [3]. All tissues are stabilized by a well-defined ECM organized by a support of fibrous proteins,

primarily collagens, elastin, fibrillin or fibronectin, which deliver the ECM with tensile strength and elasticity [5]. Cells communicate with extracellular substrates, typically the ECM and other cells, by facilitating with integrins that regulate all key cellular activities comprising adhesion, changes in cell migration, differentiation, orientation, proliferation, gene expression, and apoptosis in a synergistic way with growth factors and hormones. Cell adhesion to the extracellular matrix causes assembling of integrins into focal adhesion clusters and stimulation of intracellular signaling cascades into the cytoskeleton and the nucleus [6]. Integrins are a huge line of cell surface receptors that facilitate the extracellular cell matrix as well as intercellular connections. Integrin signaling is likewise accountable for directing the cell cycle. Integrins are influential in controlling cell death which is required for cell detachment and tissue restoration. The majorities of tissue cells propagate and transfer in an anchorage-dependent manner, which implies that tissue cells can only persist when secure transmembrane interactions are made between the cytoskeleton and the adjacent surface which could be the ECM or biomimetic material [7].

1.2 Biomaterials and Medical Devices

Metals such as stainless steel, tantalum, titanium and its alloys are broadly utilized for medical implants in trauma surgery, orthopedic and oral medicine. These metals are known to be relatively biocompatible as articulated by their comparative synergy with human tissues [8]. Biocompatibility is the capacity of the materials to operate in the existence of a suitable host for precise function [9]. Metals have the ability to deliver adequate mechanical strength, particularly under cyclic loading environments, which is important for medical devices at an affordable cost [8]. Anytime a material is exposed to the atmosphere, contamination must be recognized.

Biomaterial devices must be produced with uniform, manageable levels of contamination and need to be rid of undesirable impurities. It is extremely important that a biomaterial generates the same results and performs in the same manner at any time period [10]. Customary transplant materials usually last around 10-15 years on average and implant failures commencing from implant loosening, inflammation, infection and wear debris often transpires [1]. The surface of the material has an enormously vital role in the response of the cellular environment to medical devices. [11]

1.3 Titanium, Titania and Titanium Alloys

The mechanical strength of commercial purity (CP) titanium is comparatively low related to other metals applied in biomedical devices. The strength of this material can be amplified by alloying or strength hardening, for example: rolling and drawing, which generally come with some deprivation in biometric response and fatigue performance [8]. However, titanium has low abrasion resistance and wear due to its low hardness [12].

Titanium and titanium alloys are widely used in biomedical devices, particularly as solid tissue replacements as well as in cardiovascular and cardiac treatments, because of their advantageous properties, such as fairly low modulus, suitable fatigue strength, machinability, formability, corrosion resistance, and relative biocompatibility. The manufacturing process of titanium implants typically leads to an oxidized surface film that is frequently, plastically deformed, stressed and non-uniform. The native oxide film propagates naturally on the surface with contact to air. The outstanding biocompatibility, corrosion resistance, and chemical inertness of titanium and the majority of titanium alloys result from the titanium oxide layer [11].

In order to progress the chemical, mechanical, and biological characteristics, surface alteration of the implant is often executed. Various substrate alteration technologies concerning

titanium and titanium alloys comprise of thermal spraying, sol–gel, mechanical, ion implantation, chemical and electrochemical treatment from the viewpoint of biomedical engineering. Current research has revealed that the corrosion resistance, wear resistance, and biological qualities of titanium and titanium alloys can be enhanced utilizing the suitable substrate treatment methods while the necessary bulk traits of the materials are reserved [11].

As an element, titanium has a melting temperature of 1668 °C and maintains a hexagonal tightly packed crystal orientation (hcp) to a temperature of 882.5 °C. Titanium transitions into a body centered cubic structure (bcc) exceeding this temperature [13]. Alloying elements of titanium are composed of three groups: (1) a-stabilizers, such as Al, O, N, C; (2) b-stabilizers, such as Mo, V, Nb, Ta (isomorphous), Fe, W, Cr, Si, Co, Mn, H (eutectoid); (3) neutrals, such as Zr [11]. The equiatomic intermetallic compound TiNi displays the shape memory phenomenon that permits for the spontaneous reclamation of form after being exposed to macroscopic deformation higher than its elastic limit. Shape recovery may transpire after release of loads or heating. TiNi shape memory alloy with 55 wt% of Ni and 45 wt% of Ti is known as NITINOL. Nickel–titanium alloy is one of the most widespread materials utilized in vascular stents because of its distinctive shape memory properties [11].

By nanostructuring CP titanium, the strength of the nanostructured titanium is almost double that of conventional CP titanium. This development has been attained without the extreme ductility diminutions (to less than 10% elongation to failure) typically seen after rolling or drawing [8]. Nanostructures of TiO_2 have been extensively utilized in numerous purposes such as solar cells, photocatalysis, photoelectrolysis, biosensors and biomaterials. Anatase, rutile and brookite are the three primary crystals TiO_2 forms into [14].

1.4 Nanostructured Biomaterials

Nanomaterials are defined as materials with constituent physical units, grains, particles, fibers or other basic arrangements smaller than 100nm in at least one dimension [15]. Nanomaterials have aroused an enormous amount of consideration for refining disease inhibition, diagnosis, and treatment. Nanomaterials mimic surface properties (involving topography, energy, wettability, and chemistry) of natural tissues and display enhanced cytocompatible, mechanical, electrical, catalytic and magnetic properties compared to standard materials. These exceptional assets of nanomaterials have aided to increase tissue growth [1]. Nanomaterials can be made of metals, composites, polymers, ceramics and organic materials which include nanoparticles, nanowires, nanofilms, nanotubes, nanofibers, nanoclusters, nanorods, nanocrystals, etc. So far, many nanofabrication technologies (such as chemical etching, phase separation, chemical vapor deposition, photolithography, self-assembly processes, electrospinning, nano-imprinting, thin film deposition, and electron beam or nanosphere lithographies [16]) are obtainable to produce nanomaterials with well-ordered or unsystematic nanotopographies [1].

Production of nanostructured titanium dioxide (TiO_2) such as nanowires, nanofibers and nanotubes has roused attention due to their high surface-to-volume ratio and the capability to incite a superior level of biological manipulability contrasted to normal microstructures [17]. Etching from hydrofluoric acid can be observed below in **Figure 1.4.1**.

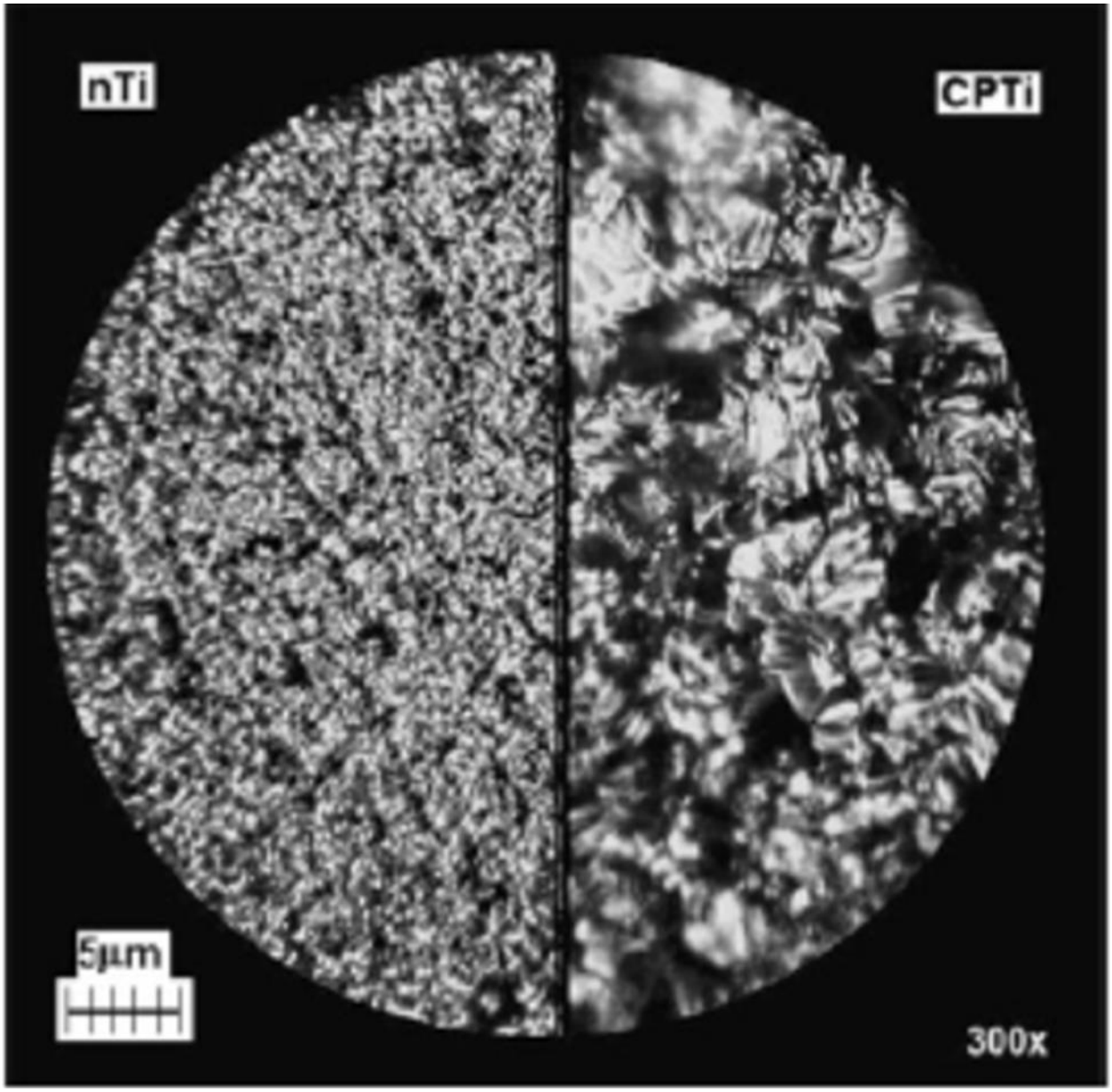

Figure 1.4.1: Hydroflouric etching of nanostructured titanium (left) and flat titanium (right). Reprinted from Valiev, Ruslan Z., et al. "Nanostructured titanium for biomedical applications." *Advanced engineering materials* 10.8 (2008): B15-B17. [8]

1.5 Titania Nanotubes Applications and Fabrication

Production of titania nanotubes has shown to have a wide range of applications including photocataylsis, fields of solar cells, sensors, photoelectrolysis and biomaterials [18]. Various images of TiO_2 nanotubes can be seen in **Figure 1.5.1**.

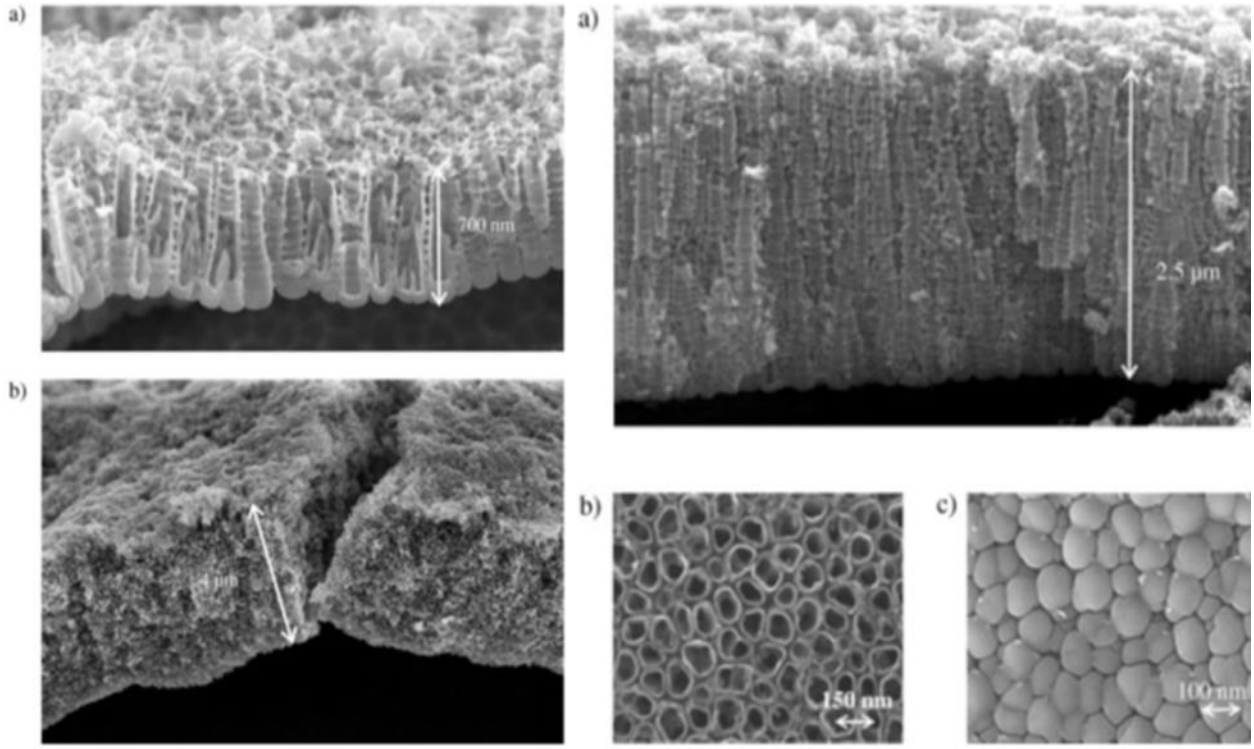

Figure 1.5.1: Varying images of TiO_2 nanotubes. Reprinted from Macak, Jan M., Hiroaki Tsuchiya, and Patrik Schmuki. "High-Aspect-Ratio TiO2 Nanotubes by Anodization of Titanium." *Angewandte Chemie International Edition* 44.14 (2005): 2100-2102 [19].

An electrochemical technique identified as anodization, a well-recognized nanosurface alteration procedure, has been used to generate vastly porous TiO_2 nanotube layers on Ti. Via the anodization of Ti in diluted hydrofluoric acid (HF) electrolyte solutions, nanotubes with various diameters and lengths can be applied into the TiO_2 films of Ti [1]. There is a fixed association concerning the anodization voltage and nanotube pore size, thus, by varying the voltage and the time the samples are run electrochemically, nanotubes with varying diameters and lengths can be

created [14]. The chief drawback of the anodization technique is that the nanotubes are amorphous and a post-annealing is necessary to crystallize them into anatase, rutile or bookite configuration. [17] The unannealed amorphous nanotubes can be tansitioned into an anatase configuration after annealing at 450 °C and to a combination of anatase and rutile after annealing at 550 °C. Conversely, the tubular structure disintegrated when annealed at 650°C [17].

Presently studied approaches of producing TiO_2 nanotubes comprise of the assisted-template method, electrochemical anodic oxidation and hydrothermal treatment [14]. The assisted-template method can be separated into two types: positive and negative templates [17]. Positive template production is utilized when oxide materials are treated on the outside surface of the template, while oxide materials are accumulated on the surface in the template's openings when negative template is utilized [20]. Both of the assisted-template procedures have the drawback that smaller nanotubes are not easy to be produced due to the limitation of the pore dimensions of the mold made from porous materials such as alumina. Furthermore, this process frequently entails extended time and burdensome procedures for preproduction and post-elimination of the templates. Elimination of the templates is completed by employing a chemical intermediate which can cause contamination because impurities cannot be entirely rid of through the practice [17].

Hydrothermal treatment has established increased thoughtfulness because this technique produces pure phase TiO_2 nanotubes with excellent crystallinity [21]. The creation of TiO_2 nanotubes by hydrothermal treatment is influenced by the initial materials, sonication preparation and hydrothermal temperature. This nanotube production technique is associated to having certain shortcomings such as the necessity for extensive reaction intervals and the requirement

for NaOH, which can cause extreme reversible inclusion that, can fabricate nanotubes that are in powder structure of unsystematic orientation [17].

Substrate alteration by nanotube layers permits not only to improve the mechanical characteristics and biocompatibility of the surface of medical implants by regulating the lateral arrangement geometry, but also offers the ability to also control the cell outcome by compacting the nanotubes with active biological signaling compounds [6].

1.6 Cell Material Interface: Method of Adhesion

Biological responses following transplantation of biomaterials comprise of wound, blood–material interfaces, temporary matrix appearance, acute inflammation, chronic inflammation, granulation tissue growth, foreign body reaction, and fibrous casing growth [7].

In the initial procedure of implantation, blood/material contacts transpire with protein adsorption to the biomaterial surface and advancement of a blood-based transitory temporary matrix that develops on and around the biomaterial. Extracellular matrix proteins are absorbed by the surface to bind cells [3]. The forms, concentrations, and orientation of these substrate-adsorbed proteins are reliant on biomaterial substrate characteristics that determine the adhesion and survival of cells. The collaboration of adsorbed proteins with adhesion receptors present on inflammatory cell masses establishes the main cellular identification scheme for implantable artificial materials and medical devices.

The provisional matrix is the preliminary thrombus/blood clot at the tissue-material boundary. The injury to vascularized connective tissue not only starts the inflammatory responses (innate immunity), but it also commences the thrombus formation comprising of the activation of the intrinsic and extrinsic coagulation schemes, the complement system, the

fibrinolytic system, the kinin-generating system, and platelets. The temporary matrix furnishes cellular, structural, and biochemical mechanisms to the progressions of wound healing and foreign body reaction. The presence of cytokines, growth factors, mitogens, chemoattractants, and other bioactive mediators within the temporary matrix delivers a rich environment of inhibiting and activating compounds competent of moderating macrophage action, alongside the proliferation and activation of other cell masses in the inflammatory and wound healing responses. The temporary matrix may be viewed as a continuous release scheme in which bioactive molecules are free to regulate ensuing stages of wound healing [7]. A summary of the foreign body reaction can observed in **Figure 1.6.1.**

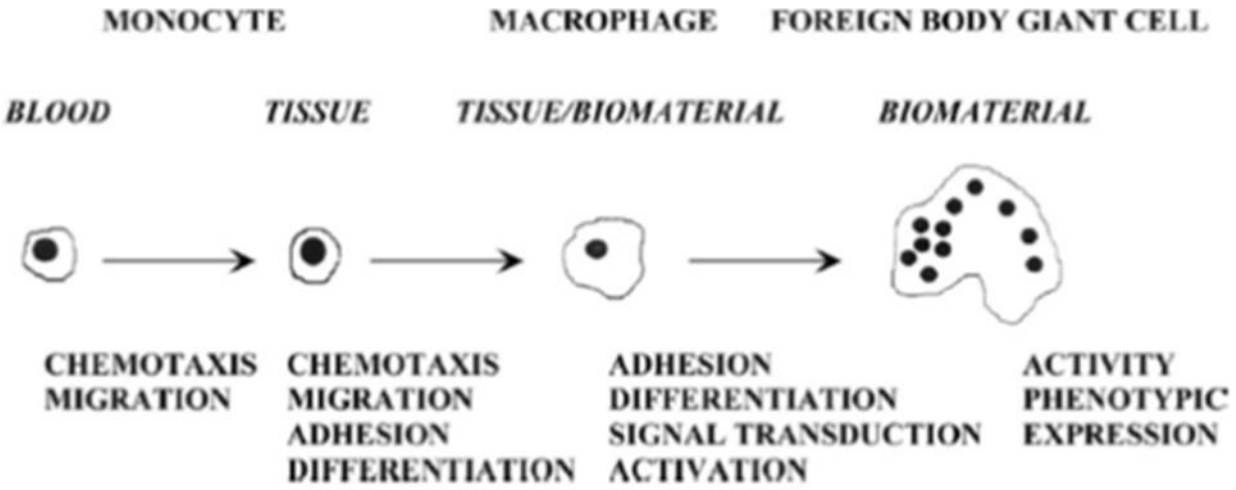

Figure 1.6.1: Summary of foreign body reaction that can occur on materials. Reprinted from Anderson, James M., Analiz Rodriguez, and David T. Chang. "Foreign body reaction to biomaterials." *Seminars in immunology*. Vol. 20. No. 2. Academic Press, 2008 [7].

The first encounter of cells to a material surface is either the formation or failure of adhesions to the surface of the material [22]. Macrophages and neutrophils are the first to attach to the implants, trailed by the development of foreign body giant cells from activated macrophages. The macrophage contact and cytokines discharged by the macrophages are thought

to draw fibroblasts and propel the foreign body encapsulation progression [11]. Succeeding the preliminary blood/material interactions and temporary matrix production, acute and chronic inflammation ensues in a sequential manner as anticipated. The level or amount of these reactions is measured by the degree of injury in the implantation process, the organ or tissue into which the implant is rooted, and the degree of temporary matrix disposition [7].

The acute inflammatory reaction with biomaterials typically resolves rapidly, typically less than one week, contingent on the level of damage at the implant location. After acute inflammation, chronic inflammation is recognized by the attendance of mononuclear cells including plasma cells, monocytes and lymphocytes. This chronic inflammatory reaction to biomaterials is frequently a small time interval and is restricted to the implant location. Chronic inflammation has been utilized to define the foreign body reaction where macrophages, monocytes, and foreign body giant cells are existent at the biomaterial border. Through biocompatible materials, prompt determination of the acute and chronic inflammatory reactions ensues with the chronic inflammatory reaction comprised of mononuclear cells normally lasting no longer than two weeks. The perseverance of the acute and/or inflammatory reactions beyond three weeks generally designates an infection. The foreign body reaction comprised of macrophages and foreign body giant cells is the last-stage reaction of the inflammatory and injury healing process succeeding implantation of a biomaterial, medical device or prosthesis [7].

1.7 Cellular Response to Biomaterials

Surface chemistry will affect cells' capability to grow, subsist, differentiate, migrate, and adhere. For example, some studies have proposed that when cells are firmly enclosed, they perform tissue-specific roles, but when they are more spread out the cells will instead decrease function and proliferate [23].

Cell area and proliferation improved with the extent of adhesiveness of the surface in the absence of stimuli from other cells [23]. A conformational transformation emerges within the adsorbed protein permitting for succeeding biological connections with the material surface [24]. Extracellular matrix (ECM) proteins are necessary for a cell to adhere to the substrate and to be able to extend [18]. Material surface chemistries facilitate specific protein (such as vitronectin, laminin and fibronectin) adsorption and bioactivity before cells adhere on transplants, further standardizing cell behavior and affecting tissue reinstitution [25].

Materials inserted in vivo at first interact with extracellular body fluids, such as interstitial fluids and blood. Body fluids comprise of proteins and amino acids that have a tendency to speed up corrosion. The pH of interstitial fluid and blood is between 7.35– 7.45 [11]. The pH drops to around 5.2 in tissue after transplantation and goes back to 7.4 within 2 weeks [26]. Allergy and toxicity transpire in vivo when metals are corroded by the body fluids, causing metal ions into the body fluid [11]. It is important for the nanomaterial to be mechanically strong, for if it is not, particles may be taken into cell later by the process of endocytosis [27]. It is generally recognized that titanium displays superior corrosion resistance and stability in vitro. There have been acknowledgements presenting the buildup of titanium in tissues next to the implant that indicates metal discharge and some amount of corrosion in vivo.

Titanium implants have numerous complications, or failures, for causes that comprise of bacterial infection, local inflammation, cell death and impaired cell healing. Therapy of these impediments can be challenging. Management of infection presently comprises lengthy progressions of high-dose oral and intravenous antibiotics to rid the infection [28]. Nevertheless, systemic drug dispensation for any situation, whether intramuscular, intravenous or topically, has limits, such as low biodistribution, poor drug solubility, absence of selectivity, uninhibited pharmacokinetics and sometimes severe side effects in other tissues [29]. Failure to eradicate bacteria at the place of infection can be preceded by continued infection as bacterial biofilms. To counteract this problem, local drug delivery of antibiotics at the implantation location is presently utilized, regularly as antibiotic-loaded cement, to thwart implant-related infections by decreasing the amount of bacteria and/or inhibiting bacterial adhesiveness to the implant exterior [30].

1.8 Cellular Response to Biomaterials Nanofeatures

Fibroblast establishment significantly increases by nanostructuring, in one particular study, the surface cell colonization for flat CP Ti was 53.0% after 72 hrs in contrast to 87.2% for nanostructured CP titanium that was machined then etched by hydrofluoric acid [8]. Histological investigation indicated that nanocrystalline hydroxyapatite (HA) coatings stimulated larger expanses of new bone growth in the rat calvaria than uncoated or conventional HA coated tantalum after 6 weeks of implantation. Comparable trends have been reported for other nanoceramics including alumina, zinc oxide and titania. This trend provides convincing confirmation that it may not matter what implant material is contrived to have nanometer surface topographies to accelerate bone growth [1]. For example, osteoblast adhesion increased by 146%

and 200% on nanophase zinc oxide (23 nm) and titania (32 nm) contrasted to microphase zinc oxide (4.9 μm) and titania (4.1 μm), respectively [31].

The foundation cell membrane interacting with the nano-featured surface will experience tensile and relaxation mechanical dynamisms that will reorganize its structures and/or open ion channels that will activate cell behavior. Supplementary research fixated in the awareness that the surface geometry and the cell signaling that manifests would be exceptionally useful in contributing to the expansion of cellular surroundings constraining preferred cell responses [2]. Studies have shown that cells react differently to varying surfaces by material and by nanofeature. These include cell proliferation, adhesion, morphology, cytoskeletal arrangement, surface antigens, and gene display [27]. Cell adhesion to nanotopography may be modified by the order, symmetry and scale of nanofeatures encountered by the cells [12]. These effects result from the initial cell adhesion or failure of adhesion [27]. The surface of a material can alter cell proteins by the interactions between a biomaterial and the cells [10]. The impact of surface nanotopography on cell gene expression and differentiation has been shown. Tendencies in cell behavior are challenging to determine due to variations in cell type, feature material, facet aspect-ratio, substrate geometry and the parameters evaluated [2].

1.9 Cellular Response to Titania Nanotubes

Human mesenchymal stem cells (hMSC) had increased adhesion on 30 nm diameter nanotubes compared without any perceptible differentiation where nanotubes with 70 and 100 nm diameters had an enormous increase in stem cell elongation, which induced differentiation into osteoblast type cells [18]. Studies on the behavior of osteoblasts and bone marrow stem cells coated to TiO_2 nanotube surfaces of increasing diameter revealed that a maximum reaction in regard to cell motility, osteogenic adhesion, proliferation, and differentiation was attained on 15 nm nanotubes contrasted to 50–100 nm nanotubes and flat TiO_2 surfaces. A potential reason for the inclination of cell types to respond better to 15 nm TiO_2 nanotube diameters could be that a layout of 15 nm may be ideal for integrin assembling on the cell surface as the extents of extracellular integrin heads are on the order of 8 -12 nm [32]. This ideal was reinforced by the assessment that cell expansion, focal contact development and paxillin phosphorylation was greatest on 15 nm nanotubes, whereas on 100 nm nanotubes apoptosis rates were largest.

Comparable outcomes were found with endothelial cells [33]; the results were thought to be unrelated on the crystal structure of TiO_2 (Anatase versus amorphous configuration), and on the occurrence of fluoride lingering from the anodization process [33]. Increased mesenchymal stem cell motility was observed on 100 nm diameter TiO_2 nanotube surfaces compared to flat Ti and smaller sized nanotubes of 50–70 nm diameters. This result is in contrast that the cell adhesion and mobility of mesenchymal stem cells was maximum on reduced diameter (~15 nm) TiO_2 nanotubes and decreased considerably with growing pore magnitude, displaying radically decreased cellular activity and a high extent of apotosis near ~100 nm diameter nanotubes. This alteration in the cell expansion performance could be triggered by the significantly dissimilar makeup of the TiO_2 nanotubes anodized, amorphous TiO_2 nanotubes versus annealed and

crystallized, anatase phase TiO_2 nanotubes and similarly the variety of cells studied: mesenchymal stem cells versus differentiated primary endothelial cells [34].The results showed that preosteoblasts migrate better and lengthened more filopodias (cytoplasmic projections) on the nanotubes substrate corresponding to the subsequent tendency: anatase-rutile > pure anatase > amorphous nanotubes [17]. An example of cell filopodia of a human osteoblast can be seen in **Figure 1.9.1** below.

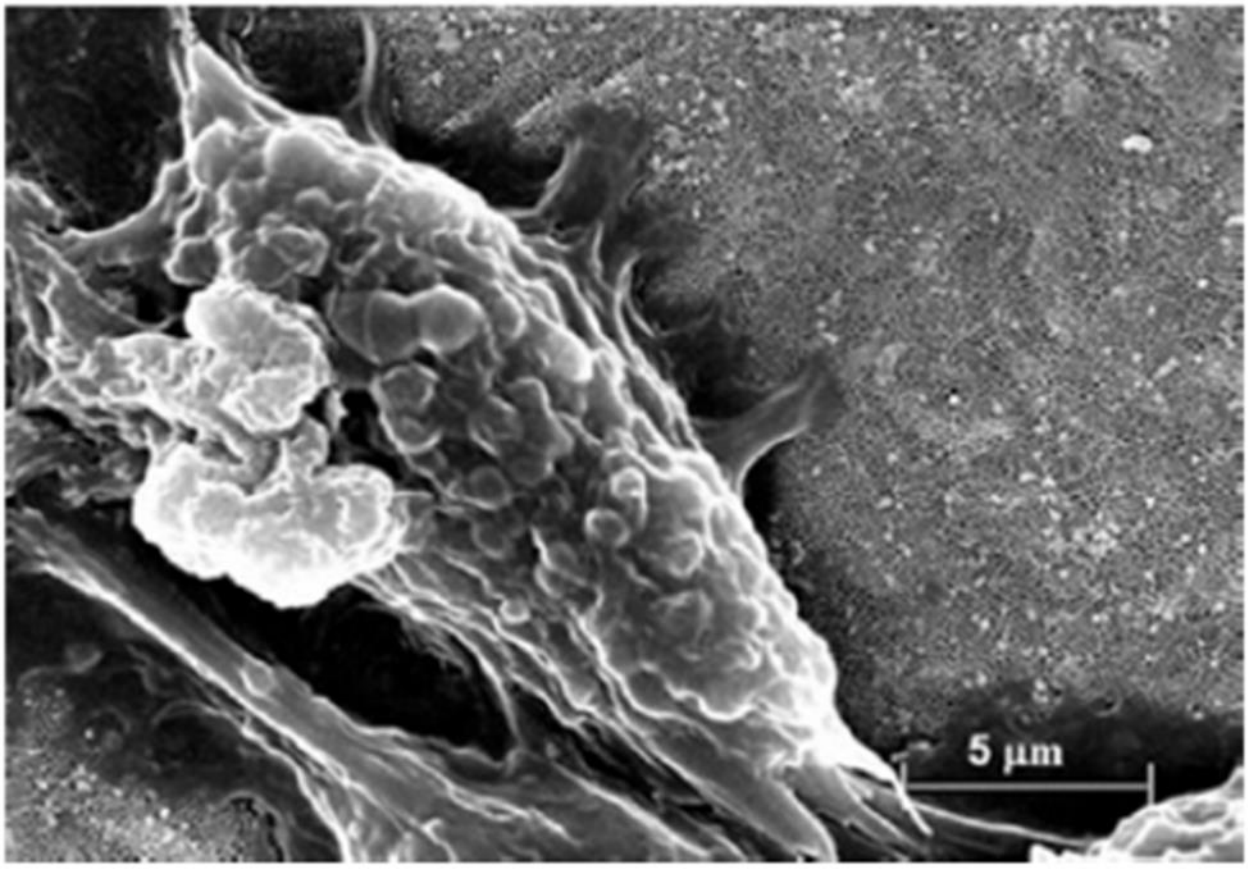

Figure 1.9.1: Human osteoblast cell on nanoporous titania surface with filopodia's attachments. Reprinted from Tan, A. W., et al. "Review of titania nanotubes: fabrication and cellular response." *Ceramics International* 38.6 (2012): 4421-4435 [17].

The pores within nanotubes can be utilized to hold various biomolecules or drugs for regulated gradual emission, the rate of which can be regulated with the nanotube diameter and

length [34]. Titania nanotubes with changeable diameters and lengths with high surface-to-volume ratio were shown to be excellent means for delivery of local drug therapies [5]. **Table 1.9.1** summarizes the findings of various cell types on titania nanotubes.

Table 1.9.1: Summary of various studies on cells grown on TiO_2 nanotubes.

Cell	***Response***
Osteoblast	Increased cell adhesion and growth with quicker extension of filopodia on Titania nanotubes contrasted with flat Ti sample. [35] Accelerated cell adhesion on nanotubes with diameters ranging from 20 to 70 nm with an optimum diameter of 70 nm and lowest at 120 nm. Proliferation rate increased along with diameters. [36] Highest cell attachment and proliferation was seen on nanotubes in anatase and rutile structures. [37] Nanotubes of 30 nm diameters were observed to have increased adhesion and proliferation. [38]
Chondrocyte	Nanotubes of 70 nm were established to be optimum. [39]
Epidermal keratinocyte and Fibroblasts	Nanotubes favored by fibroblasts but not keratinocytes. [9]
Muscle and Endothelial cells	Endothelial cells showed more extended forms whereas muscle cells were observed rounded when exposed to nanotubes. [40]
Mesenchymal stem cell	Titania nanotubes of 15 nm for cell proliferation, migration and differentiation. [6] Differentiation was much greater with nanotube diameters less than 30 nm and greatly decreased with greater diameters. [41] Optimum cell adhesion and proliferation on titania nanotubes of 15 nm diameter. [42]

1.10 Smooth Muscle Cell Response to Biomaterials

Smooth muscle cells are arranged in sheets and are found in the walls of large blood vessels, intestinal tract, uterus, airways of the lungs, and the muscles of the iris and eye lens. Smooth muscle cells (SMC)s alter vessel diameter in a process known as peristalsis in which the contraction and relaxation of smooth muscle tissue propagates down a muscular tube. This

allows blood vessels to maintain blood pressure and increase or decrease blood flow locally. SMCs have various functions which correspond to varying phenotypes ranging from synthetic to contractile as the two extremes. The diversity of the SMCs is observed in their morphology, levels of protein expression specific to SMCs, potential growth and migration traits. Synthetic SMCs have been observed as having an epitheliod or rhomboid shape where contractile SMCs have been defined as elongated, spindle shaped cells. Synthetic SMCs have been shown to have higher number of organelles involved in protein synthesis, where in contractile phenotypes many of the organelles are replaced by contractile filaments. In general, synthetic SMCs exhibit faster proliferative and migratory rates than contractile phenotypes [43].

The primary purpose of SMCs is to preserve fluidic homeostasis through communication with endothelial cells (EC)s while regulating blood pressure and flow by contraction and dilation of the blood vessel. To examine the role of SMCs as a vascular intermediary, the arrangement of SMCs can be realized through culturing SMCs on micro- and nanostructured substrates [44].

Experiments show that both makeup and arrangement of the ECM have important outcomes for SMC phenotype. The ECM is a source of cytokines and growth factors that are linked to particular ECM constituents. Changes in the ECM volume or composition precisely disturb the availability of these molecules and create another facet to the communication between extracellular matrix and biochemical constituents in the management of SMC phenotype. SMC differentiation can yield numerous phenotypes in-between the contractile and synthetic phenotypes. Synthetic and contractile SMCs can be deemed differentiated cells, though they have separate roles [43].

In adverse environments, cells in mature vessels can go through a reverse phenotypic alteration from the common contractile variety to proliferative, migratory synthetic cells. A comparable change in cell phenotype has been witnessed when vascular smooth muscle cells (VSMCs) are detached from their natural environment and repositioned in cell culture, seemingly due to the lack of the native physiological indicators that preserve and control VSMC phenotype in the wall of the vessel. Studies comparing alterations in phenotypic indicators or isolated cell cultures have shown there is phenotypic heterogeneity in VSMC in the natural vessel that essentially all VSMCs have the capacity to change phenotypes in response to environmental signals.

Arterial smooth muscle cells are subjected predominantly to cyclic tensile stresses as a consequence of the pulsatile pressure fabricated by the heart that causes cyclic expansion of the vessel wall. These mechanical forces play a vital job in maintaining cell role and phenotype. Increased matrix synthesis, increased proliferations are more characteristic of a synthetic phenotype, whereas increased contractile protein matter are typical of the contractile phenotype. The VSMC phenotype is a range, as contrasting to a distinct collection of phenotypic conditions. The nomenclatures “synthetic” and “contractile” are utilized to denote approximate locations along this range, signifying cell roles and expression of indicators that are linked with either a synthetic or a contractile purpose. Presently there are no standards for employing mechanical strains to VSMCs. The results of shear stress in the circulatory system are most regularly connected with the endothelial cells that line the vessel [45]. Summary of smooth muscle cells response to various biomaterial nanostructures can be viewed in **Table 1.10.1** below.

Table 1.10.1: Summary of various SMC studies on cells grown on different biomaterial nanofeatures.

Biomaterial Nanofeature	**Smooth Muscle Response (compared to control/s)**
Nanostructured Poly(Lactide-co-Glycolide) (PLGA)	SMC enhanced cell densities [46] SMC proliferation and adhesion were increased [47]
poly(L-lactideco-ε-caprolactone) (PLCL) nanofibers	SMC adhesion and proliferation were increased [48] SMC expressed a spindle-like contractile phenotype [49]
Nano-structured poly-caprolactone (PCL)	Greater cell adhesion and function [47]
ZnO nanoparticles	decreased viability and cell contractility [50]
electrospun silk fibroin scaffolds	promote vascular cell viability and preserve cell phenotype [51]
Nanostructured Titanium	Increased cell density and function [52]
Titania nanotubes	SMCs were ~40% smaller than flat surfaces; decreased proliferation [40]

1.11 Methods of Analysis

Material surfaces vary significantly from the bulk of the material, especially in the presence of air, specific analytical methods are required to know the various characteristics of the surface. These include surface infrared technologies, contact angle techniques, secondary ion mass spectrometry (SIMS) electron spectroscopy for chemical analysis (ESCA), scanning probe microscopes, and surface imaging techniques. These analyses allow the user to know the surface contamination including trace amounts of elements, molecular-scale features, functional group distribution and orientation among many other parameters [10].

To examine the biocompatibility of biomedical implant substrates, many diagnostic approaches exist to evaluate cellular reactions including cell adhesion, proliferation, differentiation, migration and cell death. Assessment of cell adhesion performance may comprise of qualitative and quantitative investigation of adhesion kinetics, dispersal morphology, development of stress fibers and focal contacts, as well as binding forces to the biomaterial

implant substrate. Straightforward methods to quantity cell adhesion, for example by totaling the percentage of adherent cells after a definite time of adhesion by colorimetric assays, are adequate to assess the adhesiveness of biomimetic substrates and altering constraints such as hydrophobicity, surface charge, surface elasticity or surface topography [7].

Several techniques have been defined for quantitative analysis of cell adhesion rates and kinetics (1) Adherent cells can be precisely tallied by phase contrast microscopy. (2) As a substitute, cells can be labeled with fluorescent dyes, or by firm transfection with green fluorescent protein (GFP) and the attached cells can be observed with the fluorescent microscope. (3) More quantitative methods include colorimetric assays, e.g. by staining adherent cells with crystal violet or by colorimetric amount of intracellular enzyme action; most regularly, adherent cells are lysed with detergent, and the quantities of free alkaline phosphatase are calculated by ELISA by p-nitro-pheny-phosphate (pNPP) as the color substrate. [7] Adhesive forces of cell–substrate connections can be quantitatively determined by atomic force microscopy, and specifically force spectroscopy. [7]

Cell proliferation rates on implant substrates are the result of active cell division, cell dormancy, and apoptotis or necrosis. Cell proliferation is ascertained by the proportion of growth stimulating versus inhibitory or even toxic aspects, as well as by the surface interaction and surface design of the implant materials. [7]

For numerical examination of cell mitosis of actively dividing cells, DNA synthesis can be utilized as an explicit indicator for replication. The total of marked DNA precursors such as 5-bromo-20-deoxyuridine or [3H]-thymidine assimilated into the DNA is measured either by tallying the complete quantity of labeled DNA, or by microscope identification of labeled nuclei. [5]

Cell migration is a significant progression throughout injury healing and tissue restoration, in immune responses, inflammation and implant rejection. Therefore, the degree of migration of immune cells, endothelial, cells, chondroprogenitor, osteoprogrenitor and mesenchymal stem cells from neighboring tissues into the implant location is a key constraint for assessing tissue repair capability of the implant material. As the locomotion of tissue cells in the body is sluggish (regularly a few micrometers/minute), time-lapse video microscopy is frequently utilized for gauging the velocity and course of migrating cell, by means of cell tracking sequencers. The total lengths of cell movement with regard to the beginning position are generally represented by mapping cell pathways of 10 cells shadowed by time –lapse video microscopy [53]. More elementary, but less precise methods to estimate cell migration are gap filling or wounding assays [54], which can only be utilized to investigate cell migration of simple surfaces layered with adhesive proteins such as fibronectin, laminins or collagens. A band of cells is detached, creating a cell-free breach in the cell layer. The culture is resumed, permitting cells to transfer from the wound boundary into the opening. The contracting of the breach by re-established cells after a distinct time permits valuation of comparative cell movement on identified surfaces and thus is a modest instrument to equate either the locomotion of dissimilar cell types or the cell motility of various substrates [5].

Histological stains can be utilized to determine differentiation to chondrocytes, osteoblasts, skeletal cells, smooth muscle cells, endothelial muscle cells along with other cell types that can be observed utilizing labeled antibodies to cell-specific indicators including proteins, enzymes, and cell surface molecules [5].

Several approaches have been instituted to determine apoptosis at different phases of cell death (apotosis). Most appropriate is the identification of plasma membrane depolarization by

fluorescent labeled annexin V which specially senses phosphatidylserine [55]. While this technique identifies initial phases of apoptosis, detection of proteases that mark subsequent phases of cell death. DNA disintegration is the last stage of cell death which can be identified by the TUNEL technique which reveals a run of DNA sections following gel electrophoresis [5]. A flowchart of organization of characterizing biomaterials can be seen in **Figure 1.11.1** below.

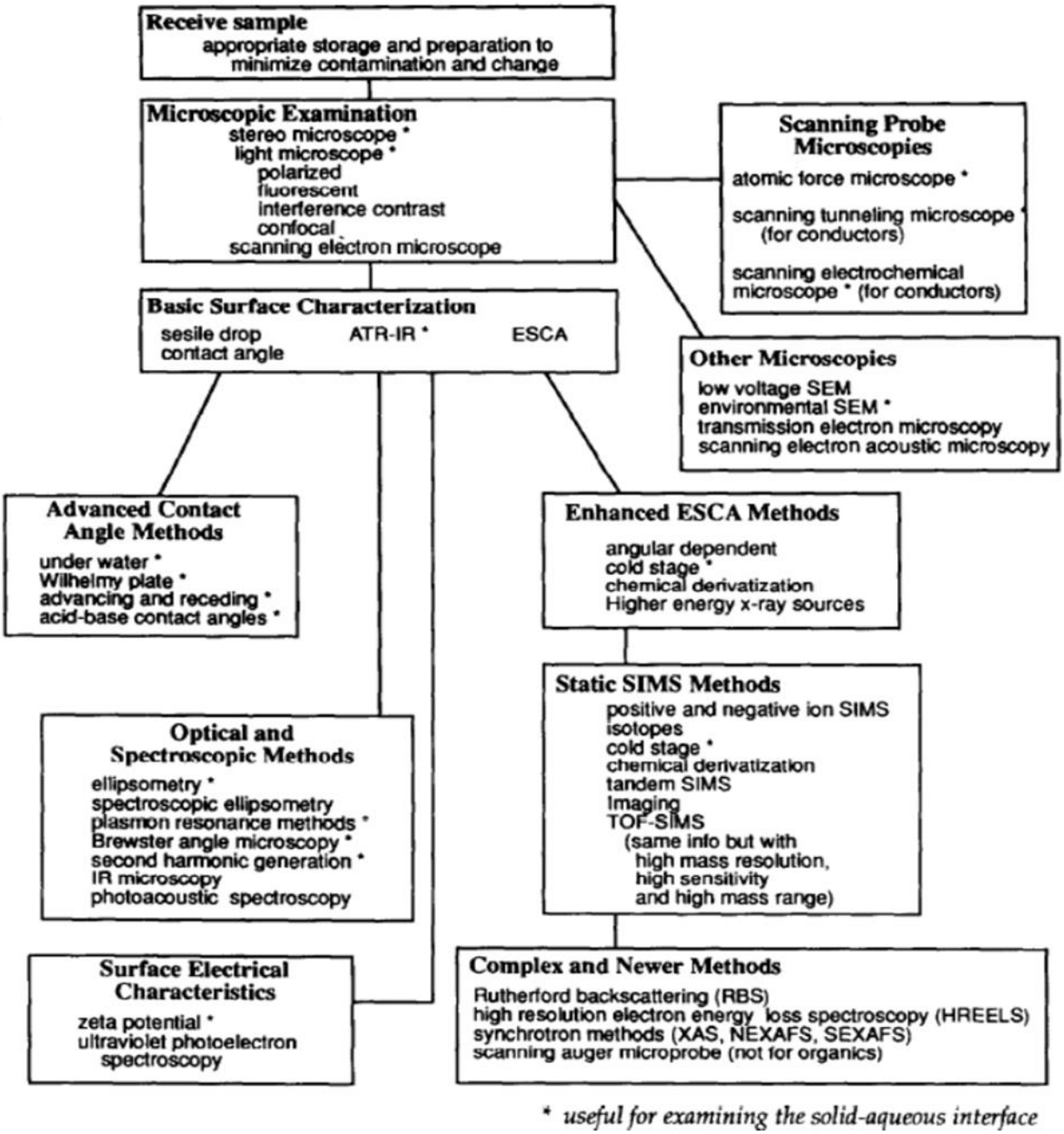

Figure 1.11.1: Arrangement of characterizing surfaces of biomaterials. Reprinted from Ratner, Buddy D. "Characterization of biomaterial surfaces." Cardiovascular Pathology 2.3 (1993): 87-100. [10]

REFERENCES

[1] Zhang, Lijie, and Thomas J. Webster. "Nanotechnology and nanomaterials: promises for improved tissue regeneration." *Nano Today* 4.1 (2009): 66-80.

[2] Martinez, E., et al. "Effects of artificial micro-and nano-structured surfaces on cell behaviour." *Annals of Anatomy-Anatomischer Anzeiger* 191.1 (2009): 126-135.

[3] Sniadecki, Nathan J., et al. "Nanotechnology for cell–substrate interactions." *Annals of biomedical engineering* 34.1 (2006): 59-74.

[4] CHAFFEY, NIGEL. "Alberts, B., Johnson, A., Lewis, J., Raff, M., Roberts, K. and Walter, P. Molecular biology of the cell." *Annals of botany* 91.3 (2003): 401-401.

[5] von der Mark, Klaus, and Jung Park. "Engineering biocompatible implant surfaces: Part II: Cellular recognition of biomaterial surfaces: Lessons from cell–matrix interactions." *Progress in Materials Science* 58.3 (2013): 327-381.

[6] Park, Jung, et al. "Nanosize and vitality: TiO2 nanotube diameter directs cell fate." *Nano letters* 7.6 (2007): 1686-1691.

[7] Anderson, James M., Analiz Rodriguez, and David T. Chang. "Foreign body reaction to biomaterials." *Seminars in immunology*. Vol. 20. No. 2. Academic Press, 2008.

[8] Valiev, Ruslan Z., et al. "Nanostructured titanium for biomedical applications." *Advanced engineering materials* 10.8 (2008): B15-B17.

[9] Smith, Barbara S., et al. "Dermal fibroblast and epidermal keratinocyte functionality on titania nanotube arrays." *Acta biomaterialia* 7.6 (2011): 2686-2696.

[10] Ratner, Buddy D. "Characterization of biomaterial surfaces." *Cardiovascular Pathology* 2.3 (1993): 87-100.

[11] Liu, Xuanyong, Paul K. Chu, and Chuanxian Ding. "Surface modification of titanium, titanium alloys, and related materials for biomedical applications." *Materials Science and Engineering: R: Reports* 47.3 (2004): 49-121.

[12] Freese, Howard L., Michael G. Volas, and J. Randolph Wood. "Metallurgy and technological properties of titanium and titanium alloys." *Titanium in Medicine*. Springer Berlin Heidelberg, 2001. 25-51.

[13] Collings, E. W. "The physical metallurgy of titanium alloys." *American Society for Metals, 1984*, (1984): 261.

[14] Smith, Barbara S., et al. "Hemocompatibility of titania nanotube arrays." *Journal of Biomedical Materials Research Part A* 95.2 (2010): 350-360.

[15] Siegel, Richard W., and Gretchen E. Fougere. "Mechanical properties of nanophase metals." *Nanostructured Materials* 6.1 (1995): 205-216.

[16] Gonsalves, Kenneth, et al., eds. *Biomedical nanostructures*. John Wiley & Sons, 2007.

[17] Tan, A. W., et al. "Review of titania nanotubes: fabrication and cellular response." *Ceramics International* 38.6 (2012): 4421-4435.

[18] Oh, Seunghan, et al. "Stem cell fate dictated solely by altered nanotube dimension." *Proceedings of the National Academy of Sciences* 106.7 (2009): 2130-2135.

[19] Macak, Jan M., Hiroaki Tsuchiya, and Patrik Schmuki. "High-Aspect-Ratio TiO2 Nanotubes by Anodization of Titanium." *Angewandte Chemie International Edition* 44.14 (2005): 2100-2102.

[20] Bae, Changdeuck, et al. "Template-directed synthesis of oxide nanotubes: fabrication, characterization, and applications†." *Chemistry of Materials* 20.3 (2008): 756-767.

[21] Swami, Nathan, Zhanwu Cui, and Lakshmi S. Nair. "Titania nanotubes: novel nanostructures for improved osseointegration." *Journal of Heat Transfer* 133.3 (2011): 034002.

[22] Curtis, A. S. G., et al. "Cells react to nanoscale order and symmetry in their surroundings." *NanoBioscience, IEEE Transactions on* 3.1 (2004): 61-65.

[23] Folkman, Judah, and Anne Moscona. "Role of cell shape in growth control." (1978): 345-349.

[24] Ketabchi, Amirhossein, et al. "Nanoporous titanium surfaces for sustained elution of proteins and antibiotics." *PloS one* 9.3 (2014): e92080.

[25] Webster, Thomas J. "Nanophase ceramics: the future orthopedic and dental implant material." *Advances in chemical engineering* 27 (2001): 125-166.

[26] Hench, L. L., and E. C. Ethridge. "Biomaterials: the interfacial problem." *Adv Biomed Eng* 5 (1975): 35-150.

[27] Curtis, A. S. G. "Tutorial on the biology of nanotopography." *IEEE transactions on nanobioscience* 3.4 (2004): 293-295.

[28] Liu, Huinan, and Thomas Jay Webster. "Nanomedicine for implants: a review of studies and necessary experimental tools." *Biomaterials* 28.2 (2007): 354-369.

[29] Tran, Phong A., et al. "Opportunities for nanotechnology-enabled bioactive bone implants." *J. Mater. Chem.* 19.18 (2009): 2653-2659.

[30] Simchi, A., et al. "Recent progress in inorganic and composite coatings with bactericidal capability for orthopaedic applications." *Nanomedicine: Nanotechnology, Biology and Medicine* 7.1 (2011): 22-39.

[31] Colon, Gabriel, Brian C. Ward, and Thomas J. Webster. "Increased osteoblast and decreased Staphylococcus epidermidis functions on nanophase ZnO and TiO2." *Journal of Biomedical Materials Research Part A* 78.3 (2006): 595-604.

[32] Takagi, Junichi, et al. "Global conformational rearrangements in integrin extracellular domains in outside-in and inside-out signaling." *Cell* 110.5 (2002): 599-611.

[33] Park, Jung, et al. "Narrow window in nanoscale dependent activation of endothelial cell growth and differentiation on TiO2 nanotube surfaces." *Nano letters* 9.9 (2009): 3157-3164.

[34] Brammer, Karla S., et al. "Enhanced cellular mobility guided by TiO2 nanotube surfaces." *Nano letters* 8.3 (2008): 786-793.

[35] Oh, Seunghan, et al. "Significantly accelerated osteoblast cell growth on aligned TiO2 nanotubes." *Journal of Biomedical Materials Research Part A* 78.1 (2006): 97-103.

[36] Yu, W. Q., et al. "In vitro behavior of MC3T3-E1 preosteoblast with different annealing temperature titania nanotubes." *Oral diseases* 16.7 (2010): 624-630.

[37] Bai, Yu, et al. "The effect of annealing temperatures on surface properties, hydroxyapatite growth and cell behaviors of TiO2 nanotubes." *Surface and Interface Analysis* 43.6 (2011): 998-1005.

[38] Brammer, Karla S., et al. "Improved bone-forming functionality on diameter-controlled TiO 2 nanotube surface." *Acta biomaterialia* 5.8 (2009): 3215-3223.

[39] Brammer, Karla S., et al. "Nanotube surface triggers increased chondrocyte extracellular matrix production." *Materials Science and Engineering: C* 30.4 (2010): 518-525.

[40] Peng, Lily, et al. "The effect of TiO 2 nanotubes on endothelial function and smooth muscle proliferation." *Biomaterials* 30.7 (2009): 1268-1272.

[41] Park, Jung, et al. "TiO2 nanotube surfaces: 15 nm—an optimal length scale of surface topography for cell adhesion and differentiation." *Small* 5.6 (2009): 666-671.

[42] Bauer, Sebastian, et al. "Size selective behavior of mesenchymal stem cells on ZrO 2 and TiO2 nanotube arrays." *Integrative Biology* 1.8-9 (2009): 525-532.

[43] Rensen, S. S. M., P. A. F. M. Doevendans, and G. J. J. M. Van Eys. "Regulation and characteristics of vascular smooth muscle cell phenotypic diversity." *Netherlands Heart Journal* 15.3 (2007): 100-108.

[44] Kim, Hong Nam, et al. "Nanotopography-guided tissue engineering and regenerative medicine." *Advanced drug delivery reviews* 65.4 (2013): 536-558.

[45] Stegemann, Jan P., Helen Hong, and Robert M. Nerem. "Mechanical, biochemical, and extracellular matrix effects on vascular smooth muscle cell phenotype." *Journal of applied physiology* 98.6 (2005): 2321-2327.

[46] Miller, Derick C., et al. "Endothelial and vascular smooth muscle cell function on poly (lactic-co-glycolic acid) with nano-structured surface features."*Biomaterials* 25.1 (2004): 53-61.

[47] Thapa, Anil, Thomas J. Webster, and Karen M. Haberstroh. "Polymers with nano-dimensional surface features enhance bladder smooth muscle cell adhesion." *Journal of Biomedical Materials Research Part A* 67.4 (2003): 1374-1383.

[48] Nisbet, D. R., et al. "Review paper: a review of the cellular response on electrospun nanofibers for tissue engineering." *Journal of biomaterials applications* (2008).

[49] Xu, C. Y., et al. "Aligned biodegradable nanofibrous structure: a potential scaffold for blood vessel engineering." *Biomaterials* 25.5 (2004): 877-886.

[50] Berntsen, Peter, et al. "Biomechanical effects of environmental and engineered particles on human airway smooth muscle cells." *Journal of The Royal Society Interface* 7.Suppl 3 (2010): S331-S340.

[51] Zhang, Xiaohui, Cassandra B. Baughman, and David L. Kaplan. "In vitro evaluation of electrospun silk fibroin scaffolds for vascular cell growth."*Biomaterials* 29.14 (2008): 2217-2227.

[52] Choudhary, Saba, Karen M. Haberstroh, and Thomas J. Webster. "Enhanced functions of vascular cells on nanostructured Ti for improved stent applications."*Tissue engineering* 13.7 (2007): 1421-1430.

[53] Echtermeyer, F., and S. Sch6ber. "E. P6schl, H. vonder Mark, and K. yon der Mark. 1996. Specific induction of cell motility on laminin by a7 integrin." *Biol. Chem* 271: 2071-2075.

[54] Lampugnani, Maria Grazia. "Cell migration into a wounded area in vitro."*Adhesion Protein Protocols*. Humana Press, 1999. 177-182.

[55] Van Engeland, Manon, et al. "Annexin V-affinity assay: a review on an apoptosis detection system based on phosphatidylserine exposure." *Cytometry*31.1 (1998): 1-9.

CHAPTER 2

FABRICATION AND CHARACTERIZATION OF TITANIA NANOTUBES

2.1 Introduction

Biomedical devices are generally made of ceramics, composites, polymers, metals and metal alloys or a combination of these materials. Titanium and titanium alloys are widely used in biomedical devices, particularly as solid tissue replacements as well as in cardiovascular and cardiac treatments, because of their advantageous properties, such as fairly low modulus, suitable fatigue strength, machinability, formability, corrosion resistance, and biocompatibility. Titanium The manufacturing process of titanium implants typically leads to an oxidized, contaminated surface film that is frequently, plastically deformed, stressed and non-uniform. The native oxide film propagates naturally on the surface with contact to air. The outstanding biocompatibility, corrosion resistance, and chemical inertness of titanium and the majority of titanium alloys result from the titanium oxide layer [1]. Examples of various titanium implantable devices can be identified in **Figure 2.1.1.**

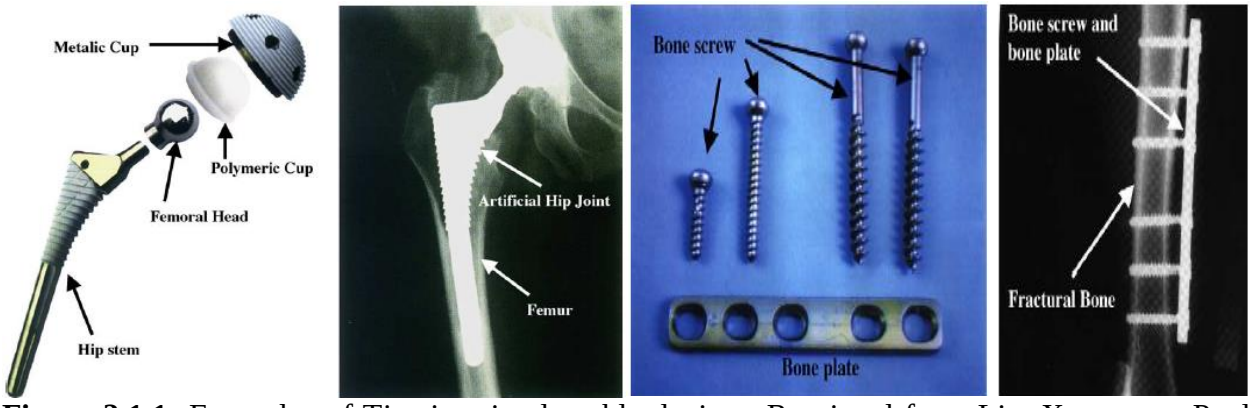

Figure 2.1.1: Examples of Titanium implantable devices. Reprinted from Liu, Xuanyong, Paul K. Chu, and Chuanxian Ding. "Surface modification of titanium, titanium alloys, and related materials for biomedical applications."*Materials Science and Engineering: R: Reports* 47.3 (2004): 49-121. [1]

Since cellular organelles and surfaces are nanometer in dimension, there is a strong need to produce medical implants with surfaces on the nanoscale. Since these transplant surfaces interact closely with nanostructured extra-cellular matrices (ECM), the characteristics of nanomaterials are crucial in promoting cell growth, migration, differentiation and proliferation as well as influencing tissue restoration [2]. Producing structures that closely resemble natural tissue on the surface of implantable devices permits for improved implant incorporation that may decrease the degree of implant rejection and infection [3,4]. Due to these findings, vertically oriented titania or titanium oxide (TiO_2) nanotubes were fabricated on the surface of commercially pure (CP) titanium that were found to be uniform and reproducible utilizing an electrochemical anodization or anodic oxidation process. Titania nanotubes mechanical characteristics were determined by field electron scanning electron microscope (SEM) JEOL JSM 6500F, crystal composition by glancing angle X-ray diffraction (GAXRD) Bruker D8, elemental composition by X-ray photoelectron spectroscopy (XPS), Phi-5800 Spectrometer and hydrophilicity by trigger command software by a goniometer, Rame-hart model 250. Nanostructured materials allow for entirely new kinds of reactions between cells and implant surfaces due to the surface area being astronomically increased and the surface topography can be fabricated to more closely resemble native tissue via a variety of different nanostructure producing techniques. Previous studies have shown that nano-structured components can have significant impacts can have on numerous tissues [6-14] including smooth muscle cells [15]. The incorporation and/or adsorption of essential proteins onto the exterior of an implant have been shown to correlate the cellular feedback of the surrounding tissue. Due to these findings, an assessment of significant proteins that may be adsorbed during and after insertion of the device was completed in vitro. The enriched cellular response from titania nanotubes with smooth

muscle tissue precipitates an appeal to demonstrate their advantageousness as a possible stent surface modification.

Anodic expansion is governed by symmetry between anodic oxide growth and chemical dissolution of the oxide on metal surfaces. When in the existence of fluoride ions, the development of a soluble fluoride compound and a diminutive ionic radius allows the compound to incorporate into the emerging titania lattice and travel through the oxide by an outside electric field [16]. Titania nanotubes are believed to form through a process where high concentrations of fluoride molecules accumulate at the base of the nanotubes, with the more soluble titania continuously dissolved and re-deposited in a tube-like structure between the generated pores. The stages of titania nanotube growth through anodic oxidation can be observed in **Figure 2.1.2.**

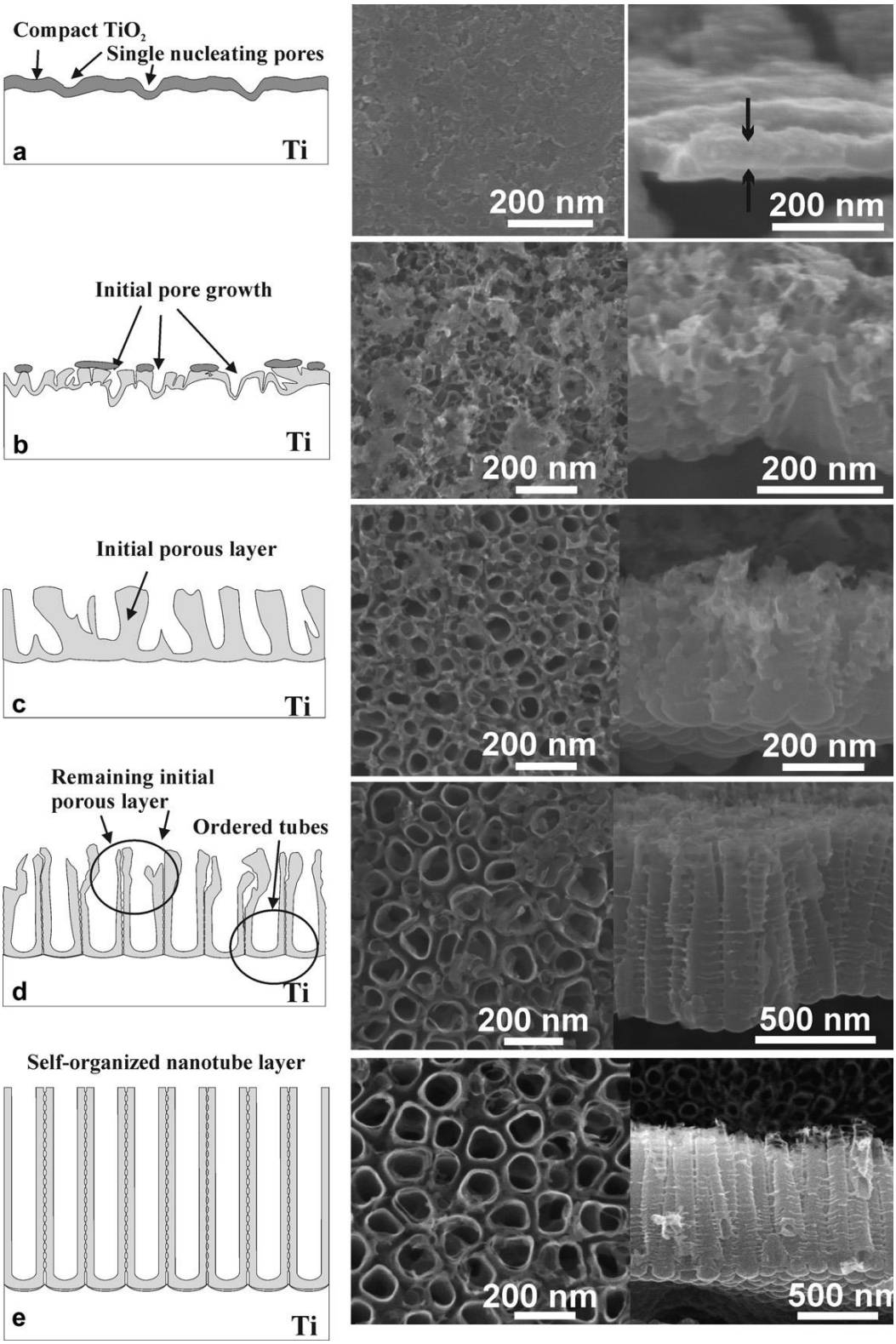

Figure 2.1.2: Periods of titania nanotube formation diagram (left) and consequent SEM imaging (right). Reprinted from Macak, J. M., et al. "Mechanistic aspects and growth of large diameter self-organized TiO 2 nanotubes." *Journal of Electroanalytical Chemistry* 621.2 (2008): 254-266 [17].

2.2 Methods for Experimentation

Nanotube morphology was determined by field electron scanning electron microscope (SEM, JEOL JSM 6500F), crystal composition by glancing angle X-ray diffraction (GAXRD, Bruker D8), elemental composition by X-ray photoelectron spectroscopy (XPS, Phi-5800 Spectrometer) and hydrophilicity or wettability of the TiO2 layers was calculated by measuring the contact angle via goniometer (Rame-hart model 250 standard goniometer) trigger command built in software that measured contact angle with time lapsed video.

2.2.1 Fabrication of Titiania Nanotubes

Titanium foils were used as substrates for anodic growth of titania nanotube layers. The electrochemical anodization process requires a fluoride electrolytic solution with titanium as the cathode and platinum as the anode and will be fabricated such as previously described [18]. The anodized nanotubes were then annealed to yield a crystalline structure from the otherwise un-annealed amorphous structure.

Commercially pure titanium sheets, (0.25mm thick, 99.7% pure) were purchased through Titanium Joe Inc. The titanium was cut to 2 cm x 2.5 cm substrate size and prepared prior to anodization with Micro 90 soap, acetone, and iso-propanol. For anodization, a conventional electrochemical cell with a two-electrode configuration was used to produce the titania nanotubes as seen in **Figure 2.2.1.** Platinum was utilized as a counter electrode. The electrolyte solution was composed of diethylene glycol (DEG, basic, 99% reagent, Sigma), 2% hydrofluoric acid (48% HF pure), 3% de-ionized water (diH_2O). Nanotube formation was produced at a constant potential at 60 volts (V) at room temperature for 24 hours to produce tubes on the order of 150 nm diameters and lengths of 1µm.

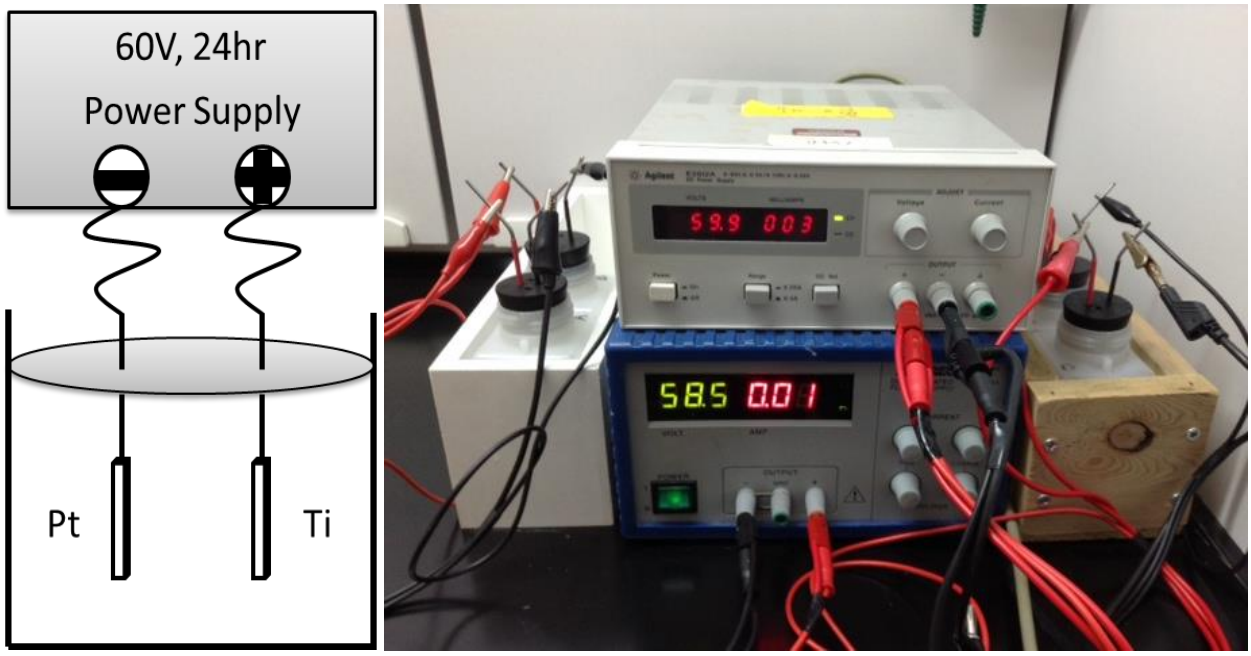

Figure 2.2.1: Diagram and actual representation of anodization process with Agilent E3612A (top) and BK Precision (bottom) 1623A DC Power Supplies.

After electrochemical treatment all nanotube substrates were immersed in isopropyl alcohol after anodization, followed by rinsing with deionized water and dried by pressurized nitrogen respectively. The substrates were then annealed at 530°C for 5 hours at a ramp rate of 15°C/min. in air utilizing the furnace in **Figure 2.2.2**.

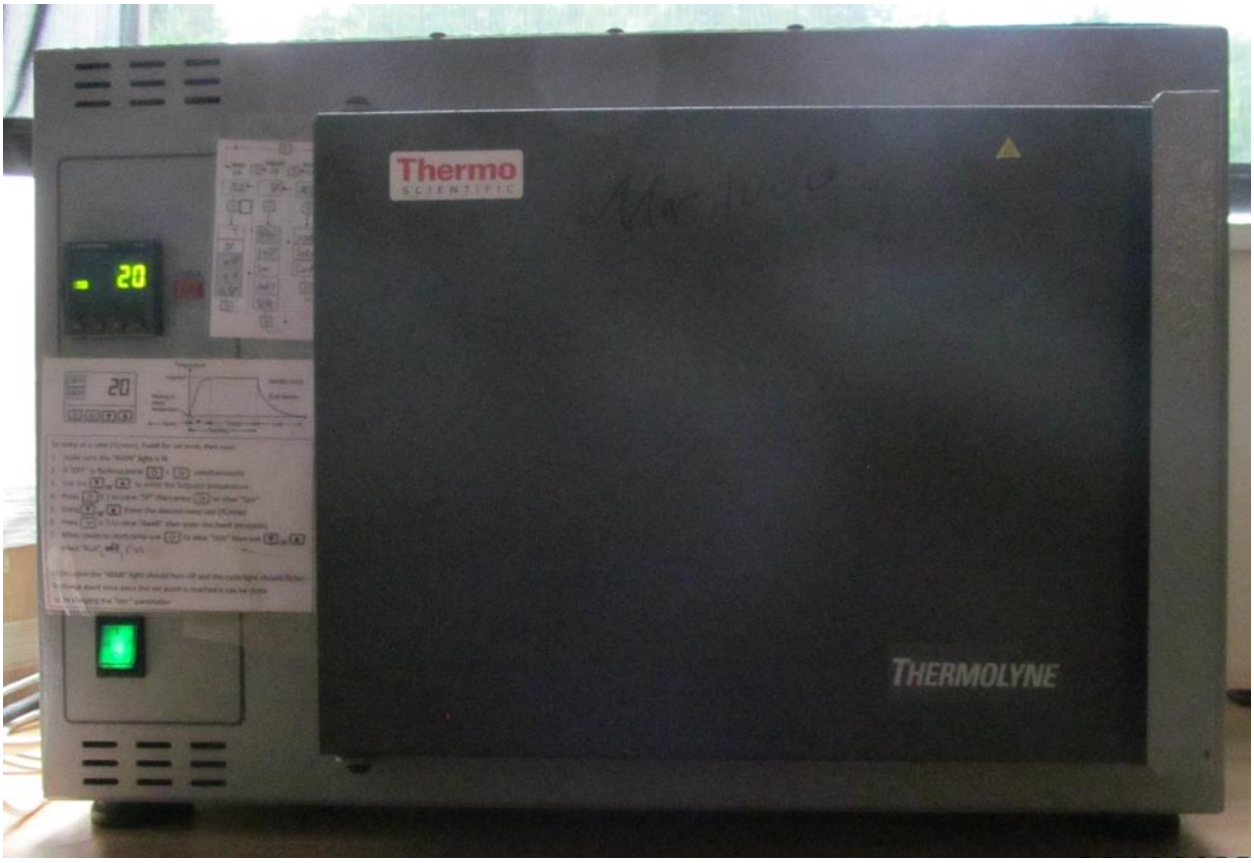

Figure 2.2.2: Thermo Scientific Thermolyne F63735 furnace used to anneal nanotubes.

2.2.2 *Morphology*

Nanotube morphology, width, length and thickness were determined by utilization of a field electron scanning electron microscope (SEM, JEOL JSM 6500F), as seen in **Figure 2.2.3**, using built in software. With the built in SEM software, distances on the SEM image were able to be determined using a measured click and drag line calculated by the SEM computer software based on the magnification of the image. Titanium and nanotube substrates were prepared by 10 nm gold coating and viewed 5 to 15 kV. Observation of SEM images of nanotube surface provided indication of reproducibility and homogeny of titania nanotubes produced under identical conditions in the laboratory.

Figure 2.2.3: Colorado State University JEOL JSM SEM 6500F at the Central Instruments Facility Imaging Laboratory.

2.2.3 Crystalline Structure

Annealed and un-annealed titania nanotubes were compared verses flat CP titanium via Brüker D-8 Discover X-ray diffractometer (Cu-Kα X-ray source, line focus), as observed in **Figure 2.2.4**, with a goniometer containing seven axes of motion. For GAXRD experiments, a scintillation detector on the diffracted beam region and a Göbel mirror was placed on the primary beam region. The Göbel mirror contains parabolically bent multilayers through a laterally graded period to attain parallel and monochromatic X-ray beams. During GAXRD investigations, the

angles of incidence were fluctuated in increments of 0.25° and trials were accomplished with soller slits (0.4° separation) on the diffracted beam side. The apparatus alignment was verified by means of a SiO_2 substrate. Substrates of 2 cm x 2.5 cm were used for analysis [19, 20].

A preliminary test was completed to find the height of the substrate by examining the radiation strikes per second as the scanner shifted from below to above the surface. The height was taken at half of the greatest intensity. A detector scan was made at low resolution with the Θ angle at zero until the initial major peak was identified in order to define the 2Θ angle. This process was reiterated from a Θ of zero to a Θ of three in increments of half a degree. Two- Θ values were chosen when a considerable increase in intensity was perceived. After the specifications were established, a detector scan was completed in the range of significance at a step side of 0.01 with a time per step of one second. The GAXRD records were then evaluated utilizing Diffract.EVA. The data was then imported into Microsoft Excel to match the crystal arrangements observed on each surface.

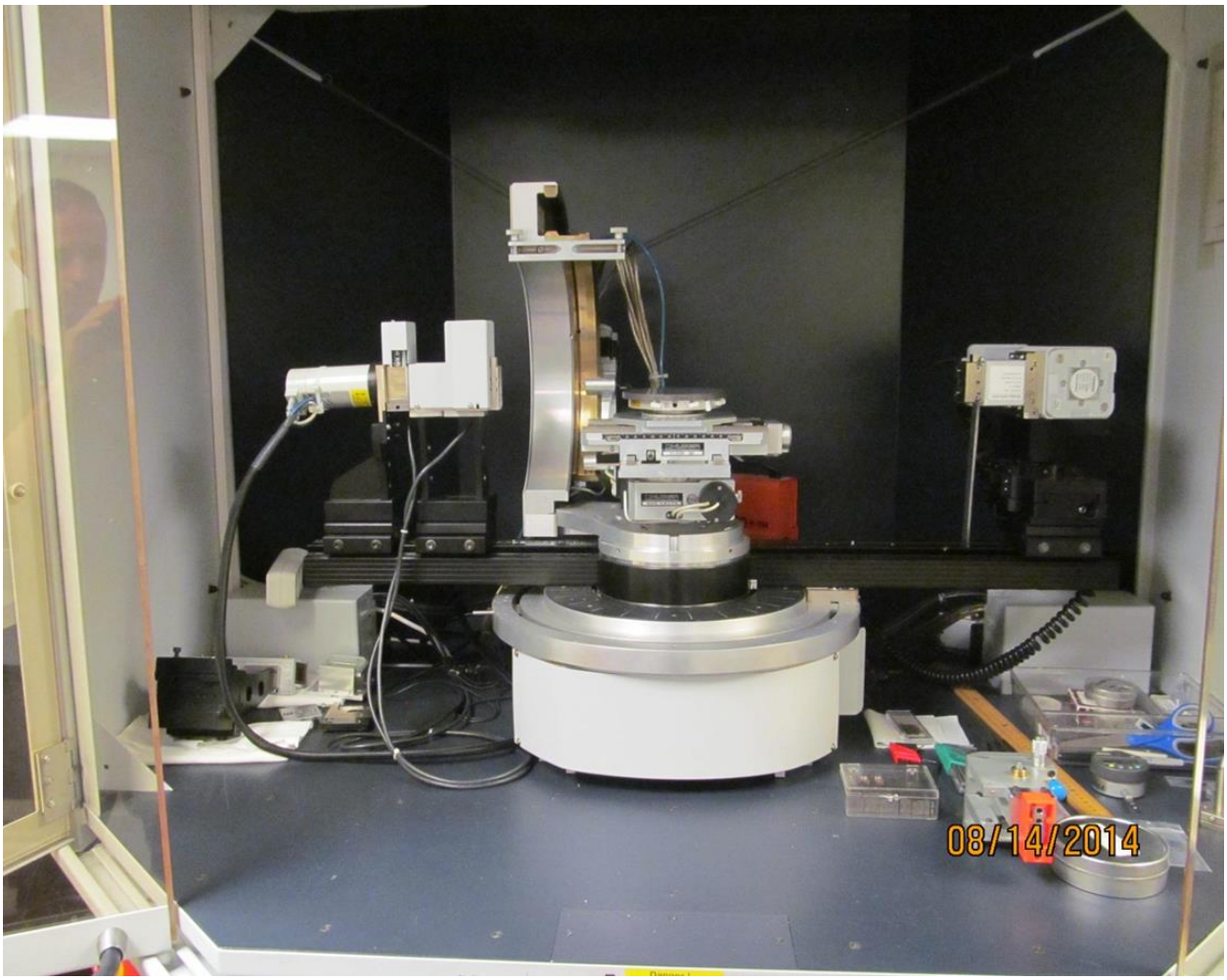

Figure 2.2.4: Colorado State University Bruker D8 XRD (Glancing Angle attachment not shown) in the Central Instruments Facility X-ray Spectroscopy and Diffraction Laboratory.

2.2.4 Elemental Composition

X-ray photoelectron spectroscopy (XPS) data was completed by an ESCA Systems X-ray Photoelectron Spectrometer 5800 system (Physical Electronics) shown below in **Figure 2.2.5**. Monochromatic Al K_α (E = 1486.6 eV) was utilized as the X-ray source. The survey spectra were collected from 10 to 1100 eV with pass energy of 187.85 eV. Data for percent elemental composition, elemental ratios and peak fit analysis were calculated using Multipack and XPS Peak 4.1 (Freeware) software [21].

Figure 2.2.5: Colorado State University ESCA Systems X-ray Photoelectron Spectrometer 5800 system (Physical Electronics) in The Central Instruments Facility X-ray Spectroscopy & Diffraction Laboratory.

2.2.5 Surface Energy and Wettability

Hydrophilicity of the nanotube and titanium surface was determined by goniometer (Rame-hart model 250 standard goniometer); seen in **Figure 2.2.6**, trigger command. Deionized water was dropped upon the surface of the substrate to measure the degree of phase separation formed between the solid/liquid interface as well as the vapor/liquid interphase. Utilizing the goniometer's trigger command software, the contact angle was measured every 0.5 seconds immediately after a 3 µm deionized water droplet struck the surface of the substrate. These

contact angle measurements were made until the software could no longer provide any results due to the contact angle being too acute to allow for an accurate reading.

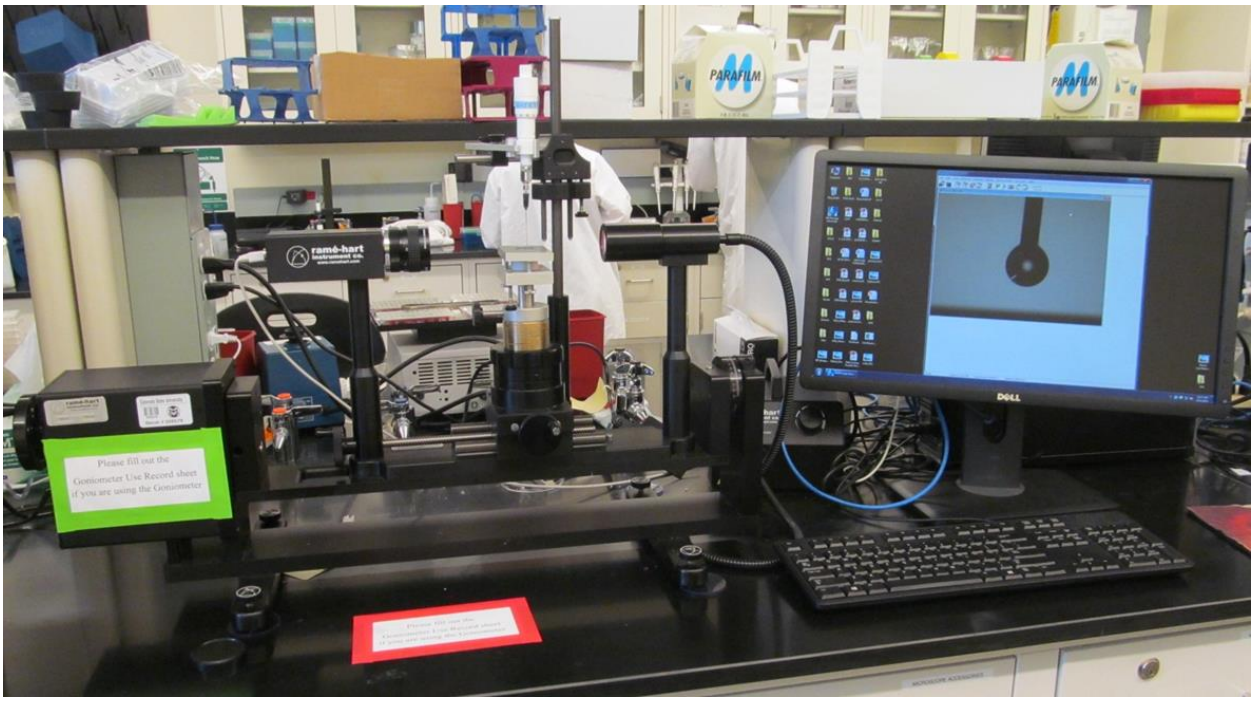

Figure 2.2.6: Rame-hart model 250 standard contact angle goniometer at Colorado State University.

2.2.6 Statistical Analysis

Each experiment was performed on at least three surfaces per experimental sample (n_{min} = 3). The quantitative results were analyzed using a two-way analysis of variance (ANOVA) model paired Tukey's post hoc test with statistical significance of $p < 0.05$. The analysis was performed using Deducer, an R based program.

2.3 Results and Discussion

For this study two topographies were compared: flat CP titanium versus titania nanotubes run at 60 volts for 24 hours and annealed at 530°C for 5 hours. The titania nanotubes were produced from commercially pure titanium from Titanium Joe Inc.

Titania nanotubes were formed by the dissolution of titanium via a fluoride containing electrolyte solution contending with its disposition back onto the body of the surface [16].

2.3.1 Morphology

By altering the parameters of the anodization process such as duration of the electric circuit, voltage, pH, quantities and species of solutes and solvents the nanotube proportions will be modified. There is a fixed association concerning the anodization voltage and nanotube pore size, thus, by varying the voltage and the time the substrates are run electrochemically, nanotubes with varying diameters and lengths can be created [22]. By varying such factors of the anodization process, titania nanotubes are able to be produced from nano- to micro- meters in length, tenths to hundredths of micrometers in diameter, and around 9 to 34 nm in tube thickness. SEM imaging of titania nanotubes at 5,000x, 10,000x and 50,000x magnification can be observed in **Figure 2.3.1**.

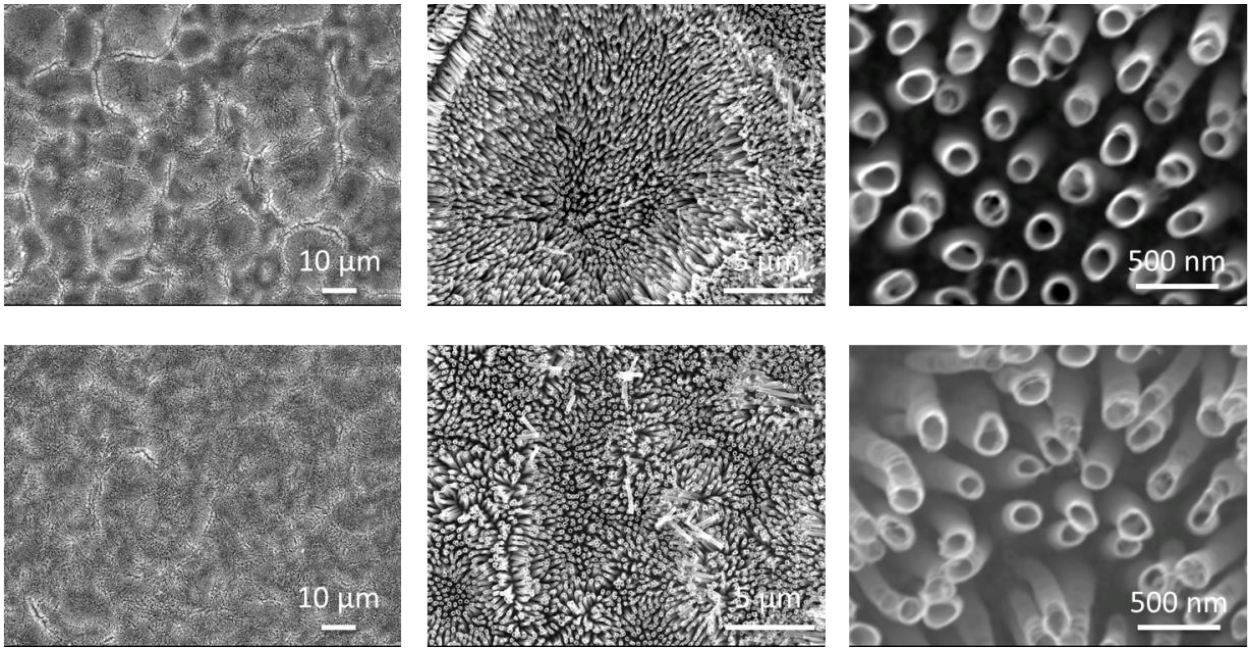

Figure 2.3.1: SEM imaging for titania nanotubes un-annealed (top) and annealed (bottom) at 5,000x, 10,000x and 50,000x respectively.

The chief drawback of the anodization technique is that the nanotubes are amorphous and a post-annealing is necessary to crystallize them into anatase, rutile or bookite configuration [22]. Diagrams of rutile and anatase crystals can be seen below in **Figure 2.3.2**. In both anatase and rutile crystals, 6 oxygen atoms surround a titanium atom in a more or less partial octahedral conformation. At the apices of the octahedron, the 2 bonds between titanium and oxygen are marginally longer with varying angles on the corners of the structure between the two structures [1]. In the annealing process, with temperatures rising above 580°C, rutile phases become more prevalent with brookite configuration seemingly always in low quantities [23]. The combinations of the different crystalline titania nanotubes will have varying material characteristics that would need to be studied on a case by case basis to make any concrete determinations on their biomedical responses comparative to each other.

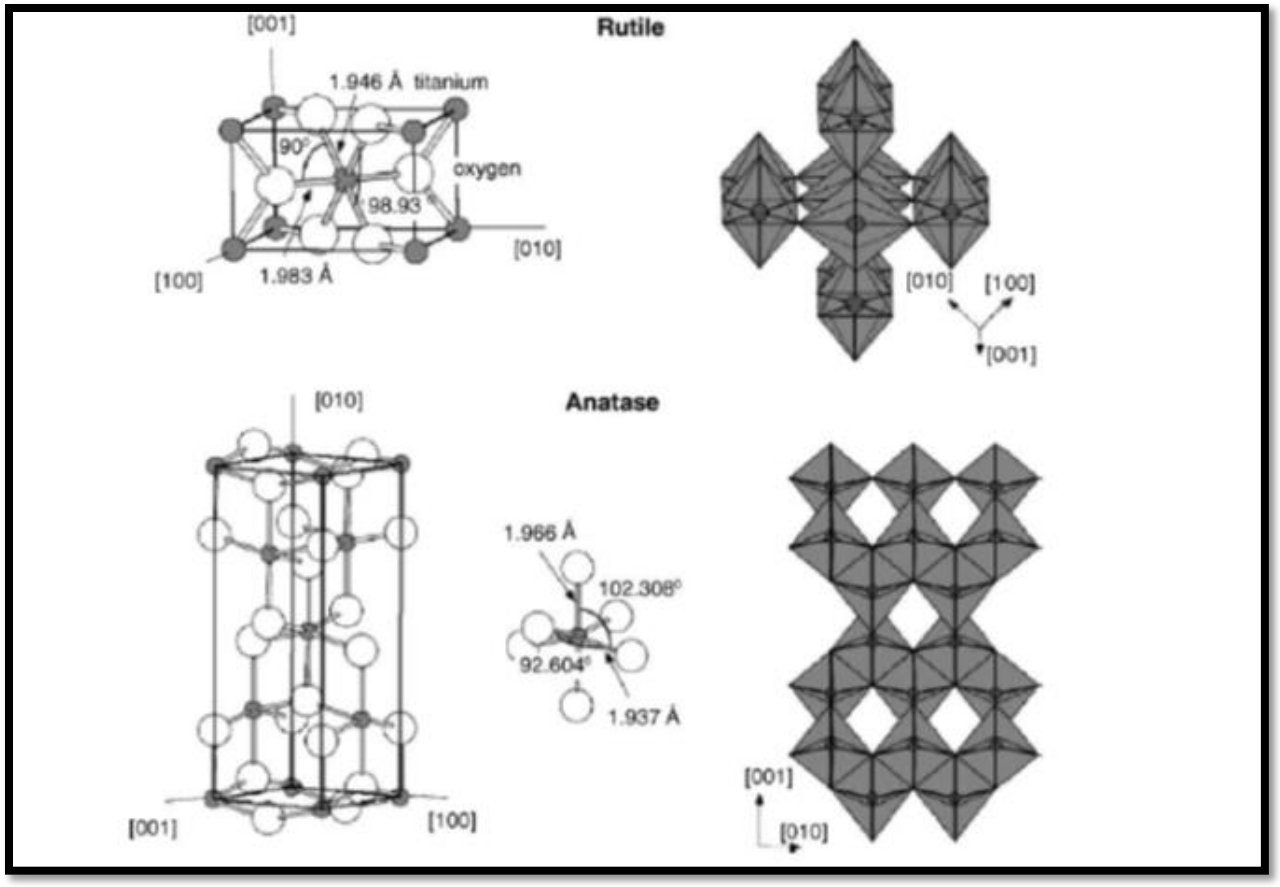

Figure 2.3.2: Illustration of rutile and anatase bulk structure. Octahedral stacking in both structures is shown on right side of figure. (Right) Reprinted from Liu, Xuanyong, Paul K. Chu, and Chuanxian Ding. "Surface modification of titanium, titanium alloys, and related materials for biomedical applications."*Materials Science and Engineering: R: Reports* 47.3 (2004): 49-121 [1].

Nanotube substrates ranged from a greenish light blue color to a bluish purple under the naked eye. From SEM imaging, the nanotube substrates ranged from 100 - 190 nm diameters, 40 -70 nm thickness and 870 - 1150 nm lengths for the annealed substrates and 120 – 170 nm diameters, 45 – 70 nm thickness and 770 - 1130 nm lengths for the un-annealed substrates as perceived in **Figure 2.3.3**. This minute differences between the two substrates is most likely by chance, with the rearrangements of atoms from the amorphous phase in un-annealed nanotubes to the crystalized annealed nanotubes changing the overall dimensions negligibly for no

significance was seen between samples for any measurements. The nanotubes were most often observed to be asymmetrical and course. Nanotube dimensions were very similar on the same substrate but differed when compared to other substrates. Nanotube lengths were found by tilting the substrate 180° and viewing under the SEM. Nanotubes were annealed with a ramp rate 15°C/second at 530° for 5 hours. No statistical difference was seen by the two-way ANOVA for diameter, wall thickness or length for un-annealed and annealed titania nanotubes.

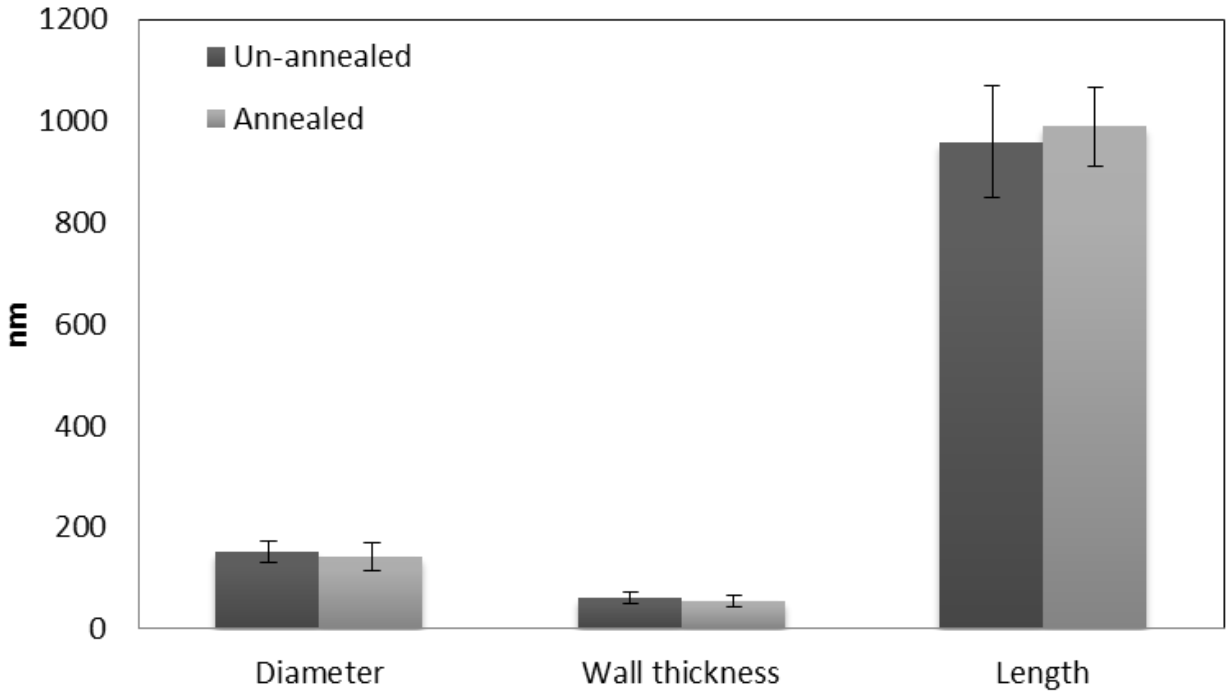

Figure 2.3.3: Un-annealed and annealed nanotubes average diameters, wall thickness and lengths based on SEM imaging.

2.3.2 Crystal Structure

The un-annealed amorphous nanotubes can be transitioned into an anatase configuration after annealing at 450 °C and to a combination of anatase and rutile after annealing at 550 °C. Conversely, the tubular structure disintegrated when annealed at 650 °C [22]. The organization

of the molecules from amorphous to various combinations of crystalline structures corresponds to varying the mechanical properties of the titania nanotubes correlating to varying their biological reaction to various tissues. By having a uniform procedure for the anodization process the titania nanotubes produced were also found to be uniform sequentially every time the process was repeated.

In **Figure 2.3.4**, varying crystalline phases were seen between flat titanium and un-annealed nanotubes versus annealed nanotubes. All substrates had titanium peaks at the same location but of different strengths. The un-annealed nanotubes and titanium substrates were seen to have the same peaks at the same places including anatase and titanium points but of varying magnitudes. The annealed nanotube substrates showed higher anatase signals than un-annealed nanotubes or titanium with the annealed substrates being the only one of three substrates that were observed to have any rutile signals. The annealed substrates also exhibited very slight brookite signals by GAXRD but not enough to elicit a definite finding.

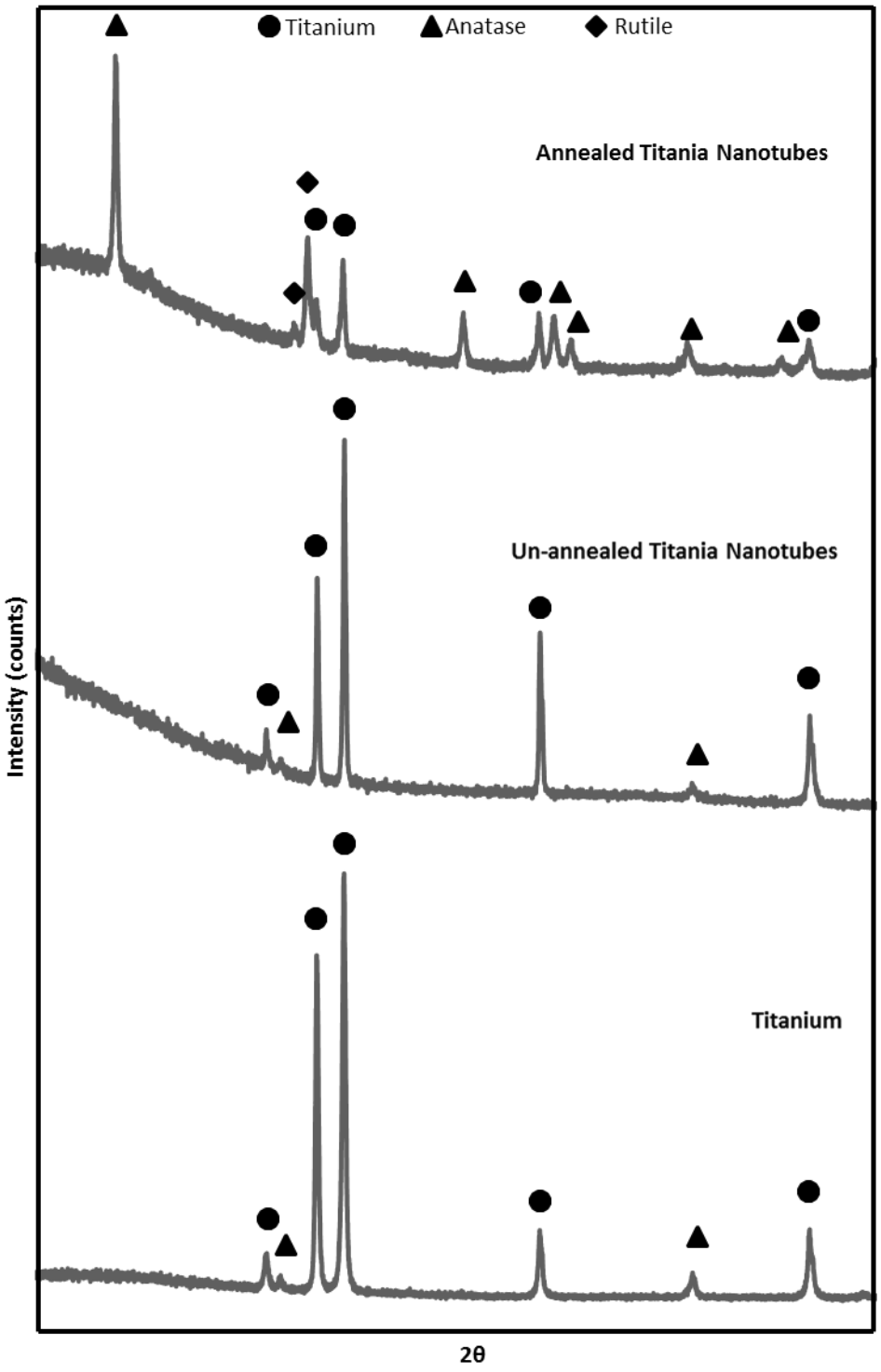

Figure 2.3.4: Spectra results from GAXRD for titanium and un-annealed and annealed nanotubes with 2θ ranging from 20° to 75° and Intensity counts per second ranging from 0 to 3000.

2.3.3 Elemental Composition

Elemental Composition was found using an X-ray Photoelectron Spectrometer for titanium, un-annealed and annealed nanotubes. The substrates were sputtered with Argon gas prior to being scanned. Low resolution survey of XPS can be observed in **Figure 2.3.5**, where from the results, one may observe the decrease in fluorine peak after annealing the nanotube substrates. The titanium peak, seen in all substrates, is well known and documented. The presence of carbon is known to be an impurity in the XPS system and any substrates exposed to air will be seen to have carbon on its surface. The oxygen peak seemed to increase after annealing the nanotubes perhaps incorporating more oxygen when transitioning from the amorphous to crystalline phases.

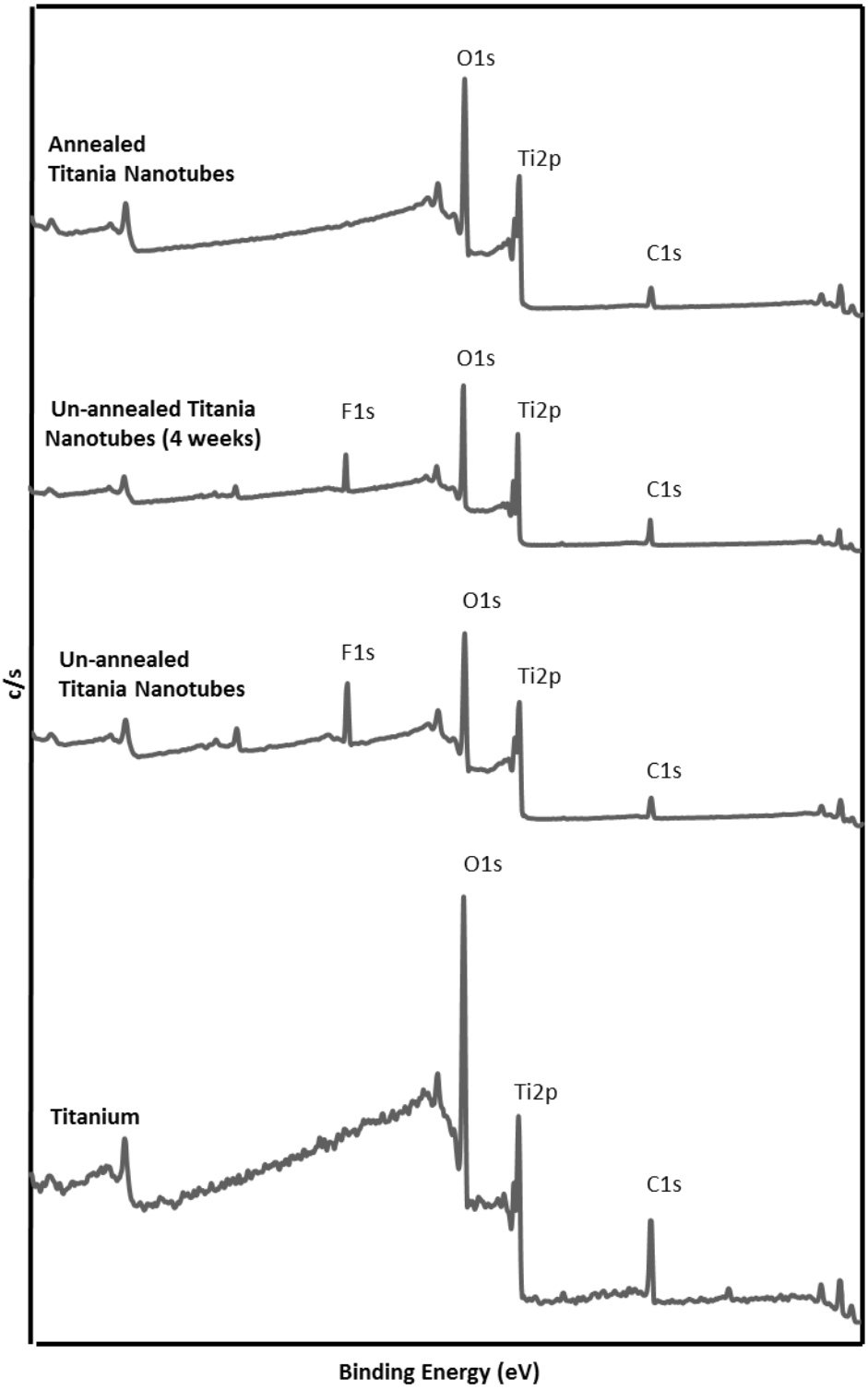

Figure 2.3.5: Low resolution survey from XPS measuring annealed, un-annealed, un-annealed after 4-weeks enclosed under normal atmosphere, and titanium.

Trace amounts of Iron, Zinc, Calcium, and Sodium were observed on the 3 substrate types, which is most likely due to impurities residing within the XPS chamber. Only Oxygen, Titanium, Carbon and Fluorine are recorded due to their more pronounced indications on cell development. Normalized atomic percentages of the surface can be seen in **Fig. 2.3.5.**

As seen in **Table 2.3.1**, residual fluorine from the anodization process decreased drastically after annealing titania nanotubes. Even after 4 weeks of idleness, the un-annealed nanotubes had a very slight drop in the fluorine amount indicating that residual fluorine on the surface decreases quite slowly with time compared to annealing. Therefore, not only does annealing allow for a crystalline structure, it more importantly drastically decreases the lingering fluorine with has been shown to be cytotoxic [17].

Table 2.3.1: Normalized elemental composition based on Spectra results from XPS for titanium, un-annealed and annealed nanotubes.

Atomic %	Titanium	Un-annealed	Un-annealed (4 weeks)	Annealed
Oxygen	55.2	46.8	47.9	57.2
Titanium	15.8	21.1	24.0	24.3
Carbon	29.0	17.1	19.1	17.5
Fluorine	0.0	15.0	9.0	1.0

2.3.4 Surface Energy and Wettability

Surface energy of a surface is very important for the biological functionality between the cells and the material surface. Surface energy and wettability of the surface has been shown to be in direct correlation. The wettability of the surface was determined with a goniometer. Depending on hydrophilic or hydrophobic surfaces, cells will have relatively different reactions to the surfaces notwithstanding other parameters. In general, cells seem to prefer hydrophilic surfaces, which is thought be due the fact cells are ~70% water and prefer conditions more similar to their natural environment.

Figure 2.3.6 demonstrates visually how the droplet decreases contact angle and height with time with slides from the video taken relatively the same time as when the first and last measurement was taken using the goniometer's trigger command software. A 3 μm droplet was the smallest amount that could be accurately measured as any smaller droplet would evaporate too quickly on the nanotube surface to allow for accurate measurements. Any droplet larger than 3 μm would have a contact angle outside the camera view which would not allow any reading for the nanotube substrates.

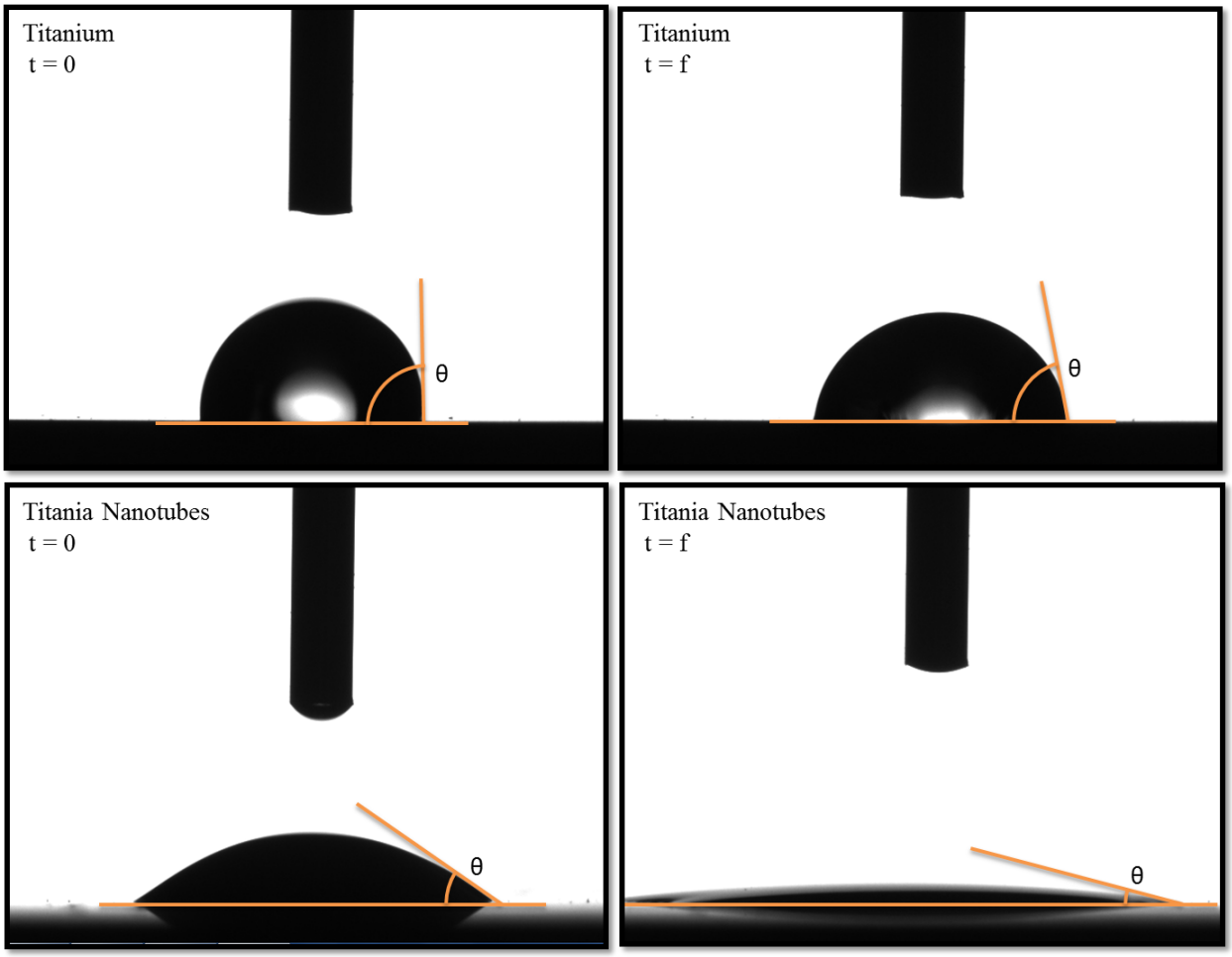

Figure 2.3.6: Goniometer testing of solid -vapor- liquid interface using deionized water for titanium and titania nanotubes.

All substrate surfaces wettability was measured by the goniometers trigger command software. The measurements were produced by placing a 3 µm drop of deionized water onto the surface of the substrate which immediately started measuring the height of the droplet and the contact angle between the solid-liquid and liquid-vapor interface every 0.5 seconds as seen in **Figure 2.3.7.** Contact angles as well as the height of the water drop decreased with time and a much more drastic decline for the titania nanotubes than the flat titanium corresponding to a much higher surface energy for the titania nanotubes.

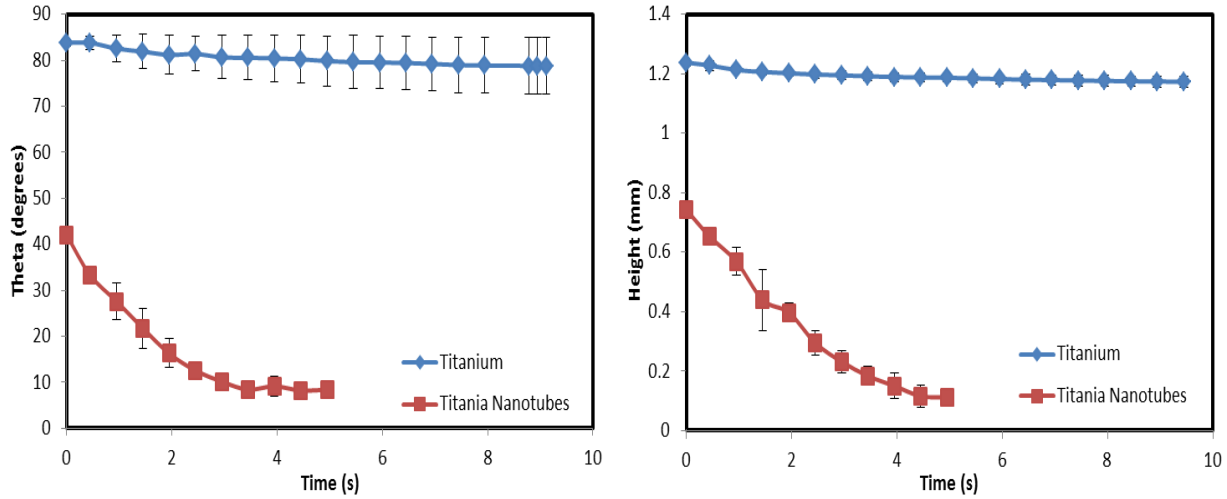

Figure 2.3.7: Contact angle and height of droplet from solid-liquid-vapor interface utilizing Rame-hart model 250 goniometer built in trigger command software.

Titanium goniometer measurements started at a contact angle of 83.79° ± 0.6364° with a height of 1.238 ± 0.0011 mm and ended with 78.72°±6.1771°and 1.173 ± 0.0195 mm in approximately 9.5 seconds. Titania nanotube goniometer measurements started at a contact angle of 42.04° ± 0.0000° with a height of 0.742 ± 0.888 mm and ended at 8.43° ± 0.0000° and 0.113 ± 0.0000 mm in approximately 5 seconds. Titanium substrates contact angle and height were constant after approximately 9.5 seconds. The titania nanotubes substrates' contact angle after 5 seconds was too acute for the goniometer software to measure the angle. Surface energy can be calculated utilizing a cosine function from the measured contact angle of the surface as seen in the equation below.

$$\mathbf{E_s = E_{lv} \cos \theta} \qquad \textbf{Equation 2.3.1}$$

In this equation the contact angle is signified by θ, E_s is the surface energy of the surface and E_{lv} is known as the energy coefficient at the liquid vapor boundary at 72.8 mJ/m^2 at 20°C for

water [24]. **Figure 2.3.8** demonstrates the surface energy of the substrates utilizing the **Equation 2.3.1.**

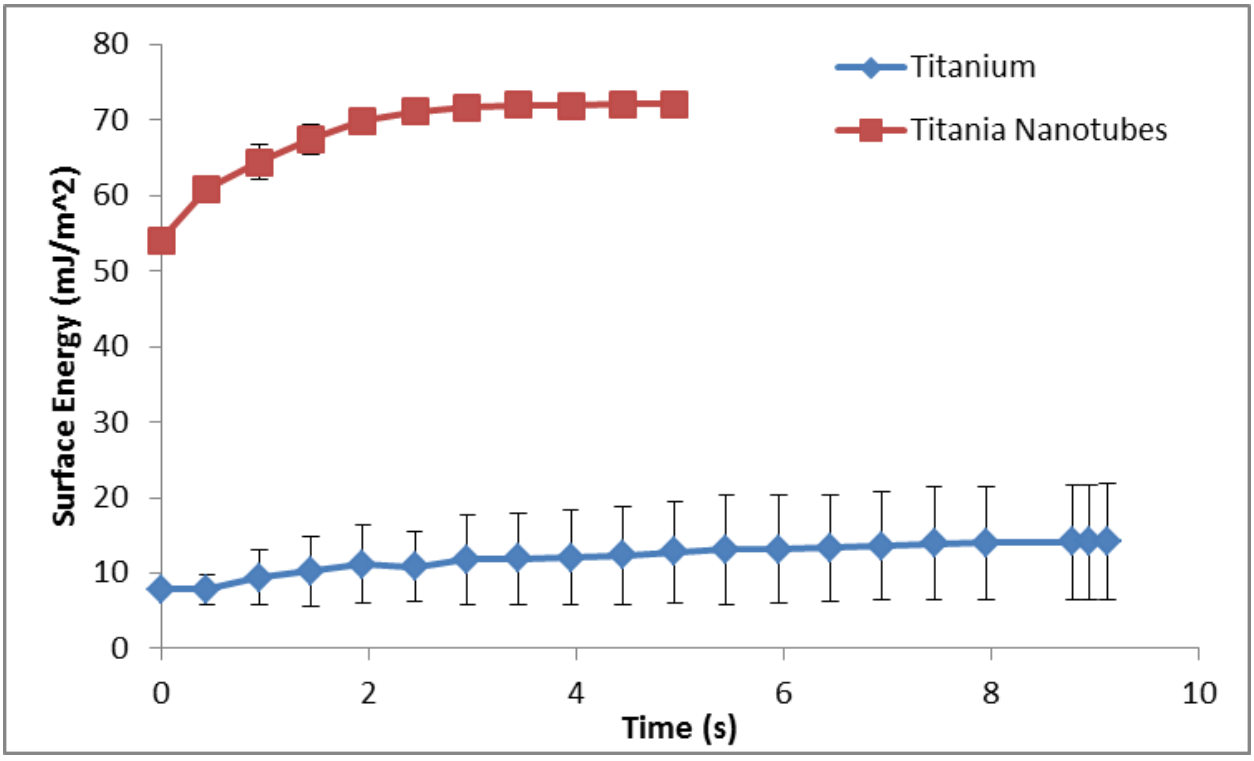

Figure 2.3.8: Surface energy calculations using equation 2.4.1 based on contact angle measurements from Rame-hart model 250 goniometer built in trigger command software.

2.4 Conclusion

The bulk material will determine how the implant is accepted at a mechanical level. The surface of an implantable material determines the how the material will be accepted at the cellular level. The surface morphology including the size and shape of the material structures as well as the chemical composition of the material can also affect the cellular response. The effect of wear and corrosiveness of the material will determine the immune response as well as the

toxicity the cells. All of these factors will determine the longevity of the implant and if it will need to be replaced. To determine the ability of titania nanotubes to be a suitable surface modification for vascular stents, this research was completed in order to determine the smooth muscle cells reaction versus flat CP titanium. The material characterization parameters that were studied in this research included surface morphology, surface energy, atomic structure and elemental composition.

Titania nanotubes were produced with a solution of deionized water diethylene glycol, and hydrofluoric acid by volume respectively. This anodization process was carried out at 60V for 24 hours followed by thorough water rinsing with high pressure air drying then annealed at 530°C for 5 hours at a 15°C/min ramp rate. SEM imaging showed the nanotube substrates ranged from 100 – 190 nm diameters, 40 – 70 nm thickness and 870 - 1150 nm lengths for the annealed substrates and 120 – 170 nm diameters, 45 – 70 nm thickness and 770 - 1130 nm lengths for the un-annealed substrates.

Slight brookite signals were noticed in the annealed substrates which could correlate to minute presence of brookite crystals in the annealed substrates. Anatase and rutile crystalline phases were observed in the annealed titania nanotubes but only slight anatase crystal phases were seen in the CP titanium and un-annealed titania nanotube substrates. To obtain increasing amounts of anatase crystal structures and any presence of rutile and brookite crystals, nanotubes must be annealed as shown by the GAXRD results in those un-annealed nanotubes and titanium substrates were observed to have very similar peaks.

Residual fluorine from, anodization was observed to decrease with time but was found to decrease much more drastically after annealing titania nanotubes. Fluoride can quickly enter cell

membranes by diffusion, especially as hydrofluoric acid and can essentially influence every stage of metabolism for humans [17, 25]. Most surfaces including polystyrene and TiO_2 with fluorine on the surface for bone, endothelial and smooth muscle cells showed increased proliferation and differentiation rates up to a threshold than those surfaces without fluorine [26, 27, 28, 29]. The relative amounts of titanium, oxygen and carbon changed slightly between each substrate.

From the goniometer contact angle measurements with the incorporation of equation 2.4.1, titania nanotubes had a surface energy approximately 46 mJ/m^2 higher than the titanium substrates at the first measurement and approximately 59 mJ/m^2 higher at 5 seconds when the trigger command could no longer read the contact angles from the titania nanotube substrates due to being to acute to quantify. These results indicate that titania nanotubes are more hydrophilic than flat CP titanium which should correlate to increased adhesion of cells if based only on the wettability of the surface.

REFERENCES

[1] Liu, Xuanyong, Paul K. Chu, and Chuanxian Ding. "Surface modification of titanium, titanium alloys, and related materials for biomedical applications."*Materials Science and Engineering: R: Reports* 47.3 (2004): 49-121.

[2] Zhang, Lijie, and Thomas J. Webster. "Nanotechnology and nanomaterials: promises for improved tissue regeneration." *Nano Today* 4.1 (2009): 66-80.

[3] Curtis, A. S. G., et al. "Cells react to nanoscale order and symmetry in their surroundings." *NanoBioscience, IEEE Transactions on* 3.1 (2004): 61-65.

[4] Biggs, Manus Jonathan Paul, R. Geoff Richards, and Matthew J. Dalby. "Nanotopographical modification: a regulator of cellular function through focal adhesions." *Nanomedicine: Nanotechnology, Biology and Medicine* 6.5 (2010): 619-633.

[5] Huschka, Ryan, et al. "Visualizing light-triggered release of molecules inside living cells." *Nano letters* 10.10 (2010): 4117-4122.

[6] Oh, Seunghan, and Sungho Jin. "Titanium oxide nanotubes with controlled morphology for enhanced bone growth." *Materials Science and Engineering: C*26.8 (2006): 1301-1306.

[7] Yu, W. Q., et al. "In vitro behavior of MC3T3-E1 preosteoblast with different annealing temperature titania nanotubes." *Oral diseases* 16.7 (2010): 624-630.

[8] Bai, Yu, et al. "The effect of annealing temperatures on surface properties, hydroxyapatite growth and cell behaviors of TiO2 nanotubes." *Surface and Interface Analysis* 43.6 (2011): 998-1005.

[9] Brammer, Karla S., et al. "Improved bone-forming functionality on diameter-controlled TiO 2 nanotube surface." *Acta biomaterialia* 5.8 (2009): 3215-3223.

[10] Brammer, Karla S., et al. "Nanotube surface triggers increased chondrocyte extracellular matrix production." *Materials Science and Engineering: C* 30.4 (2010): 518-525..

[11] Smith, Barbara S., et al. "Dermal fibroblast and epidermal keratinocyte functionality on titania nanotube arrays." *Acta biomaterialia* 7.6 (2011): 2686-2696.

[12] Park, Jung, et al. "Nanosize and vitality: TiO2 nanotube diameter directs cell fate." *Nano letters* 7.6 (2007): 1686-1691.

[13] Park, Jung, et al. "TiO2 nanotube surfaces: 15 nm—an optimal length scale of surface topography for cell adhesion and differentiation." *Small* 5.6 (2009): 666-671.

[14] Bauer, Sebastian, et al. "Size selective behavior of mesenchymal stem cells on ZrO 2 and TiO2 nanotube arrays." *Integrative Biology* 1.8-9 (2009): 525-532.

[15] Peng, Lily, et al. "The effect of TiO 2 nanotubes on endothelial function and smooth muscle proliferation." *Biomaterials* 30.7 (2009): 1268-1272.

[16] Macak, J. M., et al. "TiO 2 nanotubes: self-organized electrochemical formation, properties and applications." *Current Opinion in Solid State and Materials Science* 11.1 (2007): 3-18.

[17] Macak, J. M., et al. "Mechanistic aspects and growth of large diameter self-organized TiO 2 nanotubes." *Journal of Electroanalytical Chemistry* 621.2 (2008): 254-266.

[18] Gong, Dawei, et al. "Titanium oxide nanotube arrays prepared by anodic oxidation." *Journal of Materials Research* 16.12 (2001): 3331-3334.

[19] Schuster, M., and H. Gobel. "Parallel-beam coupling into channel-cut monochromators using curved graded multilayers." *Journal of Physics D: Applied Physics* 28.4A (1995): A270.

[20] Nagel, D. J., J. V. Gilfrich, and T. W. Barbee. "Bragg diffractors with graded-thickness multilayers." *Nuclear Instruments and Methods in Physics Research*195.1 (1982): 63-65.

[21] Kohli, Sandeep, et al. "Effect of Annealing on the Interfacial and Structural Properties of Amorphous Silicon-Hafnia Films." *Metallurgical and Materials Transactions A* 42.1 (2011): 71-75.

[22] Smith, Barbara S., et al. "Hemocompatibility of titania nanotube arrays."*Journal of Biomedical Materials Research Part A* 95.2 (2010): 350-360.

[23] Varghese, Oomman K., et al. "Crystallization and high-temperature structural stability of titanium oxide nanotube arrays." *Journal of Materials Research* 18.1 (2003): 156-165.

[24] Liu, Xiaomei, et al. "Influence of substratum surface chemistry/energy and topography on the human fetal osteoblastic cell line hFOB 1.19: phenotypic and genotypic responses observed in vitro." *Biomaterials* 28.31 (2007): 4535-4550.

[25] Chouhan, Swapnila, and S. J. S. Flora. "Effects of fluoride on the tissue oxidative stress and apoptosis in rats: biochemical assays supported by IR spectroscopy data." *Toxicology* 254.1 (2008): 61-67.

[26] Cooper, Lyndon F., et al. "Fluoride modification effects on osteoblast behavior and bone formation at TiO 2 grit-blasted cp titanium endosseous implants."*Biomaterials* 27.6 (2006): 926-936.

[27] Bačáková, Lucie, et al. "Fluorine ion-implanted polystyrene improves growth and viability of vascular smooth muscle cells in culture." *Journal of biomedical materials research* 49.3 (2000): 369-379.

[28] Bačáková, Lucie, et al. "Molecular mechanisms of improved adhesion and growth of an endothelial cell line cultured on polystyrene implanted with fluorine ions." *Biomaterials* 21.11 (2000): 1173-1179.

[29] Gazzano, E., et al. "Fluoride effects: the two faces of janus." *Current medicinal chemistry* 17.22 (2010): 2431-2441.

CHAPTER 3

TITANIA NANOTUBES EFFECT ON THE ADHESION AND PROLIFERATION OF HUMAN AORTIC SMOOTH MUSCLE CELLS

3.1 Introduction

Cell area and proliferation can be improved with the extent of adhesiveness of the surface in the absence of stimuli from other cells [1]. This is further shown in previous work that surfaces on the micro and nano scale has shown to promote cell adhesion, growth and differentiation with the greatest difference in the nano-size structure surfaces [2]. In a series of experiments in this chapter, titania nanotubes will be compared to flat CP titanium to determine the application of utilizing titania nanotubes on the surface of titanium stents via in vitro cell culture applications.

Adhesion and subsequent proliferation of human aortic smooth muscle cells (HASMC) were examined and investigated utilizing fluorescence microscopy and ImageJ software. The following experiments in this chapter attempt to measure how titania nanotubes will affect smooth muscle cell adhesion and attachment for cell propagation.

Cell viability was determined through 3-(4, 5-dimethylthiazolyl-2)-2, 5-diphenyltetrazolium bromide (MTT) assay which ascertained mitochondrial activity through the cells ability to convert colorless, soluble MMT to purple, insoluble formazan [3]. Smooth muscle cell histology was determined via SEM while the cell nucleus, cytoplasm and microfilaments were examined using various dyes and viewed under the fluorescence microscope. With the cell stained images both cell density and shape factor were determined utilizing ImageJ software.

These analyses allow qualitative and quantitative analyses to examine cellular response with the nano features of titania nanotubes and flat commercially pure (CP) titanium.

3.2 Methods for Experimentation

HASMC viability was accomplished utilizing Life Technologies™ Vybrant® MTT Cell Proliferation Assay Kit. HASMC morphology was determined by field electron scanning electron microscope (SEM, JEOL JSM 6500F)

3.2.1 Fabrication and Characterization of Titania Nanotubes

Titania Nanotubes were created and characterized as portrayed in Chapter 2. Uniform and easily reproducible titania nanotubes were fabricated from CP titanium utilizing an electrochemical reaction in a fluorinated electrolyte solution. These annealed and un-annealed titania nanotubes were compared versus titanium in their nano-morphology, crystal and elemental composition as well as their hydrophilicity. The preparation and cleansing of both substrates was completed in the same procedures.

3.2.2 Primary Cell Culture

Human aortic smooth muscle cells were purchased by Invitrogen and were taken from 1 single human donor. The Invintrogen website states the cells are stated to be 70% viable and approximately ≥500,000 cells per vial. Only passage 5 cells or less was used for experimentation since previous research has shown that passage 6 or greater SMCs have decreased functionality [4]. The medium in which the cells were cultured includes the following:

- Gibco MCDB 131 Medium

- Smooth Muscle Cell Growth Supplement (SMGS)
    - Fetal bovine serum 4.9% v/v
    - Human basic fibroblast growth factor (2 ng/mL)
    - Human epidermal growth factor (0.5 ng/mL)
    - Heparin (5 ng/mL)
    - Recombinant human insulin-like growth factor (2 µg/mL)
    - Bovine Serum Albumin (0.2 µg/mL)
- L-Glutamine (2 mmol/L)
- Penicillin-Streptomyocin (100 ug/mL)

A 1 mL frozen vial of HASMCs kept at -80°C in a Thermo Scientific Revco freezer were thawed and divided amongst 2 100mm x 20mm Greiner bio-one CELLSTAR™ vented tissue culture polystyrene petri dishes with 3 mL of supplemented media 131. The cells suspended inside the media were pipetted carefully in the petri dishes to evenly dispense the cells throughout the media solution. Another 10 mL of media was added to each dish. The cells were incubated at 5 % CO_2 at 37°C for 24 hours before replacing the 13 mL of media. After the initial 24 hours of incubation, media was changed every 48 hours until confluency was reached when approximately 70-80% of the bottom of the petri dish was composed of cells in about 5-6 days' time.

All Phosphate Buffered Saline (PBS) was sterilized prior to each procedure in this chapter. All chemicals were properly disposed of as their protocol demanded by Colorado State University (CSU) Environmental Health Services (EHS). All steps were done at 1 atm and room

temperature unless stated otherwise as incubated which took place at 37°C and 5% CO^2 in a Fisher Scientific Isotemp incubator.

3.2.3 HASMC Culture on Experimental Samples

5 x 5 x 0.635 mm samples of titania nanotubes and flat titanium were placed in Greiner bio-one CELLSTAR® 48 well plates sanitized by being immersed with 70% ethanol for 30 minutes then aspirated using a Fisher Scientific Maximum Dry pump. The samples were then immersed in PBS twice and aspirated followed by Ultra Violet (UV) exposure for 30 minutes. All steps of sterilization and cell culturing were performed in a Class II, Type A2 biosafety cabinet.

Initial smooth muscle cells were placed onto the titania nanotube and titanium samples by the following procedure: the media was aspirated from the petri dishes when they had reached appropriate concentrations or confluency (70-80% cell/area). After such time, the cells were rinsed twice with PBS then placed in 0.25% trypsin dissolved in PBS to remove the adhered cells from the surface of the petri dish. The trypsinated cells in the petri dish were viewed under Inverted Tissue Culture microscope (**Figure 3.2.1**) until about 90% of the cells were detached from the surface which was when the cells appeared round in shape, were clumped together and were suspended within the liquid. To deactivate the trypsin, 3 mL of media 131 was combined in the petri dish, which brought the trypsin concentration to a neglible amount so as not to damage the cells. The combined liquids with suspended cells were transferred to a 15 mL tubes for centrifugation for 7 minutes at 180 times gravity.

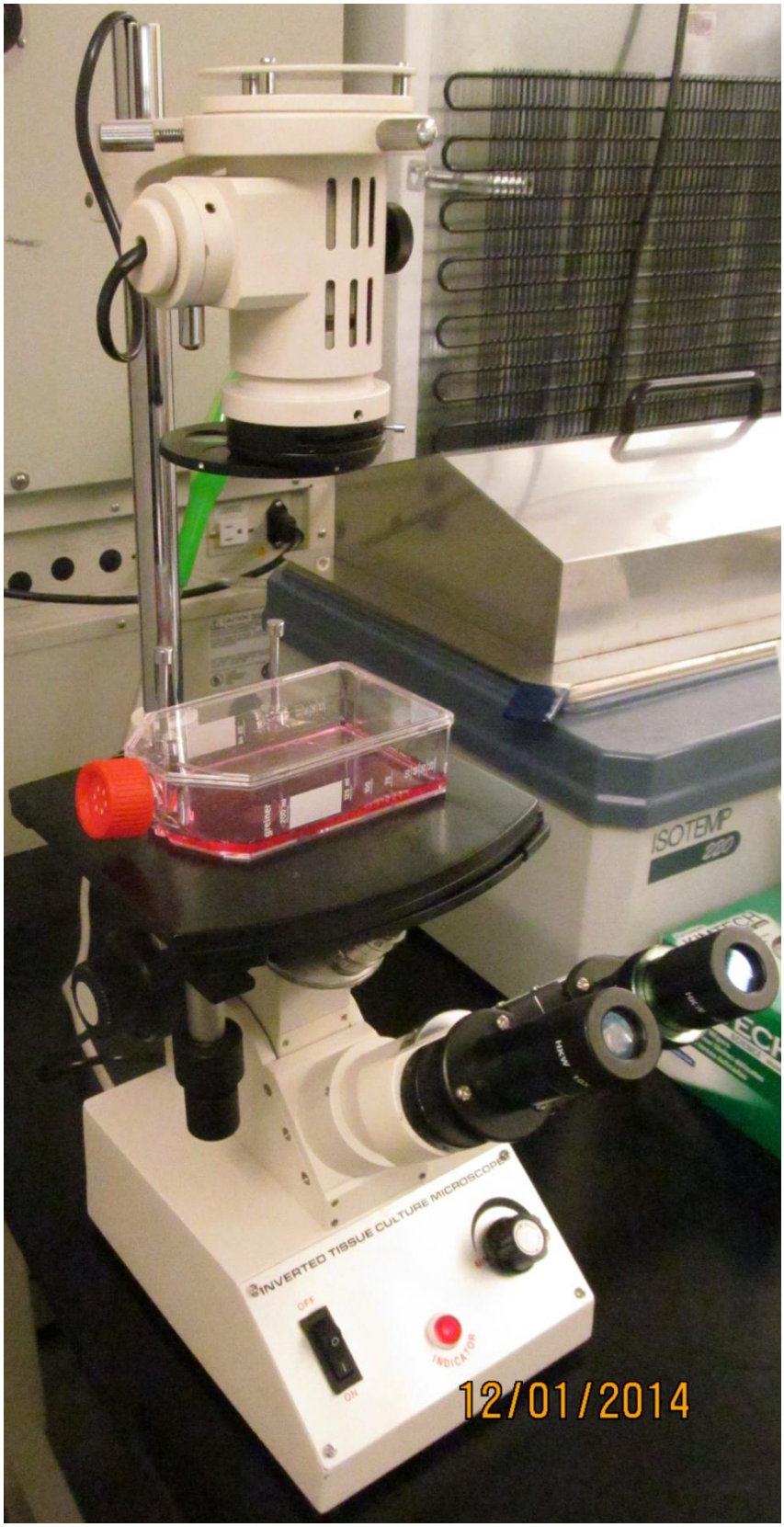

Figure 3.2.1: Colorado State University Inverted Tissue Culture Microscope at Popat Biomaterials Laboratory in Scott Bioengineering Building

After centrifugation, the cells were observed in a pellet at the bottom of the tube and the liquid supernatant above the cells was aspirated. 1 mL of PBS was added to the tube and was gently pipetted to re-dispense the cells from the pellet. After no more clumps of cells were observed, another 9 mL of PBS was added to the tube and vortexed under a low setting, using a VWR Scientific Products Vortex-Genie 2, to evenly distribute the cells throughout the PBS so an accurate cell count could be completed. The cells were then counted utilizing a Millipore Scepter™ Handheld Automated Cell Counter with a 60 µL sensor attachment which gave the number of cells in 60 µL. This concentration was then utilized to calculate the number of cells in the tube so the correct volume could be removed to acquire the demanded cell amount for initial culture on the titania nanotubes and titanium samples.

After the dilution was completed, another cell count was done using the same device and procedure as stated previously. Following the utilization of the cell counter, another dilution was made if required, to have the needed concentration and therefore, the necessary quantity of cells. The cell tube was then centrifuged again; the PBS aspirated, replaced by media and re-dispensed using the same procedure as stated formerly. The PBS was aspirated and the appropriate volume of media was added so all sample wells could begin their initial cell concentration at 20,000 HASMCs/well at 350 µL/well. This density was chosen so as to stimulate preliminary adhesion and rapid cell confluency.

Every 24-48 hours media was replaced with a volume of 350 µL/well. Cell adhesion and proliferation studies were done 1, 4 and 7 days after seeding. Cell studies included morphology examination via SEM imaging, Fluorescence Microscope imaging by fluorescent cellular staining which allowed nuclear cell counting and shape factor analysis via ImageJ, and lastly MTT viability assay.

3.2.4 Viability of HASMCs on Experimental Surfaces

HASMC viability was accomplished utilizing Life Technologies™ Vybrant® MTT Cell Proliferation Assay Kit. Prior to the assay, media was aspirated from the sample wells, with samples rinsed with PBS so as to deduct unbound cells. Samples were then placed into new wells. 1 mL of PBS was added to a 5 mg vial of MTT and afterwards vortexed to prepare the MTT solution for the assay. In new wells, the samples were placed into 350 µL of fresh media per well with the complement of 35 µL of 12mM MMT solution formerly prepared. One well was absent of any sample but filled with the MTT solution so as to be used as a negative control for comparison. All well plates with MTT solution inside were placed into the incubator for 4 hours. Sodium Dodecyl Sulfate – Hydrochloric acid (SDS-HCl) solution was utilized as it has been shown to be preferable as a solvent for formazan over Dimethyl sulfoxide (DMSO) [5]. The SDS-HCl solution was prepared by reconstituting 1 g of SDS with 1 mL of 0.01 M HCl. After incubating, 350 µL of the SDS-HCl solution was added to each well and incubated again for 6 hours. When incubation was complete, the surfaces of the samples were scraped with micropipette tips to release any bound formazan. Using a new micropipette tip for each allocation, while being careful to deter from creating any bubbles, 100 µL of formazan solution from each well was transferred to a 96 well plate. The 96 well plate was inserted into a BMG Labtech plate reader and absorbance was measured at 540 nm to ascertain the approximate viable cell population on each sample.

3.2.5 HASMC Morphology on Experimental Surfaces

To gain insight on the morphology of HASMCs in their interaction and observed phenotype with titania nanotubes and titanium substrates, SEM imaging was completed. On the

stipulated days of study, culture plate wells were aspirated so as to remove unbound cells, and placed into a series of glass petri dishes containing a variety of chemicals to fix the cells in order to prepare the samples for SEM imaging. The samples were first placed into primary fixative containing 3% glutaraldehyde (Sigma), 0.1M sucrose (Sigma) and 0.1M sodium cacodylate (Polysciences) dispersed in deionized water. After 45 minutes of being immersed in the primary fixative, the samples were transported to new wells containing a buffer solution containing all of the ingredients of the fixative minus the glutaraldehyde for 10 minutes. The samples were sequentially moved to new wells containing increasing amounts of ethanol dissolved in deionized water. The concentrations of the ethanol wells were 35%, 50%, 70%, and 100% each for 10 minutes. Finally, the samples were immersed in hexamethyldisilazane (HMDS, Sigma) for 10 minutes for dehydration of the cells. All steps were completed in a chemical hood with samples enabled to air dry after all fixation immersion steps were completed. Prior to SEM imaging, the samples were desiccated for at least 24 hours, sputtered with 10 nm of gold and imaged at 15 kV.

3.2.6 Fluorescence staining for Adhesion and Proliferation of HASMCs on Experimental Surfaces

HASMC adhered to the experimental samples were stained utilizing 4'6-diamidino-2-phenylindoledihydrochloride (DAPI) for cell nuclei, 5-Chloromethylfluorescein diacetate (CMFDA) for non-specific cytoplasm staining, and Rhodamine phalloidin for F-actin microfilament selective staining. DAPI is thought to preferentially bond in the adenine-thymine areas of DNA [6]. The cells on the experimental surfaces were imaged by Zeiss Axioplan 2

fluorescence microscope (**Figure 3.2.2**) in which DAPI was observed blue, CMFDA green and Rhodamine phalloidin red.

Figure 3.2.2: Colorado State University Zeiss Axioplan 2 Fluorescence Microscope at Popat Biomaterials Laboratory in Scott Bioengineering Building

Staining was accomplished by first aspirating the media out of all wells of samples being studied. The titania nanotubes and titanium experimental samples were rinsed twice with PBS with care not to aspirate or disturb bound HASMCs. Life Technologies™ CellTracker™ Green CMFDA was reconstituted using anhydrous dimethylsulfoxide (DMSO) and brought to a

concentration of 10 µM in new wells. The samples were then transferred to the wells containing CMFDA dissolved in PBS and placed in the incubator for 30 minutes. The CMFDA was then aspirated, the samples move to new wells filled with fresh PBS then the samples were placed back into the incubator for another 30 minutes. The samples were aspirated and rinsed with fresh PBS. The samples were placed in 3.7 % formaldehyde dissolved in PBS for 15 minutes. The samples were then rinsed with PBS then moved to new wells, immersed in 3.7% formaldehyde dissolved in PBS for 15 minutes to fix the cells. The samples were afterward rinsed twice with PBS then moved into new wells immersed in fresh PBS for 5 minutes. The wells were aspirated of PBS then 1% Triton X dissolved in PBS was added for 3 minutes. The samples were then rinsed twice with PBS then moved into new wells immersed in fresh PBS for 5 minutes. After another rinse with PBS, the samples were placed into rhodamine phallodin (5 µL per mL of PBS from 14 mM stock reconstituted using 100% methanol for 30 minutes). 300nM DAPI was added to the wells for the last 5 minutes. The samples were aspirated and rinsed twice with fresh PBS then immersed in fresh PBS until imaging with fluorescence microscope using a BP 474/28 green filter, 62 HE BP 585/35 Red filter, and 49 DAPI BP 585/50 blue filter.

3.2.7 Cell Counting of HASMCs on Experimental Surfaces

All cells were stained with CMFDA, rhodamine-phalloidin and DAPI prior to imaging with the flouresence microscope. The DAPI images were then separated from the combined filter images so that they were able to be processed through a macro in ImageJ software that allowed the computer to recognize the DAPI stain versus the background. This cell total calculation was then divided by the area of the experimental surfaces to which the cells were attached then averaged to obtain a cell count per area on each experimental surface.

3.2.8 Shape Factor of HASMCs on Experimental Surfaces

Shape factor, which is a ratio of a cell's width to length ratio, can provide some insight in the phenotype of the cell, based on its morphology. The cell shape factor was determined by comparing the diameter of the smallest circle that could incorporate the whole cell over the diameter of largest circle that could incorporate the whole cell, width over length respectively [7]. The 10x rhodamine-phalloidin stained images were separated from the DAPI and CMFDA initial combined images for shape factor analysis in ImageJ software. **Figure 3.2.3** demonstrates how shape factor was determined.

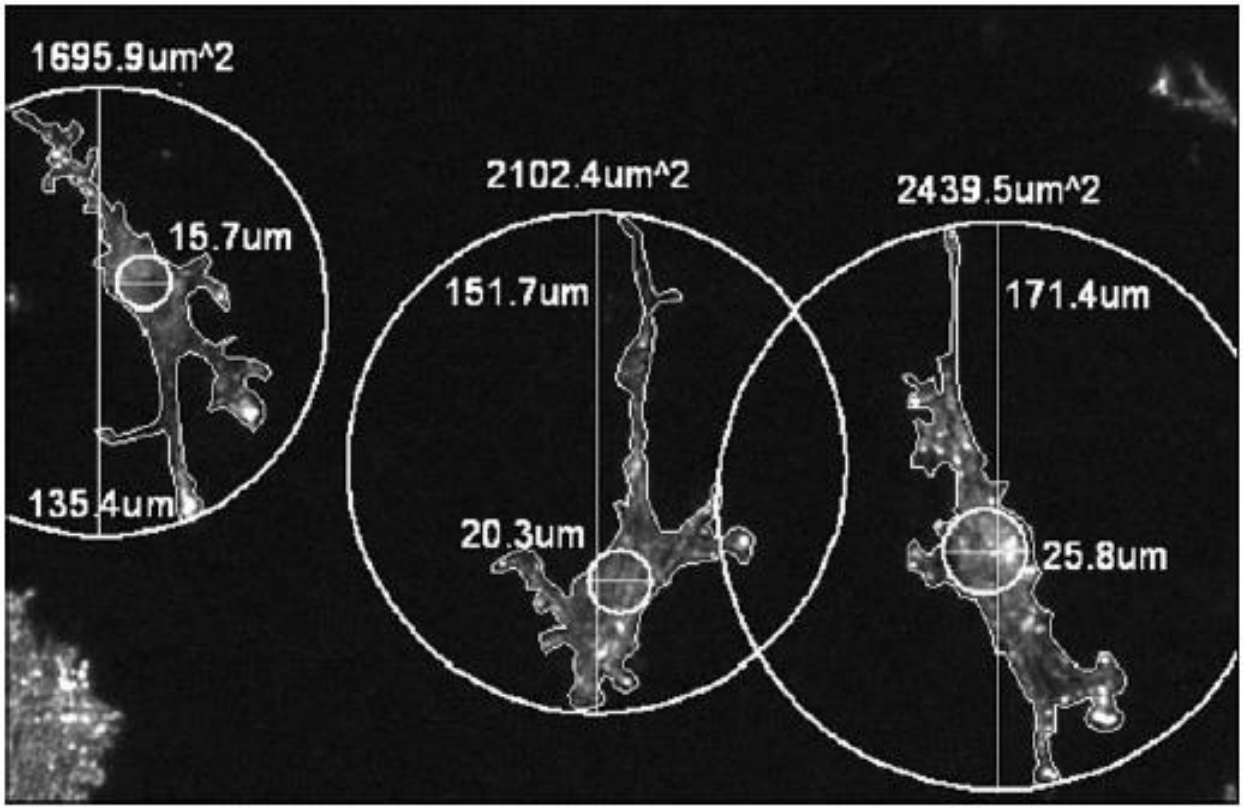

Figure 3.2.3: Shape factor diagram showing the smallest circle that could emcompass the whole cell over the largest circle to encompass the whole cell which allowed for a width over length ratio determination. Reprinted from Prasad, Ashok, Dustin Berger, and Ketul Popat. "PCL nanopillars versus nanofibers: a contrast in progenitor cell morphology, proliferation, and fate determination." *Advanced Engineering Materials* 14.6 (2012): B351-B356 [7].

3.2.9 Statistical Analysis

Each experiment was performed on at least three surfaces per experimental sample (n_{min} = 3). The quantitative results were analyzed using a two-way analysis of variance (ANOVA) model paired Tukey's post hoc test with statistical significance of $p < 0.05$. The analysis was performed using Deducer, an R based program.

3.3 Results and Discussion

To determine titania nanotubes effectiveness as a potential vascular stent surface alternative, HASMC proliferation and viability were examined on titania nanotubes as compared to flat CP titanium. Experiments to ascertain HASMC interaction with the 2 sample types were completed on days 1, 4, and 7 after initial seeding of the cells. HASMC nuclear, cytoplasmic and skeletal structures were stained by DAPI, FITC, and rhodamine phallodin respectively for subsequent imaging with a fluorescence microscope that were further processed through ImageJ to allow for cell density and shape factor values. Cellular viability was determined through the mitochondrial processing of MTT to formazan. HASMC adhesion and morphology was observed through the employment of a SEM.

Production of uniform, perpendicular from the surface titania nanotubes was accomplished through the use of an electrochemical reaction, known in literature as anodization, at 60 V for 24 hours. A solution of HF, DEG and deionized H_2O was utilized as electrolyte solution in which the nanotubes were fabricated as described beforehand [8]. Anodization of CP titanium allowed production of nanotubes ranging from 120 – 170 nm diameters, 45 – 70 nm thickness and 770 - 1130 nm lengths for the un-annealed samples and 100 – 190 nm diameters, 40 – 70 nm thickness 870 - 1150 nm lengths for the annealed samples as measured via SEM imaging. Titania nanotubes attempt to mimic surface and extracellular matrix proteins of cells by

being on a similar size scale while allowing better adhesion by the almost infinitely greater surface area of titania nanotubes compared to flat titanium and increased hydrophilicity.

3.3.1 Viability of HASMCs on Experimental Surfaces

Following day 1, 4, and 7 of primary seeding on HASMCs on titanium and titania nanotubes, the cell were subjected to MTT from a commercial assay kit. HASMC viability was determined utilizing a MTT assay which measured the change in optical density of formazan metabolized by MTT through active cellular mitochondria. This quantification of absorbance which correlates to the concentration of formazan was determined via spectrophotometric plate reader. The results of the MTT assay can be observed in **Figure 3.3.1** below. MTT two-way ANOVA revealed the main effect of day exhibited significance. Tukey Post-Hoc Test revealed a p-value of 0.698 when comparing titania nanotubes and titanium as well as a p-value of 0.34628 when comparing Day 1 to 4, 0.04836 for comparing Day 1 to 7 and 0.00412 for comparing Day 4 to 7.

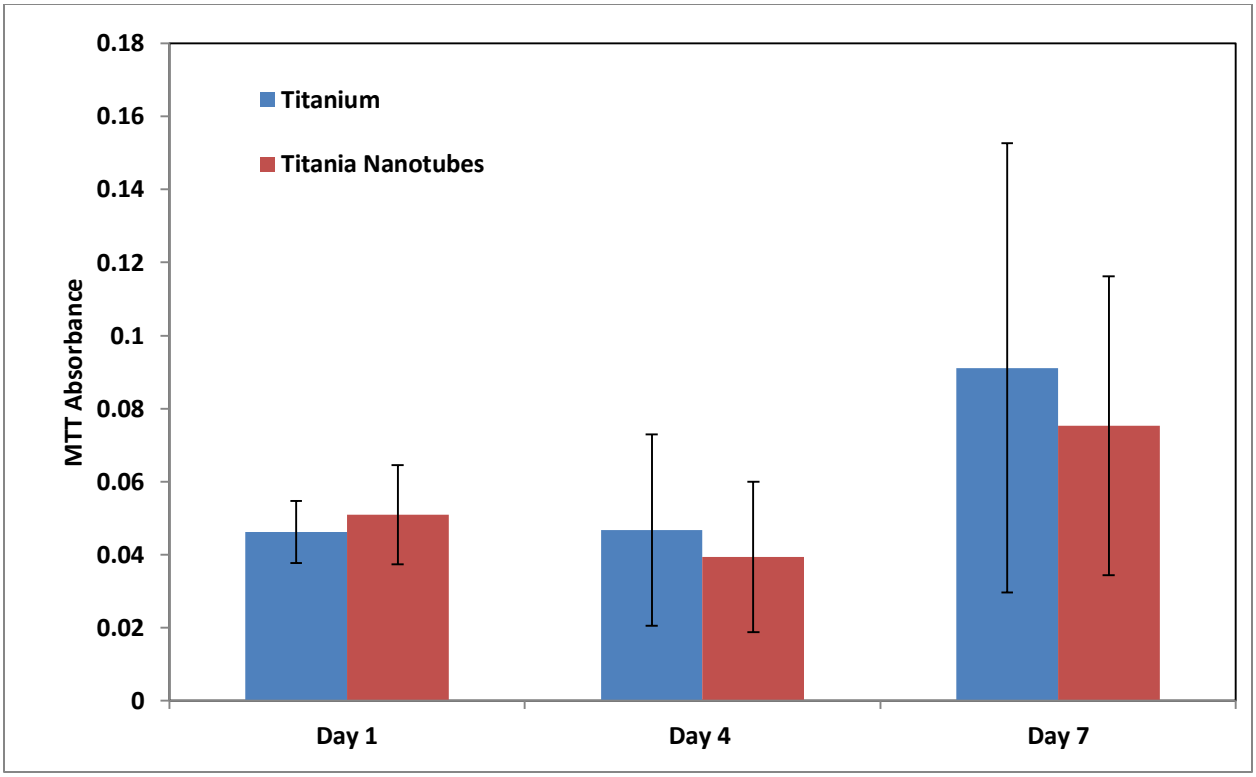

Figure 3.3.1: HASMCs' MMT viability on titania nanotubes and flat CP titanium

3.3.2 HASMC Morphology on Experimental Surfaces

HASMC morphology was evaluated after 1, 4, and 7 day after seeding of HASMCs on experimental surfaces with titania nanotubes contrasted with flat titanium. The interaction between the cells and the experimental surfaces can be observed through SEM images under 500x magnification as shown in **Figure 3.3.2**.

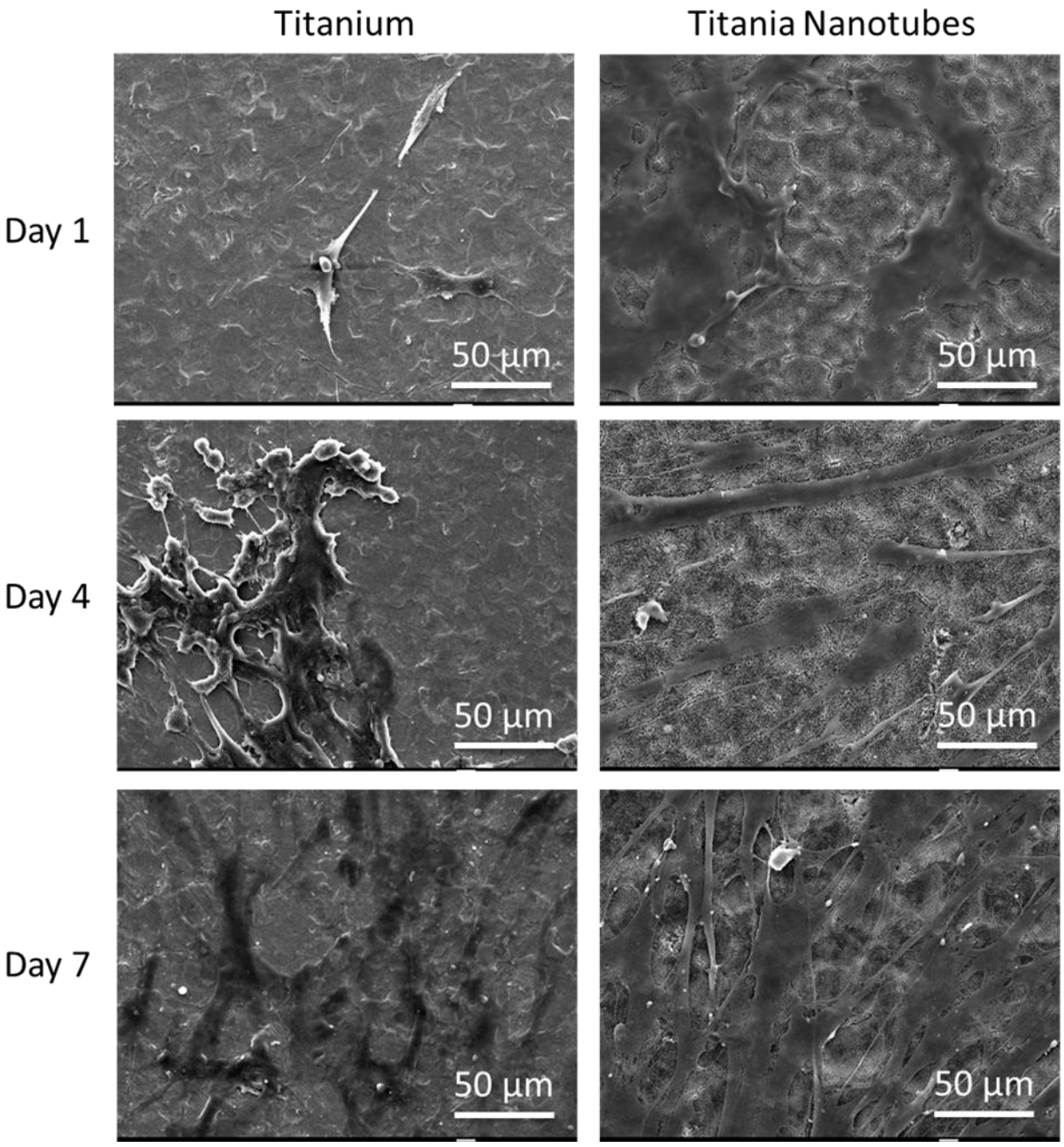

Figure 3.3.2: HASMCs on titania nanotubes and flat CP Titanium imaged with SEM at 500x at 1, 4 and 7 days after initial seeding of HASMCs.

3.3.3 Fluorescence staining for Adhesion and Proliferation of HASMCs on Experimental Surfaces

The fluorescence microscope was utilized to qualitatively examine HASMC adhesion and proliferation. Imaging with fluorescence microscopy was accomplished on days 1, 4 and 7 after initial cellular seeding on the experimental surfaces. Fluorescence microscopy images were taken in which HASMC nuclear, cytoplasmic and skeletal structures were stained by DAPI, FITC, and rhodamine phallodin respectively. These combined stain images can be viewed in **Figure 3.3.3** below and were chosen for clarity and resolution rather than a representation of average cell count per experimental sample.

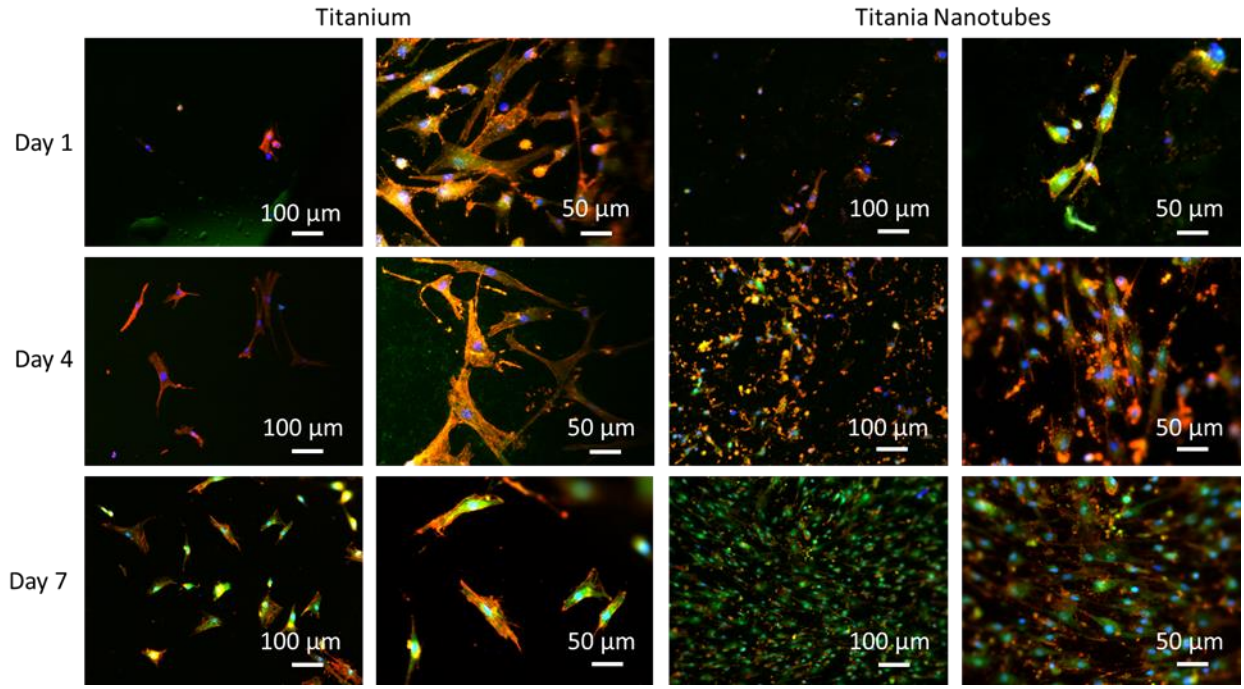

Figure 3.3.3: Fluorescence microscopy images displaying HASMC nuclear, cytoplasmic and skeletal structures were stained by DAPI, FITC, and rhodamine phallodin respectively.

3.3.4 Cell Counting of HASMCs on Experimental Surfaces

Due to employing a different filter to image each stain the fluorescence microscope's built in software allowed separation of each image by stain type. DAPI images were individually used to count the number of nuclei by ImageJ software analyzation on each image so an approximation of cell densities on each sample type could be determined as seen in **Figure 3.3.4** on days 1, 4, and 7 after initial HASMC seeding. HASMCs were seeded on experimental samples at a concentration of 20,000 cells/well. From the two-way ANOVA test, the main effect of day was found to be significant as well as the interaction between day and experimental sample. Tukey Post-Hoc Test estimate a p-value of 0.566 when comparing titania nanotubes and titanium as well as a p-value of 0.00491 when comparing Day 1 to 4, 2.2e-13 for comparing Day 1 to 7 and 4.23e-10 for comparing Day 4 to 7.

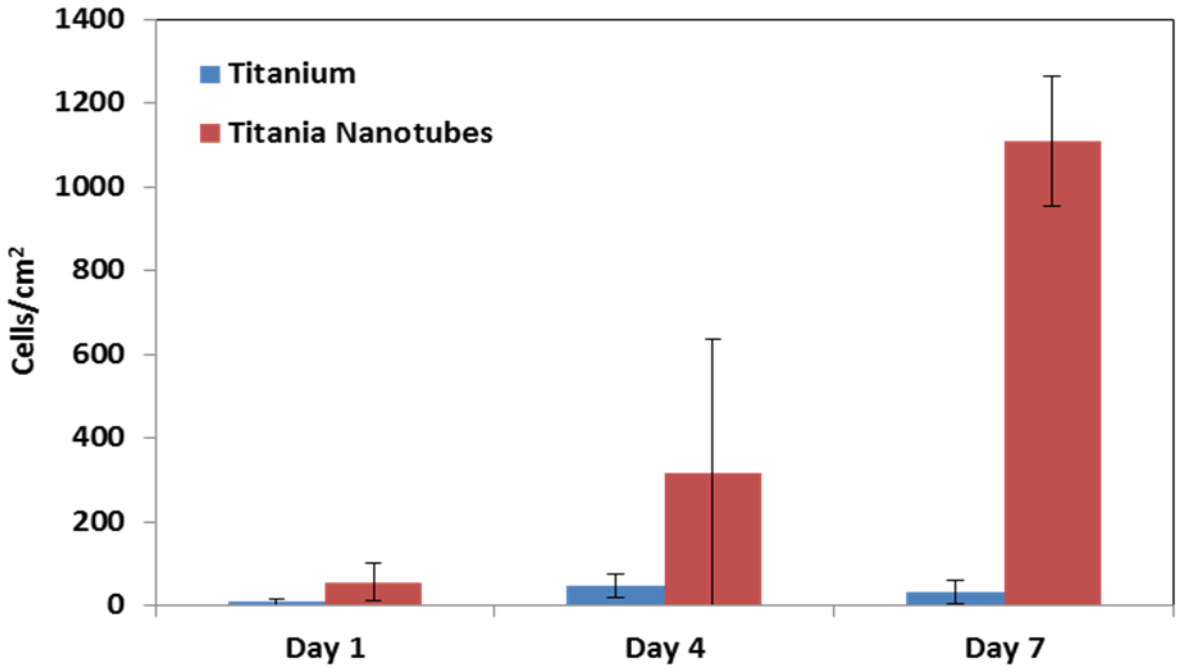

Figure 3.3.4: Smooth muscle cell populations on titania nanotubes and flat CP Titanium based on Fluorescence Imaging.

3.3.5 Shape Factor of HASMCs on Experimental Surfaces

Shape factor values were ascertained by comparing the ratio of the diameter of the largest circle that could contain an entire cell over the diameter of the smallest circle that could contain the entire cell. Rhodamine-phalloidin stained images taken from the fluorescence microscope at 10 times magnification were separated from the initial combined images of DAPI and CMFDA for shape factor analysis in ImageJ software. For this study, a shape factor value closer to 1 relates a cell to leaning to be more of a rounded, synthetic phenotype whereas a value close to 0, being more contractile. **Figure 3.3.5** demonstrates the results of the cell shape factor study. No statistical difference was seen by the two-way ANOVA for shape factor.

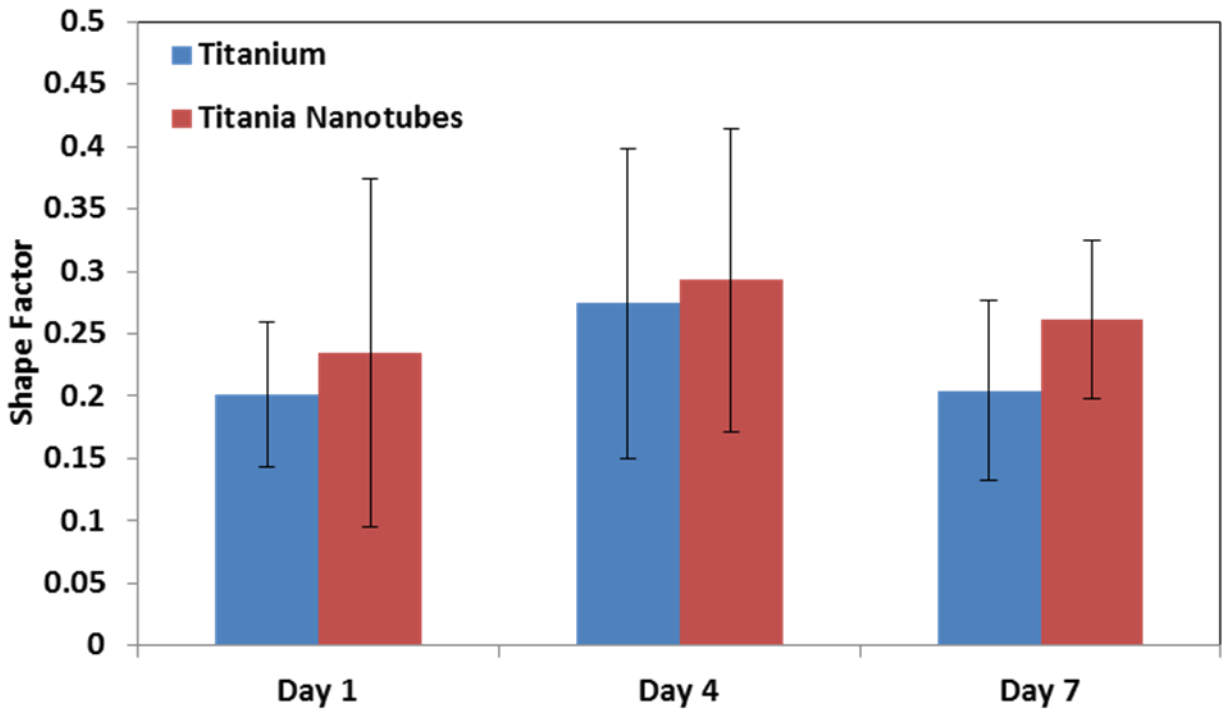

Figure 3.3.5: Human aortic smooth muscle cells' shape factor on titania nanotubes and flat CP Titanium based on Fluorescence Imaging.

3.4 Conclusion

Micro- and nanotopography has been documented to increase cellular signaling, adhesion, and proliferation of most cell types [9-19]. Despite these findings, there has been little work attempting to study the effects of nanofeatures effects on the phenotype and specific protein expression of smooth muscle cells. This study attempted to determine if titania nanotubes are a worthwhile surface modification for vascular stent applications. Human aortic smooth muscle cells cellular responses were compared between titania nanotubes and flat titanium as a control.

Morphology of the HASMCs from the SEM imaging seemed to shed little light on the mechanisms of the HASMCs except that their psuedopoditic, fingerlike projections were observed to be more pronounced on the titania nanotube samples. Fluorescence imaging concluded that HASMC stain specific cellular structures were intact.

MTT assay was utilized to determine the HASMCs mitochondria's relative output or productivity. Titania nanotube cell count exceeded that of titanium especially on day 7 and with the MTT results, which were not found to be significant, seems to signify that the individual HASMC on titanium had higher viability than titania nanotubes. This is possibly due to HASMCs on titanium being more synthetic phenotype in nature rather than shape, which was also not found to be significant, and the cells on titanium were attempting to grow and migrate more than on the nanotube samples corresponding for the need to generate more energy to power these processes by the mitochondria.

REFERENCES

[1] Folkman, Judah, and Anne Moscona. "Role of cell shape in growth control." (1978): 345-349.

[2] Flemming, R. G., et al. "Effects of synthetic micro-and nano-structured surfaces on cell behavior." *Biomaterials* 20.6 (1999): 573-588.

[3] Berridge, Michael V., Patries M. Herst, and An S. Tan. "Tetrazolium dyes as tools in cell biology: new insights into their cellular reduction." *Biotechnology annual review* 11 (2005): 127-152.

[4] Berk, Bradford C., et al. "Spontaneously hypertensive rat vascular smooth muscle cells in culture exhibit increased growth and Na+/H+ exchange."*Journal of Clinical Investigation* 83.3 (1989): 822.

[5] Young, Fiona M., Wichaya Phungtamdet, and Barbara JS Sanderson. "Modification of MTT assay conditions to examine the cytotoxic effects of amitraz on the human lymphoblastoid cell line, WIL2NS." *Toxicology in vitro*19.8 (2005): 1051-1059.

[6] Chazotte, Brad. "Labeling nuclear DNA using DAPI." *Cold Spring Harbor Protocols* 2011.1 (2011): pdb-prot5556.

[7] Prasad, Ashok, Dustin Berger, and Ketul Popat. "PCL nanopillars versus nanofibers: a contrast in progenitor cell morphology, proliferation, and fate determination." *Advanced Engineering Materials* 14.6 (2012): B351-B356.

[8] Gong, Dawei, et al. "Titanium oxide nanotube arrays prepared by anodic oxidation." *Journal of Materials Research* 16.12 (2001): 3331-3334. [6] Labeling nuclear DNA using DAPI. Chazotte B

[9] Martinez, E., et al. "Effects of artificial micro-and nano-structured surfaces on cell behaviour." *Annals of Anatomy-Anatomischer Anzeiger* 191.1 (2009): 126-135.

[10] Bettinger, Christopher J., Robert Langer, and Jeffrey T. Borenstein. "Engineering substrate topography at the micro-and nanoscale to control cell function."*Angewandte Chemie International Edition* 48.30 (2009): 5406-5415.

[11] Miller, Derick C., et al. "Endothelial and vascular smooth muscle cell function on poly (lactic-co-glycolic acid) with nano-structured surface features."*Biomaterials* 25.1 (2004): 53-61.

[12] Thapa, Anil, Thomas J. Webster, and Karen M. Haberstroh. "Polymers with nano-dimensional surface features enhance bladder smooth muscle cell adhesion." *Journal of Biomedical Materials Research Part A* 67.4 (2003): 1374-1383.

[13] Peng, Lily, et al. "The effect of TiO 2 nanotubes on endothelial function and smooth muscle proliferation." *Biomaterials* 30.7 (2009): 1268-1272.

[14] Inoguchi, Hiroyuki, et al. "Mechanical responses of a compliant electrospun poly (L-lactide-co-ε-caprolactone) small-diameter vascular graft." *Biomaterials*27.8 (2006): 1470-1478.

[15] Xu, C. Y., et al. "Aligned biodegradable nanofibrous structure: a potential scaffold for blood vessel engineering." *Biomaterials* 25.5 (2004): 877-886.

[16] Berntsen, Peter, et al. "Biomechanical effects of environmental and engineered particles on human airway smooth muscle cells." *Journal of The Royal Society Interface* 7.Suppl 3 (2010): S331-S340.

[17] Thapa, Anil, Thomas J. Webster, and Karen M. Haberstroh. "Polymers with nano-dimensional surface features enhance bladder smooth muscle cell adhesion." *Journal of Biomedical Materials Research Part A* 67.4 (2003): 1374-1383.

[18] Zhang, Xiaohui, Cassandra B. Baughman, and David L. Kaplan. "In vitro evaluation of electrospun silk fibroin scaffolds for vascular cell growth."*Biomaterials* 29.14 (2008): 2217-2227.

[21] Choudhary, Saba, Karen M. Haberstroh, and Thomas J. Webster. "Enhanced functions of vascular cells on nanostructured Ti for improved stent applications."*Tissue engineering* 13.7 (2007): 1421-1430.

CHAPTER 4

DIFFERENTATION OF HUMNAN AORTIC SMOOTH MUSCLE CELLS ON TITANIA NANOTUBE ARRAYS

4.1 Introduction

Vascular tissue has a countless amount of nanometer unevenness from the existence of nanostructured extracellular matrix proteins. Even so, a majority of vascular stents presently being employed are flat at the nanoscale. When plaque accumulation in a vessel becomes dangerous, vascular stents are often introduced into arteries as a necessary management selection to reestablish normal blood flow to various tissues [1].

The smooth muscle cell's primary vascular role is relaxation and contraction of blood vessels by altering the diameter which allows for regionalized blood pressures and flows [1]. SMCs two phenotypes, contractile and synthetic, have been observed to have flexibility to switch between phenotypes [2]. Interchanging of phenotypes is categorized by a reduction in the expression of particular differentiation proteins and amplified SMC migration, proliferation, and production of ECM constituents required for vascular renovation.

In this study, SMC specific marker proteins, including calponin (CAL) and heavy chain myosin (HCM) expression, produced from differentiation media grown HASMCs was analyzed when grown on titania nanotubes. Decreased proliferation through the employment of SMC prescribed differentiation supplemental media assisted analysis of the potential spectrums of contractile and synthetic phenotypes. ImageJ software was utilized to deduce the relative cellular expression of these proteins through immunofluorescent staining.

4.2 Methods for Experimentation

4.2.1 Fabrication and Characterization of Titania Nanotubes

Titania nanotubes were created and characterized as portrayed in Chapter 2. Uniform and easily reproducible titania nanotubes were fabricated from CP titanium utilizing an electrochemical reaction in a fluorinated electrolyte solution. These annealed and un-annealed titania nanotubes were compared versus titanium in their nano-morphology, crystal and elemental composition as well as their hydrophilicity. The preparation and cleansing of both substrates was completed by the same procedures.

4.2.2 Primary Cell Culture

Human aortic smooth muscle cells were purchased by Invitrogen and were taken from 1 single human donor. Cell culturing environments and preparation can be found in **Section 3.2.2**. Passage 5 or less cells were thawed and cultured in supplemented Gibco MCDB 131 medium and subcultured prior to seeding onto the experimental samples.

4.2.3 HASMC Culture on Experimental Samples

Experimental samples including titaniumand titanium samples were sterilized in a biosafety cabinet prior to cell seeding and onto the substrates as expressed in **Section 3.2.3**. Once the samples were sterilized, HASMCs were seeded on the experimental samples at a concentration of 20,000 cells/well. After seeding, media was replaced every 24 to 48 hours with the same media as described in **Section 3.2.2**. After 7 days of the cells being cultured on the samples, cells were grown in differentiation media that contained the following:

- Gibco MCDB 131 Medium
    - Smooth Muscle Cell Differentiation Supplement (SMDS)
        - Fetal bovine serum 1% v/v
        - Heparin (30µg/mL)
    - L-Glutamine (2 mmol/L)
    - Penicillin-Streptomyocin (100 ug/mL)

Media was stored at 4 °C. SMDS is commercially available by Invitrogen and is designed to decrease proliferation of human smooth muscle cells mainly by the increased concentration of heparin from 5 ng/mL in the SMGS growth media to 30µg/mL in the SMDS differentiation media. Previous studies have demonstrated that heparin hinders the adhesion and proliferation of smooth muscle cells in vitro and in vivo. Heparin has been shown to impede RNA and DNA synthesis, while not affecting the degree of protein synthesis [3-6].

Investigations of the cells were carried out on days 1, 4, and 7 after initial seeding in proliferative SMGS media and at days 10 and 14 when grown in differentiation SMDS media. Cell analyses included morphology investigation via SEM imaging, fluorescence microscope imaging by fluorescent labeled Calponin and Heavy Chain Myosin protein markers which permitted protein/area data. Fluorescent staining, as described in **Section 3.2.6,** allowed nuclear cell counting and shape factor analysis via ImageJ.

4.2.4 HASMC Morphology on Experimental Surfaces

In order to gain some perceptive on the morphology of HASMCs in their interaction with titania nanotubes and titanium substrates and their observed phenotype, SEM imaging was performed on days 10 and 14. Fixing of the samples prior to SEM imaging was accomplished as stated in **Section 3.2.5**. In summary, experimental samples with HASMCs cultured on the surface were subjected to a fixative containing deionized water, sucrose, sodium cacodylate and gluteraldeyde, a buffer with all the chemicals included in the fixative besides gluteraldehyde, then placed in increased ethyl alcohol concentrations then finally immersed in hexamethyl disilisone. The samples were then placed in a chemical hood to air dry. After drying, the samples were stationed in a desiccator for at least 24 hours then sputtered with 10 nm of gold and imaged at 15 kV.

4.2.5 Fluorescence staining for Differentiation of HASMCs on Experimental Surfaces

HASMCs grown on experimental samples with differentiation media were stained utilizing 5-Chloromethylfluorescein diacetate (CMFDA) for non-specific cytoplasm staining, Rhodamine phalloidin for F-actin microfilament selective staining and 4'6-diamidino-2-phenylindoledihydrochloride (DAPI) for cell nuclei. Fluorescence staining by prior mentioned stains was completed in a fashion as described in **Section 3.2.6**. In short, experimental samples with HASMCs cultured on the surface were rinsed with sterile PBS before being subjected to CMFDA (reconstituted in anhydrous dimethylsulfoxide), followed in sequence with formaldehyde, Triton X, rhodamine phallodin (reconstituted with 100% methanol), with DAPI finally being supplemented last. The samples were next aspirated and rinsed twice with fresh

PBS then immersed in fresh PBS until imaging with fluorescence microscope using a BP 474/28 green filter, 62 HE BP 585/35 Red filter, and 49 DAPI BP 585/50 blue filter.

4.2.6 HASMC Calponin and Heavy Chain Myosin Fluorescence Marker Expression

HASMC adhered to the experimental samples were stained utilizing 4'6-diamidino-2-phenylindoledihydrochloride (DAPI) for cell nuclei, and Rhodamine phalloidin for F-actin cytoskeleton staining and indirect immunofluorescence staining that marked calponin and heavy chain myosin (HCM) through the use of fluorophore by the binding of the secondary antibody. The cells on the experimental surfaces were imaged by Zeiss Axioplan 2 fluorescence microscope in which DAPI was observed blue, Rhodamine phalloidin red and specific proteins green.

At day 10 and 14, secondary or indirect immunofluorescence staining was utilized to view and determine the relative amount of proteins specific to smooth muscle cells. To remove un-adhered proteins, the differentiation media was aspirated from the experimental samples trailed by rinsing with sterile PBS. The samples were afterwards relocated to a different 48-well plate. 3.7% formaldehyde in PBS placed in the wells containing the samples to fix for 15 minutes. The samples were then washed 3 times with fresh PBS. After transferring the samples to new wells containing 1 % Triton-X in PBS for 3 minutes the samples were again washed 3 times with PBS. The samples were moved to new wells containing 10% bovine serum albumin blocking buffer for 30 minutes. Afterward the samples were retained in a solution of primary antibodies with 2 % blocking serum (dilution 1:50, Santa Cruz Biotechnology) in PBS for 1 hour. The samples were rinsed with fresh PBS 3 times and deposited into a solution of secondary fluorescently labeled antibody with 2 % blocking serum in PBS (dilution 1:100, Santa Cruz

Biotechnology) for 1 hour. All previous stated steps occurred at room temperature unless otherwise stated.

The samples were washed 3 times with PBS before following the rest of the fluorescence staining protocol of rhodamine phallodin and DAPI as previously defined in **Section 3.2.6**. The samples were imaged using the Zeiss fluorescent microscope and processed via the microscope's built in software. Cellular protein expression of HCM and calponin were ascertained by amplified fluorescence observed green in imaging.

Table 4.2.1: Blocking, primary, and secondary antibodies used for differentiated HASMCs.

	Calponin Marker	**Heavy Chain Myosin Marker**
Blocking	Bovine Serum Albumin	
Primary Antibody	CAL I: Mouse monoclonal	HCM (Y-20): Goat polyclonal IgG
Secondary Antibody	Donkey anti-goat FITC	Chicken anti-mouse FITC

4.2.7 Cell Counting of HASMCs on Experimental Surfaces

The DAPI images were separated from the combined filter images so that they were able to be processed in ImageJ software as described in **Section 3.2.7**. HASMC cellular count calculation was divided by the area of the experimental surfaces and averaged to obtain a cell count per area on each experimental surface.

4.2.8 Shape Factor of HASMCs on Experimental Surfaces

HASMC shape factor was determined by comparing the diameters of the smallest and largest circle that could incorporate the whole cell as described in **Section 3.2.8**. The 10x rhodamine-phalloidin stained images were utilized for shape factor analysis by ImageJ software.

4.2.9 Calponin and HCM Protein/Area on Experimental Surfaces

HASMCs stained with DAPI, rhodamine-phalloidin and treated with indirect immunofluorescence prior to imaging with the flouresence microscope were separated from the combined filter images by the fluorescence microscopes built in software. The green immunfluorescent images were then processed through a macro in ImageJ software that allowed the computer to recognize the green protein stain versus the background. This protein calculation was then divided by the area of the experimental surfaces to which the cells were attached then averaged to obtain a protein per area on each experimental surface.

4.2.10 Statistical Analysis

Each experiment was performed on at least three surfaces per experimental sample (n_{min} = 3). The quantitative results were analyzed using a two-way analysis of variance (ANOVA) model paired Tukey's post hoc test with statistical significance of $p < 0.05$. The analysis was performed using Deducer, an R based program.

4.3 Results and Discussion

To improve efficient biomaterial surfaces aimed in vascular repair, it is necessary to recognize how smooth muscle cells react to the surface of the implant. From this understanding, it is more likely that these surfaces will be able to stimulate SMCs to take on a more natural, contractile phenotype.

Differentiation of HASMCs was primarily determined by the use of immunofluorescence of specific proteins known to be expressed by smooth muscle cells. Synthetic SMC phenotypes are typically categorized by decreased manifestation of SMC specific proteins and intensified

relocation, growth, and production of ECM constituents essential for vascular restoration. Calponin and Heavy Chain Myosin were specifically targeted for immunofluorescence due to previous studies showing that they are key proteins expressed by differentiated smooth muscle cells [2,7-11]. The binding of the primary and secondary antibodies to these proteins demonstrate the activation and expression of these key proteins in contractile phenotype smooth muscle cells so that they are able to perform their function by regulating localized blood pressure via contracting or relaxing as a tissue. HCM presence, as yet, has not been identified in any other cells than smooth muscle. Calponin has also been seen in smooth muscle cells which are known to participate in the supervision of myosin-actin communications. This chapter attempts to understand the reaction of HASMCs to being grown on experimental surfaces for over a week while switching media in order to determine the difference in cellular reaction while under the influence of increased heparin concentration. The expression of these marker proteins was determined for 10 and 14 of culture by immunofluorescence for HASMCs grown on the experimental samples.

4.3.1 HASMC Morphology on Experimental Surfaces

HASMC morphology was evaluated after 10 and 14 day after seeding of HASMCs on experimental surfaces with titania nanotubes contrasted with flat titanium. The interaction between the cells and the experimental surfaces can be observed through SEM images under 500x magnification as shown in **Figure 4.3.1**.

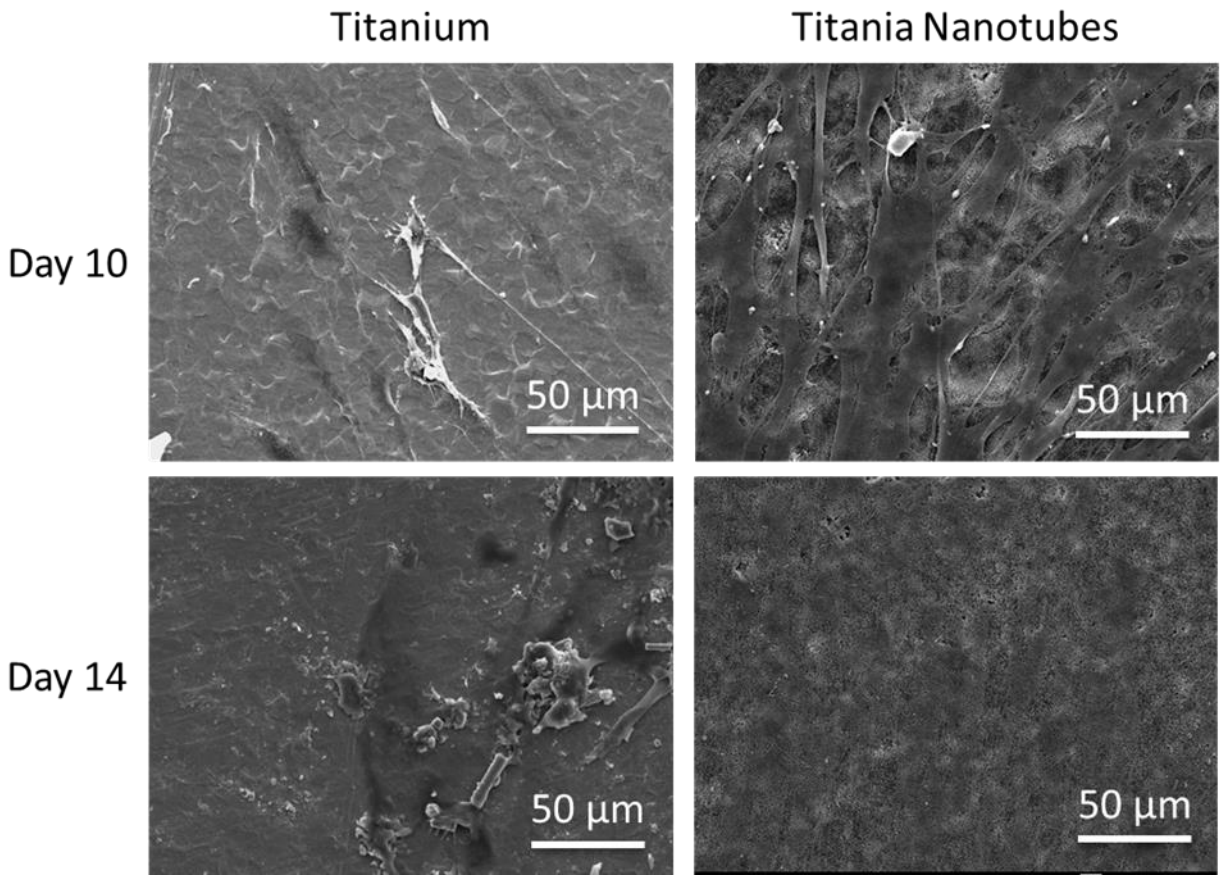

Figure 4.3.1: HASMCs on titania nanotubes and flat CP Titanium imaged with SEM at 500x at 10 and 14 days after initial seeding of HASMCs.

4.3.2 Fluorescence staining for Adhesion and Proliferation of HASMCs on Experimental Surfaces

The fluorescence microscope was utilized to qualitatively examine HASMC adhesion and proliferation. Imaging with fluorescence microscopy was accomplished on days 10 and 14 after initial cellular seeding on the experimental surfaces. Fluorescence microscopy images were taken in which HASMC nuclear, cytoplasmic and skeletal structures were stained by DAPI, FITC, and rhodamine phallodin respectively. These combined stain images can be viewed in **Figure 4.3.2** below and again were chosen for clarity and resolution rather than a representation of average cell count per experimental sample.

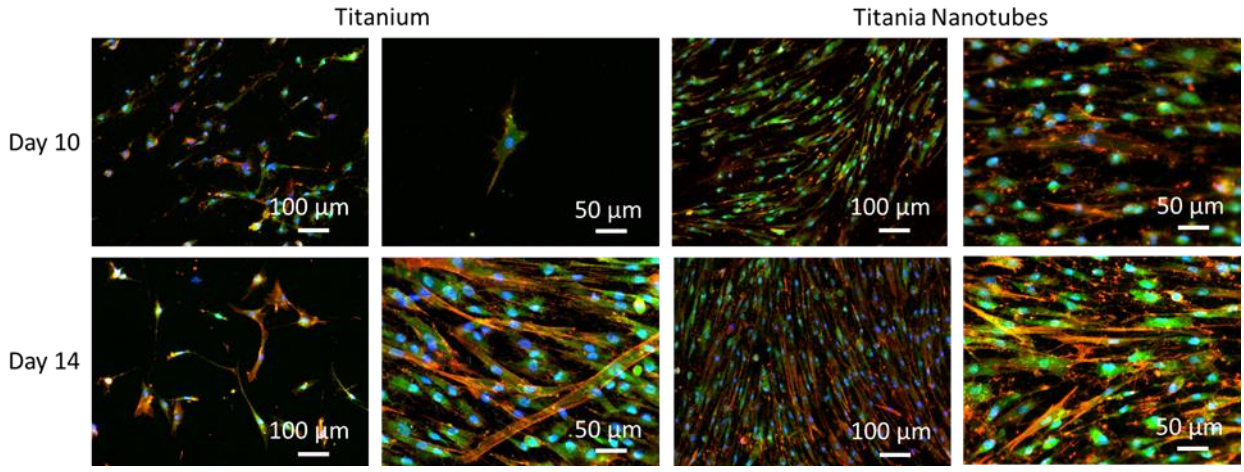

Figure 4.3.2: Fluorescence microscopy images displaying HASMC nuclear, cytoplasmic and skeletal structures were stained by DAPI, FITC, and rhodamine phallodin respectively.

4.3.3 HASMC Calponin and Heavy Chain Myosin Fluorescence Marker Expression

The fluorescence microscope was utilized to qualitatively examine HASMC differentiation of CAL and HCM expression. Imaging with fluorescence microscopy was accomplished on days 10 and 14 after initial cellular seeding on the experimental surfaces. Fluorescence microscopy images were taken in which HASMC nuclear and skeletal structures were stained by DAPI and rhodamine phallodin respectively. The green colors in the images below are from the releasing of fluorophore by the binding of secondary antibodies to the corresponding primary antibodies and specific targeted proteins, CAL and HCM. These combined stain images, chosen for their clarity, can be viewed in **Figure 4.3.3** and **Figure 4.3.4** below.

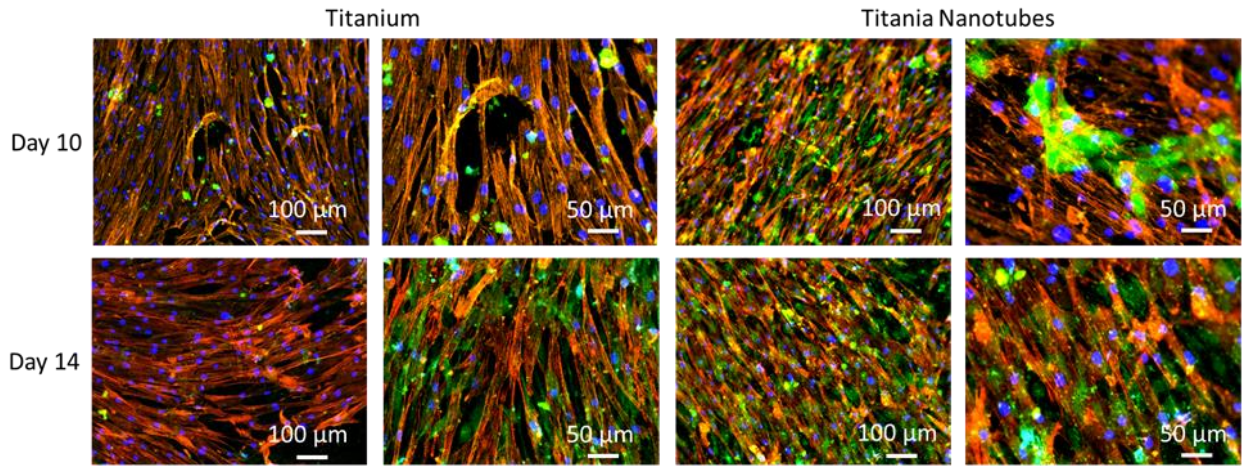

Figure 4.3.3: Fluorescence microscopy images displaying HASMC nuclear and skeletal structures were stained by DAPI, and rhodamine phallodin respectively with the green expression of the fluorophore released by immunofluorescence of calponin.

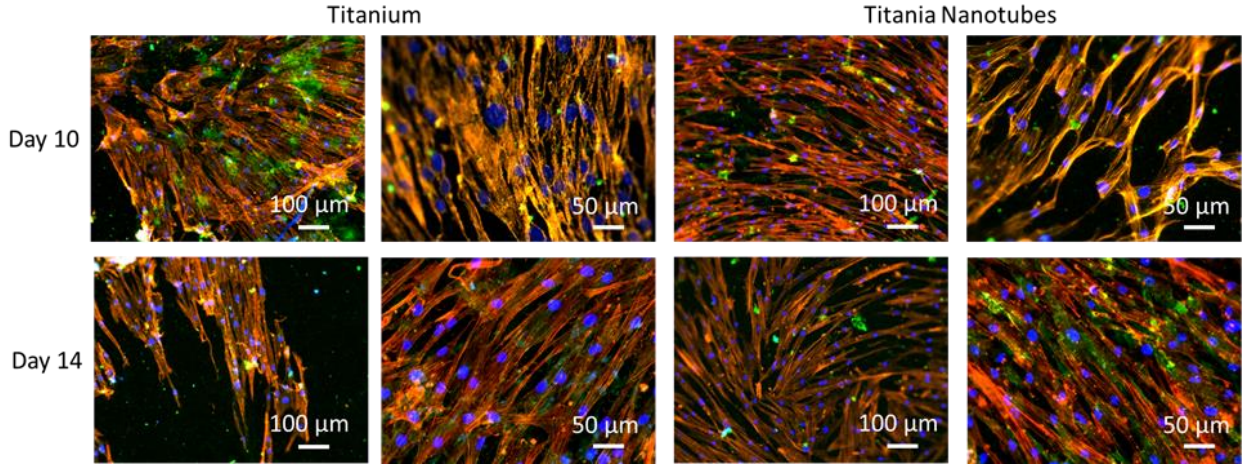

Figure 4.3.4: Fluorescence microscopy images displaying HASMC nuclear and skeletal structures were stained by DAPI, and rhodamine phallodin respectively with the green expression of the fluorophore released by immunofluorescence of heavy chain myosin.

4.3.4 Cell Counting of HASMCs on Experimental Surfaces

Due to employing a different filter to image each stain the fluorescence microscope's built in software allowed separation of each image by stain type. On days 10 and 14 after initial HASMC seeding, DAPI images were used to count the number of nuclei by ImageJ software so

an approximation of cell densities on each sample type could be determined as seen in **Figure 4.3.5.** HASMCs were seeded on experimental samples at a concentration of 20,000 cells/well.

From the two-way ANOVA test, the main effect of experimental sample was found to be significant as well as the interaction between day and experimental sample. Tukey Post-Hoc Test revealed a p-value of 8.28e-06 between nanotubes and titanium as well as a p-value of 0.788 when comparing Day 10 to 14.

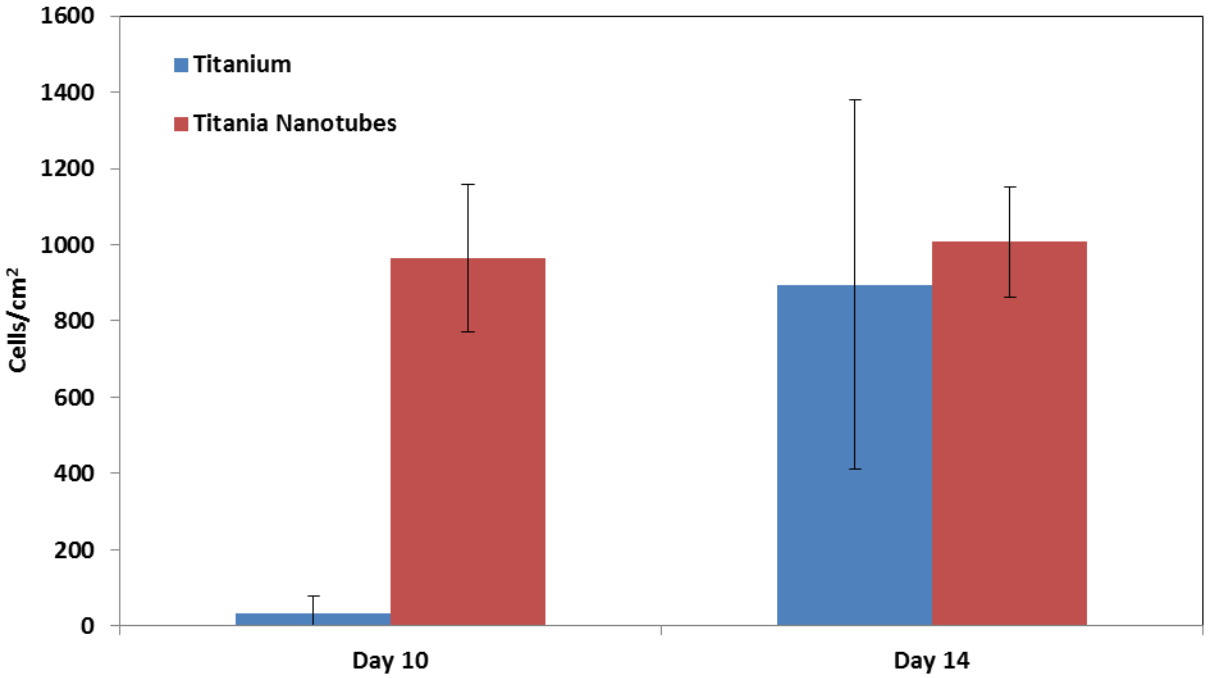

Figure 4.3.5: Smooth muscle cell populations on titania nanotubes and flat CP Titanium based on Fluorescence Imaging.

4.3.5 Shape Factor of HASMCs on Experimental Surfaces

Shape factor values were ascertained by comparing the ratio of the diameter of the largest circle that could contain an entire cell under the diameter of the smallest circle that could contain the entire cell. Rhodamine-phalloidin stained images taken from the fluorescence microscope at

10x magnification were separated from the initial combined images of DAPI and CMFDA for shape factor analysis in ImageJ software. The method for determining the shape factor was utilized in an attempt to relate a length to width ratio in order to shed light on the phenotype of the cell. For this study, a shape factor value closer to 1 relates a cell to leaning to be more of a rounded, synthetic phenotype whereas a value close to 0, being more contractile. **Figure 4.3.6** demonstrates the results of the cell shape factor study. The two-way ANOVA test had no statistical difference by shape factor.

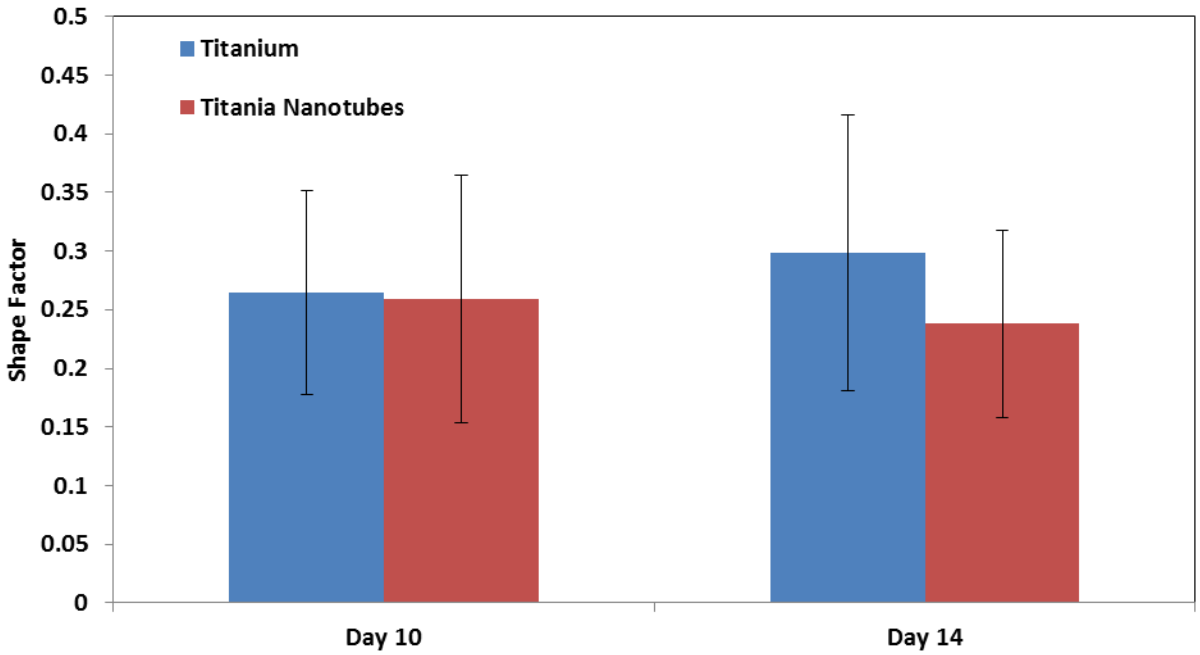

Figure 4.3.6: Human aortic smooth muscle cells' shape factor on titania nanotubes and flat CP Titanium based on Fluorescence Imaging.

4.3.6 Calponin and HCM Protein/Area on Experimental Surfaces

Protein per area calculation was ascertained by comparing the green immunfluorescent images versus the area of background as described in **Section 4.2.9**. The results for calponin and heavy chain myosin per area can be observed in **Figure 4.3.7** and **Figure 4.3.8** respectively.

From the two-way ANOVA, CAL Protein/Area showed no significant differences between days, experimental samples or the effect of experimental samples depending on the day. HCM Protein/Area two-way ANOVA demonstrated significance when the interaction between day and experimental sample was compared. Tukey Post-Hoc Test estimates that titanium exhibited nanotubes higher protein per area and a p-value of 0.289 when comparing Day 10 to 14.

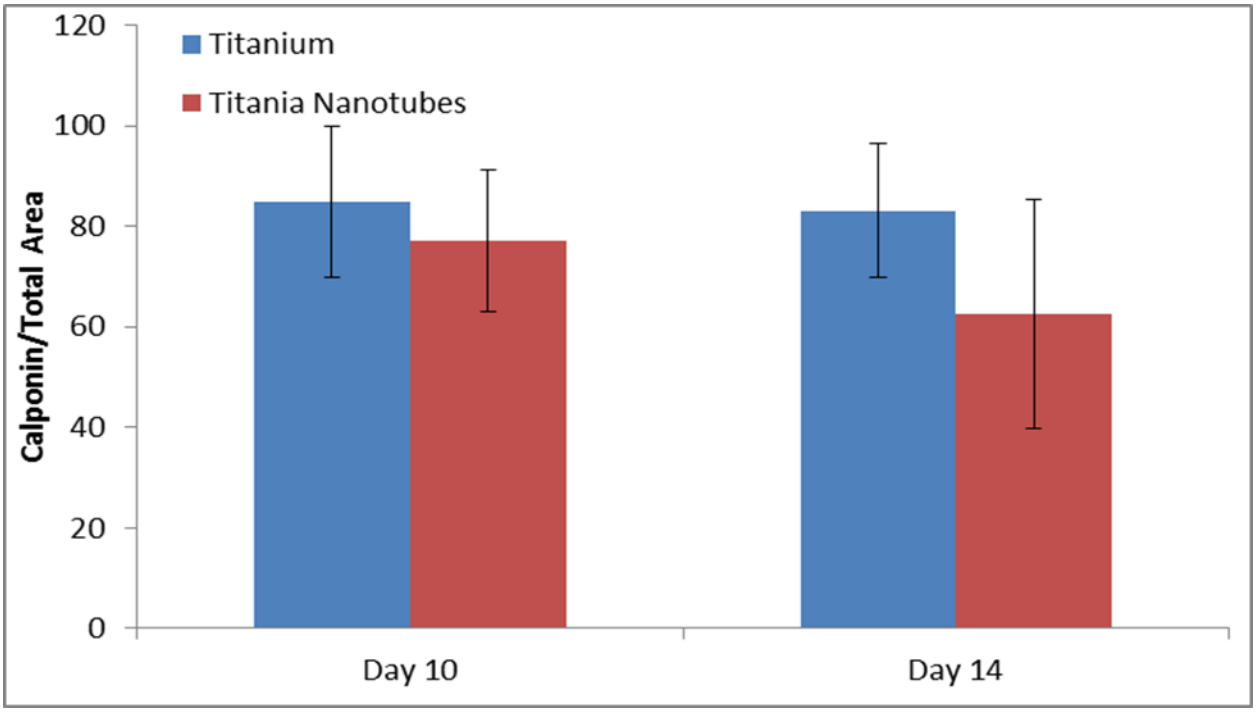

Figure 4.3.7: Protein expression of Calponin marker.

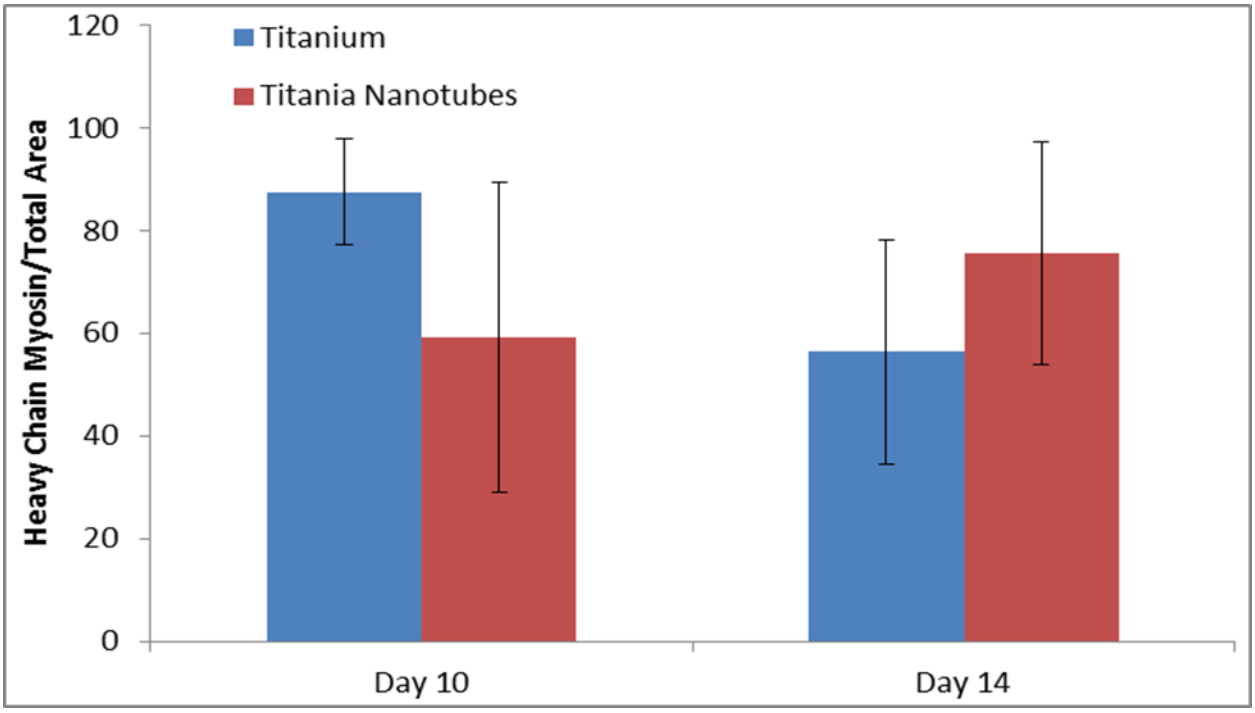

Figure 4.3.8: Protein expression of Heavy Chain Myosin marker.

4.4 Conclusion

The HASMC morphology from SEM imaging was perceived to be more spread out with longer cell extensions on titania nanotubes than titanium samples. This observation is possibly due to the cells' cytoplasmic extensions have an easier time embedding themselves in between the gapes in the nanotubes. Fluorescence staining confirmed that all cellular components as well as SMC specific marker proteins, CAL and HCM were all present on both experimental samples. Cell count was much higher on day 10 for titania nanotubes but not considerably different on day 14 for which inferences are hard pressed to be made regarding cellular population. Shape factor was not significant which correlates with the not incredible difference seen between the SMC marker proteins in that the HASMCs are not differentiating based on the topography of the surface to which they are grown on since both experimental surfaces will have a oxide layer from

being exposed to air. From this study, differentiation of HASMCs will not be observed based exclusively on the topography but some combination of mechanical, chemical and/or physiological stimulations.

REFERENCES

[1] Choudhary, Saba, Karen M. Haberstroh, and Thomas J. Webster. "Enhanced functions of vascular cells on nanostructured Ti for improved stent applications."*Tissue engineering* 13.7 (2007): 1421-1430.

[2] Peyton, Raub, Keschrumrus, Putnam. The use of poly(ethylene glycol) hydrogels to investigate the impact of ECM chemistry and mechanics on smooth muscle cells. 2006.

[3] Castellot, John J., David L. Cochran, and Morris J. Karnovsky. "Effect of heparin on vascular smooth muscle cells. I. Cell metabolism." *Journal of cellular physiology* 124.1 (1985): 21-28.

[4] Beamish, Jeffrey A., et al. "The effects of heparin releasing hydrogels on vascular smooth muscle cell phenotype." *Biomaterials* 30.31 (2009): 6286-6294.

[5] Gu, Zi, et al. "Enhanced effects of low molecular weight heparin intercalated with layered double hydroxide nanoparticles on rat vascular smooth muscle cells." *Biomaterials* 31.20 (2010): 5455-5462.

[6] Clowes, Alerander W., and Morris J. Karnowsky. "Suppression by heparin of smooth muscle cell proliferation in injured arteries." (1977): 625-626.

[7] Hao, Hiroyuki, Giulio Gabbiani, and Marie-Luce Bochaton-Piallat. "Arterial smooth muscle cell heterogeneity implications for atherosclerosis and restenosis development." *Arteriosclerosis, thrombosis, and vascular biology*23.9 (2003): 1510-1520.

[8] Stegemann, Jan P., Helen Hong, and Robert M. Nerem. "Mechanical, biochemical, and extracellular matrix effects on vascular smooth muscle cell phenotype." *Journal of applied physiology* 98.6 (2005): 2321-2327.

[9] Owens, Gary K. "Regulation of differentiation of vascular smooth muscle cells."*Physiological reviews* 75.3 (1995): 487-517.

[10] Sakamoto, Naoya, Takuya Kiuchi, and Masaaki Sato. "Development of an Endothelial–Smooth Muscle Cell Coculture Model Using Phenotype-Controlled Smooth Muscle Cells." *Annals of biomedical engineering* 39.11 (2011): 2750-2758.

[11] Miano, Joseph M., et al. "Smooth muscle myosin heavy chain exclusively marks the smooth muscle lineage during mouse embryogenesis." *Circulation research* 75.5 (1994): 803-812.

CHAPTER 5

CONCLUSION AND FUTURE WORK

5.1 Conclusions

Owing to their aptitude to vary phenotype consistent to changing physiological conditions, smooth muscle cells are essential in the advancement of vascular disease [1]. Vascular stents have the ability to widen constricted or clogged blood vessels to allow for the continued flow of nutrients by blood to tissues. The length of time that these prostheses remain effective is still limited. The stents are in constant contact with blood constituents, endothelial and smooth muscle cells and so must be in harmony with all these components. When the implant and the tissue fail to integrate properly, rejection of the prosthesis will occur. Even when integration is relatively high, the implant can still be rejected over a natural course in time by the immune response recognizing the object as foreign. In the past, research was devoted in exploring the interaction of micro- size surface features. Today, more work is focused on producing surface structures on the nanoscale. For titanium implants, titania nanotubes in particular have a fairly simple fabrication procedure, are structures on nanoscale which more closely mimic cell surface and ECM proteins while also providing a means for biochemical eluting of matter such as antibiotics and growth factors.

The purpose of this study was to examine titania nanotubes as potential surface modifications for titanium stents. This research focuses on the highly reproducible, uniform, vertically-oriented titania nanotubes interaction with human aortic smooth muscle cells' morphology, viability, adhesion, proliferation and differentiation. Titanium was used as control since, if not surface modified, would be the surface exposed to the cells. Titania nanotubes were

fabricated by an electrochemical anodization process by utilizing a fluorinated electrolyte solution. Material characterization of the experimental samples was completed through SEM imaging for morphology, crystalline structure by GAXRD, elemental composition by XPS with surface energy and wettability by goniometer.

No significant differences were found through the comparison of un-annealed and annealed titania nanotubes' diameter, wall thickness or length. Crystalline structure was very similar for titanium and un-annealed titania nanotubes but annealed nanotubes were seen to have more anatase peaks and the presence of rutile and very minimal brookite crystals. Elemental composition confirmed the drastic decrease of the residual fluorine on the surface of titania nanotubes after annealing. Surface energy of titania nanotubes were found to be at least 40 mJ/m^2 greater than flat CP titanium control.

Human aortic smooth muscle cells adhesion, viability, morphology, proliferation and differentiation were investigated over 14 days after initial cell seeding onto experimental samples. On days 1, 4, and 7 after initial seeding, studies for smooth muscle cell reaction to experimental samples included cell viability using MTT assay, cellular morphology by SEM imaging, fluorescence stain imaging by fluorescence microscopy, as well as cell counting and shape factor analysis of the fluorescence stain images by ImageJ.

The results of the previously mentioned studies point to a slightly greater cellular preference for titania nanotubes than flat CP titanium. This supposition is reported via the greater cell count and morphologically more spread out HASMCs with longer cellular cytoplasmic extensions on titania nanotubes where the rest of the other experiments on days 1, 4, and 7 showed very little difference in cellular response between the experimental samples.

Prescribed differentiation was completed by use of SMDS media that replaced the SMGS media after day 7 following initial HASMC seeding on experimental surfaces. On days 10 and 14 after initial seeding, studies for smooth muscle cell response to experimental samples included cellular morphology by SEM imaging, fluorescence staining and specific marker protein imaging by fluorescence microscopy, as well as cell counting, shape factor, and marker protein expression/area analysis of the fluorescence images.

A faintly greater cellular partiality for titania nanotubes over flat CP titanium was detected via the greater cell count and morphologically more coverage of HASMCs with more cellular extensions on titania nanotubes where the remainder of the other studies on days 10 and 14 showed very slight variance in cellular reaction between the titania nanotubes and titanium.

The overall results of the series of experiments contained in this document advocate enhanced HASMC response to titania nanotubes as compared to flat CP titanium on days 1-7 but not on days 10-14. This result suggests that there is a vast comeback in SMC growth on titanium after the SMGS media was exchanged for the SMDS media.

- No significant differences were found through the comparison of un-annealed and annealed titania nanotubes' diameter, wall thickness or length.
- Crystalline structure was very similar for titanium and un-annealed titania nanotubes but annealed nanotubes were seen to have more anatase peaks and the presence of rutile and very minimal brookite crystals.
- Elemental composition confirmed the drastic decrease of the residual fluorine on the surface of titania nanotubes after annealing.

- Surface energy of titania nanotubes were found to be at least 40 mJ/m2 greater than flat CP titanium control.
- Morphology of the HASMCs from the SEM imaging seemed to shed little light on the mechanisms of the HASMCs except that their psuedopoditic, fingerlike projections were observed to be more pronounced on the titania nanotube samples.
- Fluorescence imaging concluded that HASMC stain specific cellular structures were intact.
- Titania nanotube cell count exceeded that of titanium especially on day 7 and with the MTT results, which were not found to be significant, seems to signify that the individual HASMC on titanium had higher viability than titania nanotubes.
- HASMCs on titanium were more synthetic phenotype in nature rather than shape, which was also not found to be significant, and the cells on titanium were attempting to grow and migrate more than on the nanotube samples corresponding for the need to generate more energy to power these processes by the mitochondria.
- The HASMC morphology from SEM imaging was perceived to be more spread out with longer cell extensions on titania nanotubes than titanium samples.
- Fluorescence staining confirmed that all cellular components as well as SMC specific marker proteins, CAL and HCM were all present on both experimental samples.
- Cell count was much higher on day 10 for titania nanotubes but not considerably different on day 14 for which inferences are hard pressed to be made regarding cellular population.
- Shape factor was not significant which correlates with the not incredible difference seen between the SMC marker proteins in that the HASMCs are not differentiating based on

the topography of the surface to which they are grown on since both experimental surfaces will have a oxide layer from being exposed to air.

- Differentiation of HASMCs will not be observed based exclusively on the topography but some combination of mechanical, chemical and/or physiological stimulations.
- HASMCs grown on titania nanotubes showed more favorable results on titania nanotubes than titanium for days 1-7 but not on days 10 and 14 when the growth media was changed.

5.2 Future Work

Cellular function is controlled by the sum of the cell atmosphere, including cell-cell contacts, ECM constituents, resident chemical environments, and mechanical dynamisms. The depth of the extracellular domain is absent in these experiments, and so, there has been an great attentiveness in creating more intricate, well measured, in vitro model environments to understand vascular ecology [2].

In their natural environment, cells are surrounded by nano-topographies, in connecting with other cells; through membranes of nano-dimension arrangements or with the extra-cellular matrix (ECM). The ECM comprises predominantly of interspersed protein fibers such as proteoglycans, collagen, fibronectin and elastin. Individual proteoglycans are on the order of 330-4500 nm long and 70-85 nm diameter [3], Collagen fibrils 65-300 nm long and 10-450 nm diameter [4]with a Youngs Modulus 0.2-0.8 GPa, Hardness 0.137-0.226 GPa, Tensile Strength of 49-95 MPa [5], Fibronectin 60-70 nm long and 2-3 nm diameter [4] and Elastin elastic fibers 2.5 µm diameter with an Elastic Modulus of 1.7-2.8e-10 GPa [6] a Youngs Modulus of 0.0018-

0.0022 GPa,, and a Tensile Strength of 1.7-2.2 MPa [5]. It is therefore imperative to create implantable medical devices with similar properties.

Titania nanotubes fabricated by anodic oxidation at 60 volts for 24 hours yielded nanotube substrates ranged from 100 - 190 nm diameters, 40 -70 nm thickness and 870 - 1150 nm lengths for the annealed substrates and 120 – 170 nm diameters, 45 – 70 nm thickness and 770 - 1130 nm lengths for the un-annealed substrates. Titania nanotubes were found to have a Youngs Modulus of 70-100 GPa [6], Elastic Modulus of 1-40 GPa, and Hardness of 0.1-0.2 GPa [7].

After an implant is introduced into the body, it will be subjected to the blood and the corresponding tissue where it was placed. In the case of vascular stents, the implant would be exposed to blood, endothelial and smooth muscle tissues. Proteins from these tissues immediately respond with the surface of the implant and how these reactions occur will dictate the outcome of the implant's life.

In previous research, titania nanotubes and other micro- and nano-structured materials with a relatively low immune response offers encouraging interfaces for tissue implantation. Many titanium alloys have been utilized as biomedical prostheses due to their fairly low modulus, suitable fatigue strength, machinability, formability and corrosion resistance. Electroplating metals such as titanium or its' alloys onto ceramics or plastics would permit mechanical properties even closer in similarity of the tissue being implanted into. Electroplating of ceramics and/or plastics should be considered for future endeavors in biomedical devices. These electroplated materials could then be additionally tissue optimized by producing nanostructures on the surface as previous studies have strongly suggested nanotopographical

surfaces show superior cellular response. With many nanostructured materials, such as titania nanotubes, biochemical eluting ability such as delivery of antibiotics and growth factors for specific cell types could be modified to further increase the capacity of biocompatibility.

It may be possible that certain cell types prefer varying dimensions, elemental composition and shapes of nanostructured materials. By focusing strict attention on mimicking the tissues themselves, superior designed materials could be developed to optimize specific cellular response.

Titania nanotubes can be scratched off with fairly little force and will most always break off to some extent in handling, therefore, studies should be completed that determine the varying cellular response to increasing amounts of broken nanotubes and if there is any long term toxicological effects from having nanoparticle TiO_2 in the body.

Titania or oxide film will be always be present on both experimental samples from being exposed to air, so topography is most likely the main drive of response for this study. The same study as discussed in this document should be done with longer time frames, in vivo and with higher statistical power which would allow stronger conclusions. The effects of residual fluorine from the anodization process should be studied in its effects to the health and viability of the cells. Since not many of the tests were statistically significant from treatment to control group, titania nanotubes may have better applications in drug elution function. Studies must also be done to vary the length and width of the nanotubes to observe if more significant differences would be observed between titanium and titania nanotubes.

Cells are thought to grow more satisfactorily on electrically conductive surfaces than non-conductive surfaces. Therefore a determination of the differences of conductivity of the annealed versus un-annealed sample conductivity should be investigated.

Increasing concentrations of free fluorine anions from the anodization process left on the surface pre-annealing should be investigated on their toxicity to cells

Outcomes still vary greatly among the varying types of biomaterials and nanotopography. Until the understanding of tissue engineering and genetics has progressed far enough that purely biological implants can be produced without any immune response, the development of superior biomaterials will continue to be researched.

REFERENCES

[1] Winder, Steven J., and Michael P. Walsh. "Calponin: thin filament-linked regulation of smooth muscle contraction." *Cellular signalling* 5.6 (1993): 677-686.

[2] Stegemann, Jan P., Helen Hong, and Robert M. Nerem. "Mechanical, biochemical, and extracellular matrix effects on vascular smooth muscle cell phenotype." *Journal of applied physiology* 98.6 (2005): 2321-2327.

[3] Yeh, Ming-Long, and Zong-Ping Luo. "The structure of proteoglycan aggregate determined by atomic force microscopy." Scanning 26.6 (2004): 273-276.

[4] CHAFFEY, NIGEL. "Alberts, B., Johnson, A., Lewis, J., Raff, M., Roberts, K. and Walter, P. Molecular biology of the cell." Annals of Botany 91.3 (2003): 401.

[5] Gibson, Lorna J., Michael F. Ashby, and Brendan A. Harley. Cellular materials in nature and medicine. Cambridge University Press, 2010.

[6] Robert, Ladislas, and William Hornebeck. Elastin and elastases. Vol. 1. CRC Press, 1989.

[7] Sorkin, Jonathan A., et al. "Titania nanotube arrays as interfaces for neural prostheses." *Materials Science and Engineering: C* 49 (2015): 735-745.